Université catholique de Louvain
École Polytechnique de Louvain
ICTEAM Institute
Wireless Communication Group
Louvain-la-Neuve, Belgium

CRLB-Based Antenna Selection for Angle of Arrival Estimation

Masoud Arash

Thesis presented for the Ph.D. degree in Engineering Sciences

	Examining Committee
Advisor:	Luc Vandendorpe, UCLouvain, Belgium
Jury:	François Horlin, ULB, Belgium
	Jérôme Louveaux, UCLouvain, Belgium
	Sofie Pollin, KU Leuven, Belgium
	Marc Moonen, KU Leuven, Belgium
President:	David Bol, UCLouvain, Belgium

"Kindness is the one common language of alive beings."

Masoud Arash

To
my family
Mother and Father, Roya, Farhad, Farzad,
Amin, Amirhossein and Sara
For their undying love and support.

Acknowledgements

First and foremost, I would like to express my deepest gratitude to my supervisor, Prof. Luc Vandendorpe and my research fellows Dr. Ivan Stupia and Dr. Hamed Mirghasemi, for their unwavering support, invaluable guidance, and continuous encouragement throughout my PhD journey. Their mentorship has gone far beyond academic supervision, providing me with insights, motivation, and opportunities that have shaped both my research and personal growth. Their patience, wisdom, and dedication have made this journey not only possible but also deeply rewarding.

I am also immensely grateful to my family for their unconditional love, patience, and support during this long and demanding journey. Their belief in me, even during the most challenging moments, has been a constant source of strength. Without their encouragement and sacrifices, completing this thesis would not have been possible.

I am deeply appreciative of my colleagues and collaborators in the ICTEAM, including Nilanjan Biswas, Emre Kilcioglu, and Arash Masrouri for their support throughout my research. Their contributions have played a significant role in shaping my work. I would also like to thank the administrative and technical staff at UCLouvain for their assistance, which has been invaluable throughout my PhD.

I am sincerely grateful to the members of my PhD jury, Prof.

François Horlin, Prof. Jérôme Louveaux, Prof. Sofie Pollin, Prof. Marc Moonen and, Prof. David Bol, for kindly accepting to be part of the evaluation committee. I truly appreciate their time, consideration, and willingness to engage with my work.

This research would not have been possible without the financial support of F.R.S.-FNRS under the EOS research project MUSEWINET, for which I am truly grateful. Their support has allowed me to fully dedicate myself to my research and professional development.

Finally, I would like to thank the broader academic community and all those who have contributed to my growth as a researcher. This thesis is the culmination of years of hard work, but it is also a testament to the incredible support system I have been fortunate to have. To all those who have played a role, big or small, in helping me reach this milestone—thank you.

Abstract

The new generation of wireless systems aim to bring a breakthrough of innovations in connectivity and smart communications. The ever growing need for higher data transfer and digitization of cities require new technologies to use available resources in the most efficient way. This creates an important question: How can new technologies be leveraged to design and implement sustainable telecommunication systems?

Cellular networks, in which a fixed location base station serves a wide range of wireless devices, are the backbone of new generation of wireless systems. The base stations of such networks have to operate within several strict regulations and restrictions, due to environmental concerns related to global warming. The improvements of these networks to utilize their available resources like energy and hardware in an efficient way, play a key role in transformation toward a green communication network.

This PhD research focuses on energy efficiency improvement and resource allocation challenges within a Multiple-Input Multiple-Output (MIMO) wireless network. In this regard, the localization phase of a wireless network, that aims to achieve location information of user devices, will be the main focus of this work. In the first part, the

Cramer Rao Lower Bound (CRLB) for the angle of arrival estimation in a Multi-User Massive MIMO with linear antenna array when the received signals are accompanied by multipath signals is studied. It is demonstrated that irrespective of the distribution of multi-path signals the CRLB converges toward a deterministic value. Then, by using the obtained formulation for CRLB, a modified comprehensive version of energy efficiency in such networks in the localization phase is proposed and optimized with respect to the utilized antenna set at the base station. The optimal number of antennas to maximize the energy efficiency of the localization is presented, as well as the optimal approach to select the required number of antennas.

In the next part, we extend the CRLB analysis to planar antenna arrays in multi-user massive MIMO systems and explore antenna selection strategies for such arrays. After acquiring the CRLB formulation for a planar antenna array in a multi-user scenario, it is shown that CRLB's formulation is a combined function of AoA, that needs the (unknown) AoA's value for optimization. To overcome this problem, the expected CRLB is chosen as the criterion of antenna selection. A greedy algorithm with an optimal starting point is proposed that aims to minimize the expected CRLB.

Finally, in the last part of this thesis, we propose a real-time CRLB based antenna selection strategy whose objective function is to minimize the CRLB of a user in planar antenna arrays. First, we improve the antenna selection strategy that aims to minimize expected CRLB, from a greedy approach to an optimal analytical method. Then, we use this method to develop a two-step antenna selection strategy that aims to directly minimize the AoA CRLB of a user and further reduce the impact of unknown AoA on the selection process. In the second step of proposed antenna selection, a greedy algorithm is used with an optimal starting point whose performance is shown to be very close to the global search method.

Contents

List of Figures

List of Tables

Acronyms

2D	Two Dimensions
3D	Three Dimensions
AAoA	Azimuth Angle of Arrival
AOA	Angle of Arrival
BS	Base Station
CRLB	Cramer-Rao Lower Bound
DMC	Dense Multipath Channel
ECRLB	Expected Cramer-Rao Lower Bound
ESPRIT	Estimation of Signal Parameters via Rotational Invariant Techniques
EVD	Eigenvalue Decomposition
FIM	Fisher Information Matrix
FLOP	Floating Point Operations
GLONASS	Global Navigation Satellite System
GNSS	Global Navigation Satellite Systems
GPS	Global Positioning System
i.i.d	Independent and Identically Distributed
IoT	Internet of Things
ISI	Inter-Symbol Interference
LE	Localization Efficiency
LoS	Line of Sight

MAP	Maximum a Posteriori
MCRLB	Modified CRLB
MC	Monte-Carlo
MIMO	Multiple Input Multiple Output
ML	Maximum-Likelihood
mmwave	Millimeter Wave
MSE	Mean Square Error
MU	Multi-User
MUSIC	Multiple Signal Classification
PCRLB	Posterior CRLB
RIS	Reconfigurable Intelligent Surfaces
RMT	Random Matrix Theory
RSS	Received Signal Strength
TDOA	Time Difference of Arrival
TOA	Time of Arrival
UTs	User Terminals
w.r.t	With Respect To

CHAPTER 1

Introduction

This chapter reviews the key concepts, theoretical framework, and underlying motivations that have driven the development of this thesis. It aims to provide an overview of the fundamental ideas and research gaps that form the foundation of this study. By exploring these elements, this chapter paves the way for understanding the broader context and significance of the research questions addressed throughout the thesis.

1.1 Background

Wireless communications networks have become an integral part of today's world. Many wide spread applications like daily communications and smart transportation rely on wireless communications. These networks consist of autonomous devices equipped with sensors that provide various services to numerous users. However, meeting ever-growing demands requires wide expansion of infrastructure and energy consumption. The management of existing resources like hardware and energy remains a challenge. Existing approaches often fall short to provide a balanced service while meeting environmental concerns about energy consumption.

The new generation of wireless systems have the potential of providing reliable services with minimal energy consumption by optimally using the available resources. The multi-service wireless networks are capable of using same infrastructure for different applications. For example, a wireless Base Station (BS) can use some of its resources like antennas and available energy budget for data transfer between users, while utilizing the remaining resources for providing location-based services to the users. The optimal use of these available resources are challenging. Different services have different requirements that demands certain resources to be dedicated for them. Limited available hardware is required to support varying number of users at different times, while maintaining a certain quality of service. Also, in densely populated areas, e.g. cities, there are firm regulations about radiated power by wireless providers, limiting the available options for designers.

The evolution of wireless systems toward next-generation networks such as 5G and beyond has brought about transformative changes in communication technologies. With the advancement of hardware quality alongside theoretical analysis, many revolutionary ideas are proposed for the next generations of wireless systems. The utilization of multiple antennas in the BSs to exploit spatial diversity of environment has shown great potential for reliable communications. The use of available information in a network like the location of users is proven to greatly benefit both quality of service to the users and optimal usage of energy budget. As another example, the use of intelligent surfaces in urban areas is another powerful tool to reform and adapt the environment toward more reliable communications. The individual specifications of each of these technologies, alongside their collaboration to solve the challenges of the next generation of wireless systems is the topic of many recent studies.

1.2 Motivation

The ever-growing demand for higher data rates in wireless systems, alongside the limited frequency resources and transmit power, has driven wireless system designers to explore new ideas to fulfill these requirements. In previous generations of wireless systems, the deployment of multi-antenna techniques demonstrated substantial improvements in data throughput, spectral efficiency, and link reliability. More recently, numerous studies have revealed the great potential of utilizing a large number of antennas at base stations (commonly referred to as massive MIMO) to enable simultaneous transmission to multiple users and to enhance overall network capacity and efficiency [1, 2].

However, one of the key challenges that remains is the efficient use of antennas in these systems. The utilization of numerous antennas is not only computationally demanding but also energy intensive, since each antenna requires associated RF chains, power amplifiers, and signal processing hardware [3]. This challenge is particularly pressing in commercial 5G base stations, where energy consumption has already become a major operational cost for mobile network operators [4]. The issue is expected to intensify in 6G systems, where sustainability and carbon footprint reduction are explicit design goals [5]. Furthermore, the number of active users in a cell can vary significantly over time, especially in IoT and sensor networks, where traffic patterns are sparse and intermittent. In such scenarios, it is neither optimal nor necessary to activate all available antennas at all times. Optimized antenna selection methods are therefore essential to reduce hardware complexity, operational costs, and energy usage while maintaining high performance in real-world deployments.

The relevance of optimized antenna selection extends beyond theoretical studies. Numerous research studies have demonstrated its applicability in large-scale wireless networks, where carefully designed selection strategies can significantly improve both spectral and energy efficiency [6–8]. In practice, antenna selection is typically based on criteria such as maximizing the received signal-to-noise ratio (SNR), minimizing interference, or achieving an optimal trade-off between energy consumption and spectral efficiency. Depending on the system requirements, strategies may prioritize antennas with the strongest channel gains, or employ location- and context-aware approaches that exploit user distribution to enhance coverage and efficiency. Such works highlight the importance of efficient antenna usage not only as a means of reducing system complexity, but also as a practical enabler for sustainable operation in next-generation wireless systems.

In addition, localization—the process of determining the position of devices within a network—has become a cornerstone functionality in modern wireless systems. Beyond being a fundamental enabler for applications such as autonomous driving, intelligent transportation systems, smart city infrastructure, and emergency response services, localization is also highly relevant for the optimization of communication itself [9,10]. In massive MIMO systems, user location information can be exploited to design location-aware antenna selection and beamforming strategies, thereby reducing interference, improving link quality, and significantly cutting down unnecessary energy usage. Despite this practical importance, relatively few studies have tackled the problem of energy efficiency in the localization phase of wireless networks, even though it is directly linked to both service quality and network sustainability.

By focusing on improving the energy efficiency of the localization process within the context of MIMO systems with large number of antennas, this research addresses a critical aspect of modern wireless networks, to facilitate the deployment of energy-efficient, high-performance wireless networks that are capable of supporting the exponential growth of connected devices and diverse applications.

1.3 Research Questions

In order to approach the aforementioned challenges, we outline the primary research questions that are addressed in this thesis. These questions are designed to navigate the investigation into improving energy efficiency and performance in the localization phase of massive MIMO systems. Each question aligns with the major contributions discussed in each chapter of this thesis.

1. **How does multiple signal paths in Massive MIMO systems contribute to the accuracy of localization?**
    - What is the standard way to measure this accuracy?
    - How do these multiple signal paths benefit the location accuracy?
2. **What is the best way to balance performance and energy consumption in localization phase within Massive MIMO systems?**
    - How can we measure the benefits versus the costs of location tracking?
    - How many antennas should we use to get the best balance?
3. **How can one select the best subset of antennas to maximize localization accuracy in Massive MIMO systems?**
    - If fewer than available antennas have to be used, what is the most effective way to select a subset of antennas when not all of them are needed?
    - How can we make the process of antennas selection, faster and simpler in Massive MIMO systems?
4. **In planar antenna arrays where the accuracy depends on unknown parameters, how should we select the antennas?**
    - How can we use available information to remove the dependency of accuracy on unknown parameters?
    - Is there a way to reduce the effects of unavailable information of the antenna selection procedure?

1.4 Objectives and Major Contributions

In chapter 2, we will study the basic terminologies of localization and introduce the concepts that will be used in the future chapters. This chapter aims to introduce and define the key terms and principles that are essential for understanding the broader context of this research.

In chapter 3, the CRLB for AoA estimation in a linear antenna array when the received signal at the BS is accompanied by multipath signals according to the DMC model, is analyzed. It will be proved that regardless of the distribution of multipath signals, CRLB for AoA almost surely converges toward a deterministic expression in the MU massive MIMO setting. Afterward, a refined version of a performance metric, named Localization Efficiency (LE), is presented, using a comprehensive energy consumption model. Then, an antenna selection method is presented that minimizes the CRLB for AoA when the number of utilized antennas is smaller than the total available antennas.

In chapter 4, the CRLB analysis for AoA estimation in DMC model is extended to planar antenna arrays in Multi-User Massive MIMO systems. Then, the problem of antenna selection for localization phase is studied in these arrays. To overcome the lack of knowledge of AoA that is a non-separable part of CRLB formulation in planar antenna arrays, the expected CRLB is proposed as the cost function of the antenna selection. Finally, a greedy antenna selection algorithm with optimal starting point is proposed to minimize the expected CRLB of Azimuth.

chapter 5 focuses on addressing the issue of limited knowledge of AoA in the antenna selection procedure in planar antenna arrays for a single user. In the first part of this chapter, the presented antenna selection method, when the objective is to minimize the expected CRLB of AoA, is improved to an optimal strategy. Then, in the second part a two-step antenna selection strategy is devised whose objective is to minimize the CRLB of AoA (not its expectation). This method will make use of the antenna selection method that minimizes expected

CRLB, but will go further on reducing the effects of an unknown AoA on the antenna selection process.

1.5 Notation

Throughout this thesis, a certain mathematical notation is used for clarity. The boldface lower case is used for vectors, $\boldsymbol{x}$, and upper case for matrices, $\boldsymbol{X}$. $\boldsymbol{X}^*$, $\boldsymbol{X}^T$, $\boldsymbol{X}^H$ and $\boldsymbol{X}_{m,k}$ denote conjugate, transpose, conjugate transpose and (m,k)th entry of $\boldsymbol{X}$, respectively. $\mathbb{E}_x\{.\}$ denotes expectation w.r.t x, $Card(.)$ is cardinality of a set, $j = \sqrt{-1}$, $|\ .\ |$ stands for absolute value of a given scalar variable, tr is trace operator, $\odot$ is Hadamard product operator, $\otimes$ is Kronecker product operator, $\xrightarrow{a.s.}$ means Almost Sure convergence and $diag(\boldsymbol{x})$ is a diagonal matrix whose diagonal entries are the elements of $\boldsymbol{x}$. Also, $\boldsymbol{I}_K$ is $K \times K$ identity matrix. When $\boldsymbol{y} = [y_1\ \ y_2\ \ \ldots\ \ y_p]^T$ and $\boldsymbol{x} = [x_1\ \ x_2\ \ \ldots\ \ x_q]^T$, we define $(\frac{\partial \boldsymbol{y}}{\partial \boldsymbol{x}})_{p,q} = \frac{\partial \boldsymbol{y}_p}{\partial \boldsymbol{x}_q}$.

CHAPTER 2

Background and Motivations

This chapter defines and explains the fundamental concepts that form the foundation of this thesis. This chapter serves as a theoretical framework, introducing key terms, principles, and theories that will be referenced throughout the subsequent chapters. By establishing a clear understanding of these basic concepts, this chapter aims to provide readers with the necessary background knowledge to follow the arguments and analyses presented later in the thesis.

2.1 Localization in Wireless Systems

The history of localization in wireless communications is a story of technological innovation driven by the need for precision and efficiency in location-based services. The localization is generally defined as acquiring the information about the physical location of User Terminals (UTs) in a wireless network [11]. Early developments in this field can be traced back to the mid-20th century with the advent of radar technology, which enabled rudimentary forms of object detection and tracking. However, it wasn't until the late 20th and early 21st centuries that localization in wireless communications truly flourished. GNSS localization methods, initially developed for military purposes, became accessible to civilians in the 1980s, revolutionizing navigation and paving the way for location-based services. Initially designed to provide connectivity and coverage, the cell towers started to take part in localization as mobile devices became ubiquitous. Early techniques for localization in cellular networks relied on signal strength and timing measurements between mobile devices and nearby cell towers, known as cell ID or cell sector identification. These methods allowed for estimates of a device's location. Advancements such as enhanced cell tower density, and improved signal processing algorithms significantly enhanced localization accuracy. Nowadays, with the widespread adoption of smartphones and the rollout of 4G and 5G networks, localization in cellular mobile networks has become an integral part of numerous applications, including location-based services, emergency response systems, and targeted advertising. In the following the three main areas of localization are introduced.

2.1.1 GNSS

Global Navigation Satellite Systems (GNSS) represent a constellation of satellites orbiting Earth, providing precise positioning, and timing information to users worldwide. The primary functioning of GNSS involves a network of satellites continuously transmitting signals containing time and positioning data. These signals are received by GNSS receivers, such as those found in smartphones, vehicles, and specialized navigation devices. By calculating the time it takes for signals to reach the receiver from multiple satellites, along with the satellites' known positions, the receiver can determine its own position on Earth with remarkable accuracy. GNSS systems like GPS (Global Positioning System), GLONASS (Global Navigation Satellite System), Galileo (European Union), and BeiDou (China) offer global coverage and work in a similar fashion, with slight variations in technology and constellation configuration. The applications of GNSS span various sectors, including transportation, agriculture, surveying, emergency response, and telecommunications. In transportation, GNSS enables precise vehicle navigation, leading to safer and more efficient travel.

In agriculture, it facilitates precision farming techniques by providing accurate location data for planting, fertilizing, and harvesting. GNSS also plays a crucial role in surveying and mapping, allowing for the precise measurement of land boundaries and geographical features. Furthermore, it aids emergency response efforts by enabling search and rescue teams to quickly locate individuals in distress. Overall, GNSS has become an indispensable tool in modern society, empowering countless applications that rely on accurate positioning and timing information.

2.1.2 Radar Localization

Radar localization is a technology used to determine the position and velocity of objects by emitting radio waves and analyzing the reflected signals. This method relies on the principle of measuring the time delay between the transmission and reception of radio waves to calculate the distance to an object. By deploying radar systems equipped with special antennas, radar localization can accurately track the location and movement of targets in various environments, including air, land, and sea. Radar localization finds extensive application in aviation for aircraft navigation, collision avoidance, and air traffic control. In maritime settings, radar systems aid navigation, monitor vessel traffic, and detect obstacles such as icebergs or other ships. Additionally, radar is used in automotive applications for adaptive cruise control, collision avoidance systems, and autonomous vehicle navigation. Radar localization is achieved through sophisticated signal processing algorithms that analyze the received signals' phase, frequency, and amplitude to extract information about the target's position, speed, and direction of movement. This technology continues to evolve with advancements in radar hardware and software, offering enhanced accuracy, reliability, and versatility across a wide range of applications.

2.1.3 Cellular Localization

In order to satisfy the requirements of today's world, the next generation of wireless systems requires access to a new level of information. The information, such as location, device type, and environment in which the service is provided, enables wireless systems to deliver customized services. Cellular localization, involves determining the geographic location of a mobile device or user within the coverage area of cellular base stations. This process relies on various techniques, including received signal strength (RSS) measurements, time of arrival (TOA), time difference of arrival (TDOA), and angle of arrival (AOA). Cell towers continuously exchange signals with mobile devices, and by analyzing the strength and timing of these signals, cellular networks can estimate the device's location relative to nearby towers. More and more precise localization is achieved through the evolution of wireless systems and their utilized methods.

The applications of cellular localization are diverse and influential. Location-based services leverage cellular localization to offer features such as mapping, navigation, and location-based advertising. Emergency services utilize cellular localization to quickly respond to distress calls and locate individuals in need of assistance. Additionally, cellular localization enables network optimization, allowing mobile operators to efficiently manage network resources and improve coverage in densely populated areas. Overall, cellular localization has become an essential component of modern mobile networks, enhancing user experiences and enabling a wide range of valuable services.

On the one hand, many applications, like navigation systems, auto-driving cars and emergency services, directly use and require continuous and accurate location of UTs [12]. On the other hand, indirect usage of UTs' location information paves the way for better resource allocation, like frequency and power, alongside improved quality of service in the wireless networks [13]. For example, with the help of location information, higher data rates with higher energy efficiencies can be transferred to more UTs by beamforming at the

BS [9,14].

2.2 Localization Parameters

In every area of localization certain parameters and information are used to achieve the location data. For instance, the AoA, ToA and RSS are examples the information that is used by either some or all of localization methods. Various combinations of these information can be used together based on the requirements of a localization method.

In the past years, many research works are conducted to study the localization methods of UTs in a wireless system. Estimation of UTs location is done with respect to a BS that provides the wireless network for UTs in a certain area, like wireless cellular networks. The most used information to obtain location information in such networks include AoA, ToA and RSS. Each of these information contribute to a specific location information of a UT.

2.2.1 Received Signal Strength

RSS refers to the power level of a wireless signal as it is received by a receiver antenna. It quantifies the intensity of the signal at the receiver's location. RSS-based localization methods use measurements of signal strength obtained from multiple receivers to estimate the distances between the transmitting UT and the receivers. By combining these distance estimates, the location of the transmitting device can be inferred.

2.2.2 Time of Arrival

ToA represents the precise moment at which a wireless signal arrives at a receiver relative to a reference time. It measures the propagation delay between the transmission of a signal and its reception. ToA-based localization techniques use the differences in arrival times of signals at multiple receivers to estimate the distances between the transmitting UT and the receivers, allowing for the determination of

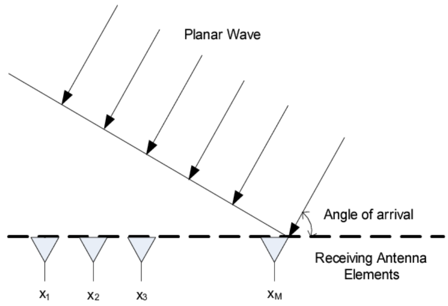

Figure 2.1: AoA of a planar propagating signal at a linear antenna array.

the device's location.

2.2.3 Angle of Arrival

AoA refers to the direction from which a wireless signal arrives at a receiving antenna array (Fig. 2.1). It is a measure of the angle between the direction of propagation of the signal and a reference axis. AoA is often used in wireless localization to estimate the spatial location of UTs based on the angles at which their signals are received by multiple antennas or sensor nodes.

AoA offers several advantages over ToA and RSS in the context of wireless cellular networks. One significant advantage of AoA is its ability to provide spatial information by using a single antenna array, not requiring multiple distributed antenna over an area. This information then can be used for beamforming without any need for further processing, facilitating the optimization of available resources (like energy) and enhancing the performance (like higher data rates and less interference). This advantages is further pronounced in the wireless systems that implement large number of antennas in one single compact array, like Massive MIMO systems, or Intelligent Reconfigurable Surfaces. Moreover, AoA-based localization is less susceptible to environmental factors that can affect signal propagation, such as interference and signal attenuation, making it more robust and reliable for many applications. These advantages made AoA the topic of many research works in the past decade, especially when the use of MIMO systems with more and more antennas became practical.

In general, the AoA estimation methods are divided into two groups of model based and data driven methods, based on their underlying design scheme.

Model-based methods rely on mathematical or physical models to describe the relationship between input data and the desired output. These models are often based on known principles or assumptions about the wireless systems in which AoA s being estimated. A model-based approach involves using mathematical equations that describe how electromagnetic waves propagate through a medium and interact with sensors or receivers to determine the AoA. These methods typically require knowledge of the system's parameters and may involve solving complex equations. Numerous Model-based methods have been proposed and modified for the AoA estimation. The most well know examples are MUltiple SIgnal Classification (MUSIC) [15] and estimation of signal parameters via rotational invariant techniques (ESPRIT) algorithms [16]. These two algorithms were the basis for development and modification of many AoA estimation methods since their introduction.

Data-driven methods, on the other hand, learn patterns and relationships directly from data without relying on explicit mathematical models or assumptions. These methods leverage machine learning algorithms to analyze large datasets and extract meaningful information. In the context of estimating angle of arrival, a data-driven approach might involve training a machine learning model, such as a neural network, using data collected in a wireless system in different situations. The model learns to map input features of the received signals to their corresponding AoA through iterative optimization based on the training data. Data-driven methods are often more flexible and can adapt to complex patterns in the data, but they may require substantial amounts of training data and computational resources. An example of Data-driven methods are the well studied fingerprinting approaches, that try to map the desired environment in variable resolutions.

2.3 Cramer-Rao Lower Bound

The CRLB is a statistical tool that plays a crucial role in assessing the accuracy and precision of parameter estimation. The CRLB indicates the minimum possible error variance of an unbiased estimator for a given parameter of interest. In other words, it provides a fundamental limit on how well one can estimate an unknown parameter based on noisy observations [17].

The CRLB is particularly important in wireless communication systems due to the inherent limitations and uncertainties in the wireless channels. The wireless channel introduces various types of distortions, such as multipath fading, interference, and noise, that can affect the accuracy of signal processing algorithms. The CRLB can help to quantify the impact of channel impairments on the estimation accuracy. Also, because the CRLB is a characteristic of a wireless system and a function of its settings, it is independent from the methods that are used for estimation. This makes the CRLB a valuable performance metric that can help wireless communication system designers to develop more robust and reliable systems.

The CRLB in a wireless system is affected by several factors. Specific settings of a wireless network is reflected by the CRLB that makes it useful as a tool to explore the pros and cons of various designs. Some of these effects are directly observed in the CRLB formulation, such as noise variance, received signal power. On the other hand, some parameters indirectly affect CRLB formulation, like the number and configuration of antennas at the BS, and the number and correlation of desired parameters for estimation.

Using multiple antennas at the BS makes it possible to use spatial diversity for estimating desired parameters. The more antennas that are used for receiving a signal, the more information is available for the estimation process. Also, the geometric arrangement of antennas at the BS greatly influences the CRLB of a wireless system. If the receiver antennas are well-spaced and optimally positioned, the localization accuracy improves. Conversely, densely clustered or poorly distributed antennas lead to a larger CRLB.

Moreover, when multiple parameters are estimated simultaneously (as opposed to individually), several effects come into play that is reflected by the CRLB. The CRLB is defined as the inverse of Fisher Information Matrix (FIM), which in turn is a measure of whole available information [18]. When several parameters like RSS, TOA and AoA are being estimated, they are often interdependent and are correlated. In such cases, the FIM becomes a block matrix, with each block corresponding to a parameter. The off-diagonal elements represent the cross-covariance between parameters. These cross-covariances are captured by the CRLB and they reveal how uncertainties in one parameter affect the estimation of another. Understanding of these effects is crucial for designing robust localization algorithms and achieving optimal performance in wireless networks.

2.4 Massive MIMO

Massive MIMO represents a revolutionary paradigm in wireless communication, achieved by deploying an large number of antennas. These systems offer several key features: spatial efficiency, 3D beamforming, and energy efficiency. The concept of Massive MIMO relies on exploiting the spatial dimension of a wireless channel to increase the capacity and reliability [19]. Massive MIMO enables simultaneous communication with multiple users, significantly boosting spectral efficiency. Its dynamic beamforming capabilities allow precise coverage in three dimensions, providing more degrees of freedom. Moreover, focusing radiation toward intended users minimizes interference, leading to energy-efficient communication. The applications of Massive MIMO are diverse: it is a cornerstone of 5G networks, promises higher data rates, improved capacity, and seamless connectivity. Additionally, it supports massive connectivity for Internet of Things (IoT) devices, enabling smart cities, industrial automation, and more.

Massive MIMO holds immense promise for precise localization of UTs. These systems offer high resolution spatial information that can be used for accurate localization, especially AoA estimation [20, 21]. Also, the multitude of antennas, mitigates fading effects caused by reflections and multipath propagation, as well as making it very difficult for jamming and spoofing attacks. In addition, the use of massive antenna arrays would enable more efficient use of the time and frequency resources by enabling the simultaneous localization of multiple UTs [22].

2.5 Energy Efficiency

Energy efficiency is a critical factor in the design of wireless communication systems, as it directly impacts the performance, cost, and sustainability of these systems. It is a critical aspect of modern communication systems, given the increasing demand for high-speed data transmission and the proliferation of wireless devices. The study of energy efficiency is particularly important because excessive radiation from wireless devices has raised concerns about potential health risks. Lower radiation levels can reduce interference with other electronic devices, improving the overall performance and reliability of wireless networks. Also, the energy management in battery-powered devices, where energy resources are limited, not only extends the battery life of devices but also reduces the overall environmental impact, contributing to sustainability goals. Efficient energy use not only extends the battery life of devices but also reduces the overall environmental impact, contributing to sustainability goals. Therefore, energy efficiency contributes not only to the sustainability and cost-effectiveness of wireless communication systems, but also to the reduction of radiation levels, enhancing the safety and reliability of these systems.

Hence, improving the energy efficiency of wireless communication systems has become a key research focus in recent years. Several studies have proposed various techniques and strategies to enhance energy efficiency in wireless communication systems, such as power control, resource allocation, transmission scheduling, and network densification.

Moreover, the importance of energy efficiency in wireless communication systems is further highlighted by the emergence of new wireless technologies and applications, such as 5G and the IoT, which require high-speed, reliable, and ubiquitous wireless connectivity with low latency and high mobility. These requirements pose significant challenges to the design and operation of wireless communication systems, particularly in terms of energy consumption and sustainability.

As an essential part of any future wireless systems, localization part plays a key role in designing an energy efficient wireless network. localization processes can consume significant energy, especially when high precision is required. Therefore, studying the energy and performance trade-off in the localization part of wireless systems is of paramount importance.

2.6 Antenna Selection

Antenna selection is one of the critical aspects of MIMO wireless communication systems, significantly boosting their efficiency while preserving a certain level of service quality. The fundamental principle of antenna selection is to pick a subset of antennas from a larger array, optimizing the system's performance based on specific criteria such as signal strength, channel conditions, or energy efficiency.

This technique offers a practical solution to various challenges inherent in MIMO systems. One of the main uses of antenna selection in wireless communications is to improve the energy efficiency of the system. Measurements have shown that around 60% of total power consumption of a cellular network is in the BS. Also, 75% of this power is used for signal processing (10%) and power amplifiers including the feeders (65%). Both of these power consumptions scale with the number of utilized antennas in the BS. The power consumption of signal processing part depends on the type of processing algorithms that are used and is usually a polynomial relation. On the other hand, the power consumption of amplifiers scale linearly with number of utilized antennas. Utilizing antenna selection can significantly reduce both of the aforementioned power consumption parameters. In fact, antenna selection is one of means toward making the power consumption, proportional to the network load.

Furthermore, antenna selection facilitates the assignment of different antennas to different services, thereby enabling multi-service wireless communications. Another compelling reason for antenna selection is that utilizing all available antennas in non-peak traffic hours might lead to an accuracy level exceeding the system's requirements, thereby generating unnecessary computational complexity. This is particularly relevant in Massive MIMO systems, where the large number of antennas can result in high computational complexity and energy consumption.

In essence, antenna selection allows for a more efficient use of resources, leading to improved network longevity, reduced energy costs, and lower radiation levels. Therefore, antenna selection is not just a technical strategy; it's a vital aspect of sustainable and efficient wireless communication. It's an area of ongoing research with significant implications for the future of wireless technology.

CHAPTER 3

Energy Efficiency in AoA Estimation

In the next generation of wireless systems, massive MIMO offers high angular resolution for localization. By virtue of large number of antennas, AoA of User Terminals (UTs) can be estimated accurately. Measurements of Dense Multipath Channel (DMC) indicate multipath signals contribute up to 95% of total link power. This fact urges the necessity of studying the contribution of multipath signals accompanying dominant path in AoA estimation. In this section, we obtain a deterministic form for $CRLB$ in multi-user scenario when contribution of multipath signals is considered. We do this when the multipath signals are independent and identically distributed (i.i.d) with arbitrary distribution. Afterward, a redefinition of localization efficiency function for multi-user scenario is presented and optimized with respect to (w.r.t) the number of antennas. When only a subset of available antennas is used, we prove that $CRLB$ can be minimized w.r.t which set is used. An antenna selection strategy that minimizes $CRLB$ is proposed. As a benchmark, we apply the proposed antenna selection to MUltiple SIgnal Classification (MUSIC) algorithm and study its efficiency.

3.1 Introduction

Massive MIMO systems are considered as one of the key candidates for the upcoming generation of wireless networks [2]. These systems utilize a large array of antennas, which opens up numerous possibilities for enhancing wireless system performance, such as increased capacity, spatial diversity, and reduced latency [2]. Notably, these systems provide high precision for various localization techniques, particularly AoA and the orientation of User Terminals (UTs) [20, 21]. Massive MIMO systems enable precise estimation of the AoA of individual multipath signals within a system [23] and offer higher multipath resolution in the angle domain [24]. Additionally, the deployment of extensive antenna arrays allows for more efficient utilization of time and frequency resources by facilitating the simultaneous localization of multiple UTs [22].

Various types of localization with different goals are introduced and studied in the literature. Anchor-based schemes, where UTs' locations are estimated relative to an anchor, are among the most popular methods [25]. In these approaches, techniques such as RSS, DTOA, and AoA estimation are employed to determine UTs' locations. The performance of these methods is typically compared with the CRLB, which provides a lower limit on the estimation error for any unbiased estimator [18].

3.1.1 CRLB of AoA estimation

Several studies have investigated the CRLB in the context of massive MIMO systems. For a planar antenna array, [26] approximated the CRLB for a fading-free channel. In [11], the authors derived the CRLB as a function of instantaneous parameters for AoA, angle of departure, delay, and orientation estimation of UTs under different scenarios, considering both Line of Sight (LoS) and Non-LoS dominant paths. In [27], the CRLB for AoA and channel gain was obtained in a massive

MIMO system with a planar array for a single UT. The authors in [10] approximated the CRLB for a single UT case of a planar array in the Millimeter Wave (mmWave) scenario, taking into account multipath effects.

All the works in [11]- [10] assumed an identical channel coefficient from each UT to all the antennas at the BS. This implies that all antennas are fully correlated, resulting in zero spatial diversity for the antenna array. The main hypothesis behind this common assumption is that all UTs experience channels where one or a few dominant paths carry most of the received signal's power to the BS. Previous studies on localization in massive MIMO systems provide valuable insights into the information that can be extracted from the dominant components of the channel (if present), with the apparent consequence that if those components are shadowed, the CRLB of systems may increase indefinitely. It is important to note that this assumption might contradict the original goal of developing massive MIMO technologies as an efficient solution to provide seamless and reliable links between UTs and BS, even in the absence of LoS or clear dominant paths. This consideration is supported by many studies of massive MIMO systems, such as [13], which assume that UTs have independent channel coefficients for different antennas.

Moreover, the same infrastructure can be utilized for both localization and data transmission. To avoid zero spatial diversity, which results from fully correlated channels, antennas are arranged to achieve independence. For example, in mmWave scenarios, a separation of a few centimeters can achieve this. This indicates a clear discrepancy between studies on data transmission and localization in massive MIMO systems. The question that arises here is how the CRLB changes when different antennas have different channel coefficients. In other words, can we leverage the presence of multipath signals in massive antenna arrays to extract AoA information and demonstrate the contribution of these multipath signals to the CRLB?

The DMC channel model is adopted in this work to represent propagation environments where, in addition to the dominant signal path, the received signal is significantly influenced by a large number of diffuse multipath contributions. Unlike classical multipath models that explicitly add a finite set of propagation paths with deterministic angles and delays, the DMC model treats the effect of scattering in a stochastic manner. In this framework, the aggregate contribution of many unresolved local scatterers in the vicinity of the UT is modeled as a diffuse component, superimposed on the dominant path. This approach captures a key characteristic of rich scattering environments that are particularly relevant for the study of (massive) MIMO systems [28].

The underlying hypothesis of the DMC model is that each antenna element receives not only the direct or dominant path, but also an additional stochastic contribution originating from a cloud of local scatterers around the UT [29,30]. As a result, the channel coefficients at different antennas become partially correlated through the common scattering environment, while still exhibiting randomness due to the diffuse nature of the multipath. Measurement campaigns support this assumption, showing that the diffuse multipath power in DMC scenarios can account for as little as 10% and up to 95% of the total link power [31, 32]. The DMC model has been observed mainly in measurements at frequencies relevant to cellular communications, typically between $\sim$ 400 MHz and 5.3 GHz, where rich scattering from buildings, various surfaces on like windows and vehicles is common [30].

By adopting this model, we explicitly hypothesize that the presence of dense multipath is a dominant mechanism shaping the statistical behavior of the channel. Consequently, evaluating the performance of localization methods and the behavior of the CRLB under the DMC assumption provides a realistic and robust characterization of system performance in rich scattering environments.

In this context, [33] was the first to address the issue of i.i.d. channel coefficients for AoA estimation. However, due to mathematical complexities of $CRLB$ analysis, [33] only provides the probability of AoA detection for a single UT. The first objective of this work is then to bridge this gap by presenting a deterministic expression of the CRLB for multiple UTs, assuming i.i.d. channel coefficients between antennas. To achieve a deterministic $CRLB$, various methods have been proposed to remove the effects of instantaneous nuisance parameters (e.g., fading channel coefficients) in $CRLB$. In [34], Miller and Chang introduced a performance metric obtained by taking the expectation from the $CRLB$ w.r.t. the nuisance parameter, while in [35] the authors defined a Modified $CRLB$ ($MCRLB$) by taking an expectation from Fisher Information Matrix (FIM). The drawback of these approaches is that the proposed metrics rely on the specific channel probability distribution. This issue is escalated in MU MIMO systems. This work proposes a deterministic and closed-form solution for the $CRLB$ in MU massive MIMO systems, considering the contribution of multipath signals with arbitrary distribution.

To achieve this, we utilize Random Matrix Theory (RMT) to demonstrate that the $CRLB$ of a MU massive MIMO system almost surely converges toward a deterministic function of the channel variance, regardless of the channel coefficient distributions. We also show that $CRLB$ for AoA estimation always converges toward a finite value, meaning that with the help of multipath signals, AoA information can always be extracted, even when the dominant path is in poor condition. This result is of particular importance to give a theoretical foundation to those techniques, such as those proposed in [12, 14, 20, 36, 37], which aim to exploit multipath signals to extract or refine AoA estimation.

3.1.2 Energy Efficiency

Massive MIMO technology can efficiently and reliably locate multiple user terminals (UTs) using limited time and frequency resources. However, the increased energy consumption of these systems can compromise these benefits. Recently, many research works have focused on the energy efficiency of massive MIMO systems [13, 38]. In [13], the authors indicated that a complete model for these systems should include the energy use of different parts, like hardware and signal processing units. Some parts, such as those for computation and hardware, use more energy as the number of antennas increases. Accordingly, several research works have examined how performance metrics change when considering a detailed energy consumption model [19,39]. Efficiency in localization has been studied only in few works, mainly at the network level. In [40] authors introduced the product of error and power consumption as a measure of efficiency in wireless sensor networks. Similarly, [41] used the inverse of this product to provide a tangible interpretation of this criterion in similar settings, obtaining $CRLB$ through simulations. Yet, more attention is needed on the concept of efficiency in localization, as it reveals important trade-offs.

To address this issue, in the second part of our work, we redefine a Localization Efficiency (LE) function for in-depth studies in multi-user (MU) scenarios. We start by formulating the LE function that incorporates critical performance metrics, using the derived CRLB for a typical system, the number of UTs, and total energy consumption. Unlike previous studies, we utilize a comprehensive energy consumption model. Interestingly, the study of $CRLB$ shows that by using a subset of available antennas, both the behavior and formulation of the $CRLB$ change, based on which set of antennas is utilized. Next, we study the antenna selection and find the set that minimizes $CRLB$ when only a subset of available antennas is used. Moreover, we show that the optimal number of antennas differs for different antenna selection methods. Finally, to analyze LE and antenna selection in simpler system models, the MUSIC algorithm is studied. The contributions of this section are summarized as follows:

- CRLB for AoA estimation of a MU massive MIMO system is derived in a deterministic form under DMC channel model with arbitrary distribution, using RMT methods.

- Efficiency function for localization is redefined as a function of system parameters to evaluate localization methods, and it is used to study the trade-off between performance and energy consumption.

- Antenna selection for localization is introduced, and a selection strategy that minimizes $CRLB$ is presented. LE is reformulated in this case, and the optimal number of antennas is obtained for this selection method.

- As a case study to show how LE of a method can be studied, LE of MUSIC algorithm based on its exact required computations is derived and studied. Also, different antenna selection methods are studied for this algorithm.

The remainder of this chapter is organized as follows. In Section 3.2 we introduce our system model. $CRLB$ is calculated for different channel models of BS antennas in Section 3.3. LE is formulated in Section 3.4. All of these are then used to study the idea of antenna selection in Section 3.5. LE of the MUSIC algorithm is dealt with in detail in Section 3.6. In Section 3.7, numerical results are used to validate the theoretical analysis and make comparisons of LE under various scenarios. Finally, the major conclusions are drawn in Section 3.8.

3.2 System Model

We consider the uplink of a single-cell mmwave communication MU massive MIMO system with a BS at the center of the cell, equipped with M antennas, equally separated by a distance d (Fig. 3.1). The choice of the linear array is due to wide studies of these arrays in the literature [11, 14], its various advantages in AoA estimation [42], and mathematical clarity. There are K single antenna UTs whose AoAs are distributed uniformly over the upper half of the cell, i.e. $AoA_k \sim U[0, \pi]$. In this system, BS estimates AoA of UTs and channel coefficients using the pilot signals transmitted by UTs with wavelength λ. The first antenna at the top of the antenna array is the reference

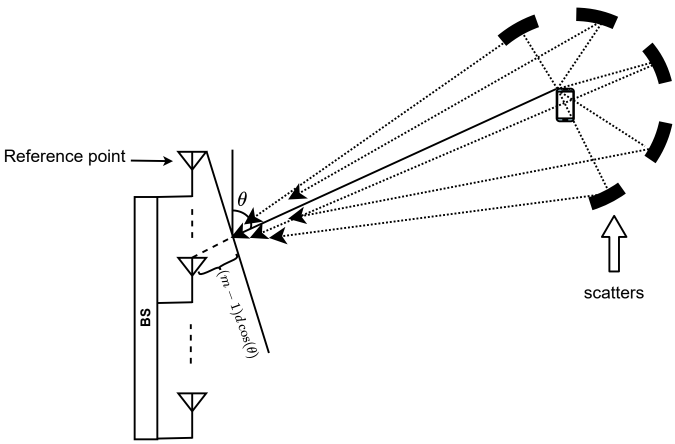

Figure 3.1: DMC channel model with multipath signals in the vicinity of the dominant path.

point w.r.t. which the AoA is measured. In the MU scenario, UTs transmit their pilot signals at the same time and frequency.

Here the DMC channel model of mmwave communication is considered, originally introduced in [29]. This model also is part of the COST 2100 channel model [30] (Fig.4, when DMC affects each antenna, separately). In this model, there are local scattering objects in the users' vicinity, as illustrated in Fig.3.1. There is a dominant path that defines the Angle of Arrival (AoA), shown with the solid line in Fig. 3.1, accompanied by many multi-path signals that are originated by scatters at the vicinity of the user, depicted by dotted lines. Such a channel can be modeled as a random variable with a mean equal to the channel coefficient of the dominant path and a variance that accounts for the sum of all the multi-path signals.

When the signal arrives at the antenna array as a plane, depending on the AoA, the received signal at the mth antenna will travel a path little longer (or shorter depending on θ) with respect to the signal's path for the reference point. This extra distance is shown in Fig.3.1 with a dashed line and if we consider the first antenna as the reference point, it is equal to $(m-1)d\cos(\theta)$. The steering vector models the phase difference that is caused due to this difference in path length. The important point is that as the multi-path signals are in the vicinity of each antenna's dominant path, they will also travel the same path, with a little difference depending on the scatters effect. So, the phase of the multi-path signals at the mth antenna can be modeled as a random variable, with the mean equal to $2\pi\frac{(m-1)d\cos(\theta)}{\lambda}$. The random variations around the mean models the induced phase due to the randomness of the aggregated multi-path signals. This is why the random part that accounts for the multi-path is also multiplied by the steering vector. The total observed channel coefficient for the kth UT at the mth antenna at the BS can be written as

$$\begin{aligned} g_{m,k} &= \sqrt{l(r_k)}(h_{d_k}e^{-j\frac{2\pi r_k}{\lambda}}e^{-j\frac{2\pi}{\lambda}d(m-1)\cos(\theta_k)} \\ &\quad + \check{h}_{r_{m,k}}e^{-j\alpha_{m,k}}e^{-j\frac{2\pi}{\lambda}d(m-1)\cos(\theta_k)}) \\ &= \sqrt{l(r_k)}e^{-j\frac{2\pi}{\lambda}d(m-1)\cos(\theta_k)}(\bar{h}_k + \hat{h}_{r_{m,k}}) \\ &= \sqrt{l(r_k)}e^{-j\frac{2\pi}{\lambda}d(m-1)\cos(\theta_k)}h_{m,k}, \end{aligned} \tag{3.1}$$

where $l(r_k)$ is the large scale fading of the kth UT, h_{d_k} is the amplitude of the dominant path, r_k is the length of the dominant path, $\check{h}_{r_{m,k}}$ and $\alpha_{m,k}$ are the amplitude and phase of aggregated multipath signals at the mth antenna. Also, $\bar{h}_k = h_{d_k}e^{-j\frac{2\pi r_k}{\lambda}}$ and $\hat{h}_{r_{m,k}} = \check{h}_{r_{m,k}}e^{-j\alpha_{m,k}}$. Finally, $h_{m,k}$ is a random variable with a mean equal to $\bar{h}_k$ and variance equal to σ_h^2 that accounts for the power of the multipath signals from the kth user at the mth antenna. Therefore, the received signal at the BS side can be written as

$$\boldsymbol{y} = \boldsymbol{G}\boldsymbol{s} + \boldsymbol{n}, \tag{3.2}$$

in which $\boldsymbol{G}$ is $M \times K$ channel matrix between M BS antennas and K UTs, $\boldsymbol{s} \in \mathbb{C}^{K\times 1}$ is the vector of transmitted pilots and $\boldsymbol{n} \sim$

$\mathcal{CN}(0, \sigma_n^2 \boldsymbol{I}_M)$ is additive noise. Matrix $\boldsymbol{G}$ is composed as

$$\boldsymbol{G} = (\boldsymbol{A}_{Rx} \odot \boldsymbol{H})\boldsymbol{Q}^{\frac{1}{2}}, \tag{3.3}$$

where

$$\boldsymbol{A}_{Rx} = [\boldsymbol{a}_{Rx}(\theta_1) \;\; \boldsymbol{a}_{Rx}(\theta_2) \;\; \ldots \;\; \boldsymbol{a}_{Rx}(\theta_K)] \tag{3.4}$$

contains $M \times 1$ steering vectors of BS antenna array response for K UTs in which

$$\boldsymbol{a}_{Rx}(\theta_k) = \frac{1}{\sqrt{M}}[1 \;\; e^{-j\beta\cos(\theta_k)} \;\; \ldots \;\; e^{-j(M-1)\beta\cos(\theta_k)}]^T, \tag{3.5}$$

θ_k is kth UT's AoA for $k \in \{1, 2, \ldots, K\}$ and $\beta = \frac{2\pi d}{\lambda}$. $\boldsymbol{H}$ is an $M \times K$ matrix whose (m, k)th element, $h_{m,k}$, is fast fading coefficient between kth UT and mth BS antennas

$$h_{m,k} = h^r_{m,k} + jh^i_{m,k}, \tag{3.6}$$

and

$$\begin{aligned} &\mathbb{E}\{h^r_{m,k}\} = \mathcal{R}e\{h_{d_k}\}, \;\; \mathbb{E}\{h^i_{m,k}\} = \mathcal{I}m\{h_{d_k}\}, \\ &\mathbb{E}\{|h^r_{m,k}|^2\} - (\mathbb{E}\{h^r_{m,k}\})^2 = \mathbb{E}\{|h^i_{m,k}|^2\} - (\mathbb{E}\{h^i_{m,k}\})^2 = \sigma_h^2, \end{aligned} \tag{3.7}$$

for $m \in \{1, 2, \ldots, M\}$ and $k \in \{1, 2, \ldots, K\}$. $\boldsymbol{Q}$ is a $K \times K$ diagonal matrix whose kth diagonal element is $l(r_k)$. Also, for simplicity, we define received signal to noise ratio at the BS side as

$$\rho_k \triangleq \frac{|s_k|^2 l(r_k)}{\sigma_n^2}. \tag{3.8}$$

Remark 1. *Our model assumes that there are K UTs, and each of them has one AoA. The same model can still be used if one wants to consider multiple AoAs for each UT, e.g., due to reflections. For example, a system with K UTs where each UT has a single AoA, can also be interpreted as a system with $\frac{K}{2}$ UTs where all UTs have two AoAs (or any other combination). The point of our system model is* *to consider that there are K independent AoAs to be estimated, no matter whose those AoAs are.*

Remark 2. *It is worth mentioning that an "angle of arrival" is not necessarily the geometric angle of a UT to the BS. For example, when there is no LOS, an angle of arrival is the angle of a reflection. How an angle of arrival is connected to the geometric angle of a UT requires the knowledge of geometry of the environment. This is outside the scope of this work, but interested readers are recommended to see [37, 43].*

3.3 CRLB

In this section, we derive a deterministic formula for the $CRLB$ of AoA estimation for MU massive MIMO settings where multipath signals' contribution is considered. We assume that the channel coefficients are random but known and so not needed to be estimated. Vector of desired parameters will be

$$\boldsymbol{\eta}_\theta = [\theta_1 \;\; \theta_2 \;\; \dots \;\; \theta_K]^T. \tag{3.9}$$

Defining $\hat{\boldsymbol{\eta}}_\theta$ as the unbiased estimation of $\boldsymbol{\eta}_\theta$, the Mean Square Error (MSE) of the estimator is lower bounded as [18]

$$\mathbb{E}_{\boldsymbol{y}|\boldsymbol{\eta}_\theta}\{(\boldsymbol{\eta}_\theta - \hat{\boldsymbol{\eta}}_\theta)(\boldsymbol{\eta}_\theta - \hat{\boldsymbol{\eta}}_\theta)^T\} \geq \boldsymbol{CRLB}_\theta = \boldsymbol{J}_{\theta,\theta}^{-1}, \tag{3.10}$$

where $\boldsymbol{J}$ is FIM and is defined as [18]

$$\boldsymbol{J}_{\theta,\theta} = \mathbb{E}_{\boldsymbol{y}|\boldsymbol{\eta}_\theta}[-\frac{\partial^2 \ln f(\boldsymbol{y}|\boldsymbol{\eta}_\theta)}{\partial \boldsymbol{\eta}_\theta \partial \boldsymbol{\eta}_\theta^T}] = \mathbb{E}_{\boldsymbol{h}|\boldsymbol{\eta}_\theta}\{\mathbb{E}_{\boldsymbol{n}|\boldsymbol{\eta}_\theta}[-\frac{\partial^2 \ln f(\boldsymbol{y}|\boldsymbol{\eta}_\theta)}{\partial \boldsymbol{\eta}_\theta \partial \boldsymbol{\eta}_\theta^T}]\}, \tag{3.11}$$

where $f(\boldsymbol{y}|\boldsymbol{\eta})$ is the likelihood function of the received signal. From [18] (page 525 and proof on page 563)

$$\mathbb{E}_{\boldsymbol{n}|\boldsymbol{\eta}_\theta}[-\frac{\partial^2 \ln f(\boldsymbol{y}|\boldsymbol{\eta}_\theta)}{\partial \boldsymbol{\eta}_\theta \partial \boldsymbol{\eta}_\theta^T}] = \frac{2}{\sigma_n^2}\mathcal{R}e[(\frac{\partial \boldsymbol{w}}{\partial \boldsymbol{\eta}_\theta})^H \frac{\partial \boldsymbol{w}}{\partial \boldsymbol{\eta}_\theta}], \tag{3.12}$$

where

$$\boldsymbol{w} \triangleq \boldsymbol{G}\boldsymbol{s} = \frac{1}{\sqrt{M}} \begin{bmatrix} \sum_{i=1}^{K} h_{1,i} s_i l(r_i) \\ \sum_{i=1}^{K} h_{2,i} s_i l(r_i) e^{-j\beta\cos(\theta_i)} \\ \vdots \\ \sum_{i=1}^{K} h_{M,i} s_i l(r_i) e^{-j(M-1)\beta\cos(\theta_i)} \end{bmatrix}. \tag{3.13}$$

By taking derivative w.r.t θ, we have

$$(\frac{\partial \boldsymbol{w}}{\partial \boldsymbol{\eta}_\theta})_{m,k} = \boldsymbol{X}_{m,k} = \frac{j\beta(m-1)\sin(\theta_k) h_{m,k} s_k l(r_k) e^{-j(m-1)\beta\cos(\theta_k)}}{\sqrt{M}}. \tag{3.14}$$

for $m \in \{1, 2, \ldots, M\}$ and $k \in \{1, 2, \ldots, K\}$. So, using Eq. 3.10, $\boldsymbol{CRLB}_\theta$ will be

$$\boldsymbol{CRLB}_\theta = \boldsymbol{J}_{\theta,\theta}^{-1} = \frac{\sigma_n^2}{2} (\mathbb{E}_{\boldsymbol{h}|\boldsymbol{\eta}_\theta} \{\mathcal{R}e(\boldsymbol{X}^H \boldsymbol{X})\})^{-1}. \tag{3.15}$$

Using the following lemmas from the random matrix theory, we prove that for any distribution of $\boldsymbol{H}$, $\boldsymbol{CRLB}_\theta$ almost surely converges toward a deterministic closed-form expression that is a function of system parameters, such as the number of antennas and variance of channel coefficients.

Lemma 1. *Let $\boldsymbol{\Sigma} \in \mathbb{C}^{N\times N}$, be a matrix with uniformly bounded spectral norm. Let $\boldsymbol{x} \in \mathbb{C}^N$, be a random vector with i.i.d. entries of zero mean, variance $\frac{1}{N}$ and eighth order moment of order $O(\frac{1}{N^4})$, independent of $\boldsymbol{\Sigma}$. Then*

$$\boldsymbol{x}^H \boldsymbol{\Sigma} \boldsymbol{x} - \frac{1}{N} tr(\boldsymbol{\Sigma}) \xrightarrow{a.s.} 0, \tag{3.16}$$

as $N \to \infty$.

Proof. See [44]. □

Lemma 2. *For $\boldsymbol{\Sigma} \in \mathbb{C}^{N\times N}$, be a matrix with uniformly bounded spectral norm, $\boldsymbol{x}$ and $\boldsymbol{y}$ two vectors of i.i.d. variables such that $\boldsymbol{x} \in \mathbb{C}^N$*

and $\boldsymbol{y} \in \mathbb{C}^N$ *have zero mean, variance* $\frac{1}{N}$ *and fourth order moment of order* $O(\frac{1}{N^2})$*, we have*

$$\boldsymbol{x}^H \boldsymbol{\Sigma} \boldsymbol{y} \xrightarrow{a.s.} 0. \tag{3.17}$$

Proof. See [44]. □

Lemma 3. *For large* M*, when* $\cos(\theta_1) \neq \cos(\theta_2)$*, for* $\boldsymbol{\Sigma} = diag(\frac{1}{M^2}, \frac{4}{M^2}, \ldots, 1)$*, we have*

$$\mathcal{R}e\{\boldsymbol{a}_{Rx}(\theta_1)^H \boldsymbol{\Sigma} \boldsymbol{a}_{Rx}(\theta_2)\} \xrightarrow{a.s.} 0. \tag{3.18}$$

Proof. See Appendix A. □

Using these lemmas and independence of the channel distribution from the number of antennas at the BS, the following theorem gives the deterministic expression for $\boldsymbol{CRLB}_\theta$.

Theorem 1. *In a massive MIMO system with large number of antennas,* $\boldsymbol{CRLB}_\theta$ *converges toward a deterministic form as*

$$\boldsymbol{CRLB}_\theta \xrightarrow{a.s.} \frac{3}{\beta^2(M-1)(2M-1)} \boldsymbol{S}, \tag{3.19}$$

in which $\boldsymbol{S}$ *is an* $K \times K$ *diagonal matrix with*

$$\boldsymbol{S}_{k,k} = ((|h_{d_k}|^2 + 2\sigma_h^2)\rho_k \sin^2(\theta_k))^{-1}, \quad k \in \{1, \ldots, K\}. \tag{3.20}$$

Proof. See Appendix B. □

It is seen from Eq. 3.19 that in a massive MIMO system, regardless of channel distribution, instantaneous $CRLB$ tends toward a deterministic value. Although other definitions like Miller-Chang version [34] or $MCRLB$ [35] obtain a deterministic form for $CRLB$, they use expectation that requires the knowledge of channel coefficients' distribution. By contrast, our obtained expression requires only the knowledge of channel coefficients' variance and is applicable even when the distribution of channel coefficients is unknown.

$CRLB$ in a MU massive MIMO system is inversely related to the second-order of the number of antennas that is in accordance with previous analysis of these systems in [10, 27]. When the number of antennas is large enough, the effects of the multipath signals that accompany the dominant path signal are in terms of general channel statistics instead of their individual realization, allowing designers to understand the amount of information they can recover from the channel. Also, the σ_h^2 term in Eq. 3.19 prevents $CRLB$ from growing indefinitely when the dominant path-signal is in poor condition. This is because as the number of antennas grows, it is almost surely improbable that all antennas be in poor condition simultaneously. So, even if few antennas have a low fading coefficient, not all of the information in the system is lost, and AoA can still be extracted. The same phenomenon also happens for channel capacity in these systems [13].

Several works have recently attempted to use multipath signals with different channel coefficients to improve their estimation accuracy, such as [12, 20, 37]. One of the main uses of multipath signals is in Fingerprinting localization method [45]. In this method, the area in which localization will be done is divided into separate subsections. Each subsection is distinguished from others based on the channel that BS sees from that subsection. Here, if the path-loss signals are considered, subsections can be sharply distinguished from one another. Moreover, by considering the multipath signals in [36] authors extracted location information (including AoA) with weak dominant path signal, using neural networks. In [14] authors presented a method to extract AoA in i.i.d. Rician channels. These works are examples of how the multipath signals can be used to extract or refine the AoA information. Our results are in accordance with these works and provide the theoretical background that $CRLB$ in such scenarios is finite, and estimating AoA is possible.

In the rest of the section, we focus on the system's energy efficiency in the AoA estimation part and how the utilization of antennas can affect the efficiency. This is important when one wants to use a subset of total available antennas for AoA estimation.

3.4 Localization Efficiency

In this section, we formulate LE function, which will aggregate the benefits and costs of a localization method. To make a general criterion for different kinds of localization, we use parameters that are included in most of the localization methods. On the one hand, these parameters are the number of simultaneously localized UTs and the method's localization accuracy as benefit parameters. On the other hand, the system's total energy consumption in the localization phase is a cost parameter.

3.4.1 Accuracy Function

Accuracy is one of the major evaluation parameters in localization [46, 47]. Different works have studied the accuracy function of localization methods and optimized it w.r.t. various parameters. Generally, accuracy is defined as the trace of the inverse of equivalent FIM [46, 48], or as the inverse of square root, the trace of the $CRLB$ matrix [47]. Although it is possible to use other definitions of $CRLB$ like those in [34] and [35], in the LE function, as we have achieved a deterministic expression for $CRLB$, we use the inverse of the square root of its trace for the accuracy function

$$Accuracy = \frac{1}{\sqrt{tr(\boldsymbol{CRLB}_{\theta})}}. \tag{3.21}$$

3.4.2 Energy Consumption

Nowadays, one of the critical parameters of a wireless system is energy consumption [13]. Due to growing concerns about energy, designers have to carefully consider their systems' energy consumption and include it in system characterization. Analyzing the energy consumption of a system indicates at what cost a performance is obtained. For example, wireless systems' energy efficiency has been widely used to describe performance trade-off between rate and energy consumption [13, 19].

In order to conduct a comprehensive investigation, it is of paramount importance to consider the energy consumption of all parts of a wireless system. In addition to transmitted power, in a massive MIMO system, the energy consumption of system hardware should also be considered to obtain a comprehensive model [13]. For instance, the energy consumption of antennas' RF-chains and processing units that scale with the number of antennas is not negligible in massive MIMO systems. In the following, we investigate different parts of the total energy consumption function according to our system model.

Transmitted Energy

In the uplink of a wireless system, UTs transmit pilots to become localized by the BS. Usually, this energy is vital as UTs have a limited energy budget. Pilot signals are predefined with a certain energy. This energy is linearly related to the number of UTs. Therefore, transmitted energy of all K UTs (in Joules) will be

$$E_{tr} = \zeta W \frac{tr(\boldsymbol{s}\boldsymbol{s}^H)}{\omega} = \frac{W\zeta}{\omega} \sum_{i=1}^{K} |s_i|^2 \ \ (J), \tag{3.22}$$

in which ζ and W are duration and bandwidth of transmitted pilots, respectively, and $\omega \in (0, 1]$ is UT's RF amplifier efficiency (and it is constant during pilot transmission time) [38].

Processing Energy

We assume that the BS carries out all of the required processing. As far as LE is concerned, these processes include the detection of pilots and running localization algorithm. This energy is proportional to the number of operations, which in turn is a function of system parameters such as M and K. To evaluate this part's energy consumption, one needs to calculate the number of required operations of an algorithm and the computational efficiency of BS processing hardware. Generally, Maximum-likelihood (ML) method that obtains $CRLB$ has the calculation complexity of K^M [49]. This is the worst case, and there may be ways to reduce the number of required calculations. Sub-optimum algorithms have M^3 order of complexity, at most, but they do not necessarily obtain $CRLB$. We study one of these algorithms in section 3.6. Hardware computational efficiency, $L_{BS}(FLOP/J)$, is usually expressed as the number of Floating Point Operations (FLOP) per Second per Watt that hardware consumes [13]. So, assuming the same time as pilot transmission is used for processing, the processing energy consumption, E_p, for ML will be formulated as

$$E_p = \frac{K^M}{L_{BS}} W\zeta \quad (J). \tag{3.23}$$

Hardware Energy Consumption

Generally, the hardware of a wireless system can be divided into two parts:

- Infrastructure part of a system that includes backhaul systems and network part, static circuit energy consumption and so on, which use constant energy and are necessary for system maintenance. Energy consumption of this part is independent from the number of antennas at the BS but may depend on the number of UTs [38].
- RF-chains of BS and UTs' antennas that are proportional to the number of BS antennas and number of UTs.

Therefore, hardware energy consumption, E_h will be

$$E_h = \zeta(MP_{BS} + KP_{UT} + P_{fix}) \quad (J), \tag{3.24}$$

where P_{BS} and P_{UT} are the power consumption of the hardware of each antenna (like RF-chains) in BS and UTs, respectively, and P_{fix} accounts for all powers that are not related to M (however, it can be depend on K).

Therefore, total energy consumption will be

$$E_t = E_{tr} + E_p + E_h. \tag{3.25}$$

Finally we can formulate LE as

$$LE = \frac{K(Accuracy)}{EnergyConsumption} = \frac{K}{(E_t)(\sqrt{tr(\boldsymbol{CRLB_\theta})})}. \tag{3.26}$$

Replacing all equations by their formula, LE will be obtained as

$$LE = \frac{1}{\sqrt{3}\zeta\sqrt{tr(\boldsymbol{S})}} \times \frac{K\sqrt{\beta^2(M-1)(2M-1)}}{(\frac{W}{L_{BS}}K^M + MP_{BS} + KW\sum_{i=1}^{K}\|s_i\|^2 + KP_{UT} + P_{fix})}. \tag{3.27}$$

Eq. 3.27 indicates that how many degrees of accuracy is achieved for every joule that is consumed. So, for example, $LE = 1$ means that for one joule of energy consumption the lowest obtained error is one radian. In this equation, LE is a function of several system parameters, such as M, K, and θ. Although designers usually cannot control some parameters such as UT's AoA or their number, they do have access to the number of BS antennas. As LE reflects a trade-off between accuracy and energy consumption, this creates an opportunity that can be used to design a system that operates at the optimal point of this trade-off. For example, a common scenario that happens in reality is that number of UTs varies drastically at different times, and it is not necessarily efficient to use all of the antennas for any number of UTs. In this case, to maximize LE, BS should use a portion of the total available antennas. It should also be noted that as studying power consumption (instead of energy consumption) is also very important for certain applications in wireless systems, like beamforming and precoding [50], one can modify the LE function in Eq. 3.27 to a function that reflects efficiency in watts (instead of Jouls) by simply removing the parameter that accounts for the time that is allocated to the localization. To do this, one needs to remove ζ from Eq. 3.27.

In order to optimize Eq. 3.27 w.r.t. the number of antennas, first, the method that will select the utilized antennas should be devised. This is because how the antennas are selected changes the formulation of LE and consequently changes the optimal number of antennas. Next, with the help of the new formulation of LE when optimal antenna selection is employed, we optimize the number of utilized antennas.

3.5 Antenna selection

In this section, we analyze the effect of antenna selection in a massive MIMO system for localization. When the number of utilized antennas is smaller than total available antennas, e.g., due to LE optimization or fewer available RF-chains, there is an opportunity that if a specific set of antennas are deployed, LE can be improved even more. Energy consumption of the system in Eq. 3.25 is a function of the number of antennas and is independent from which antennas are being used. On the other hand, in addition to the number of antennas, $\boldsymbol{CRLB_\theta}$ is a function of the set of antennas that are being used. To show this, we recall Eq. B.24 that states $\boldsymbol{CRLB_\theta}$ is inversely proportional to $tr(\mathbf{\Sigma})$. Assuming optimal number of antennas (or available RF-chains) is F, to minimize $\boldsymbol{CRLB_\theta}$, $tr(\mathbf{\Sigma})$ has to be maximized by choosing a subset of utilized antennas $\mathcal{S}$. It should be noted that in this case, the $\frac{1}{M}$ and $\frac{1}{M^2}$ coefficients in Eq. B.1 and Eq. B.3, are changed to $\frac{1}{F}$ and $\frac{1}{F^2}$, respectively. So, we have

$$\begin{aligned} &\max_{\mathcal{S}\subset\{1,\ldots,M\}} \sum_{x\in\mathcal{S}} \frac{(x-1)^2}{F^2} \\ &s.t.\ \ Card(\mathcal{S}) = F. \end{aligned} \tag{3.28}$$

Optimal solution for this problem consists of the last F antennas

$$\mathcal{S}^* = \{(M-F), \ldots, M-1\}, \tag{3.29}$$

that results in the maximum value for the trace as

$$\sum_{x=M-F}^{M-1} \frac{x^2}{F^2} = \frac{6M(M-F-1)+(F+1)(2F+1)}{6F}. \tag{3.30}$$

and minimum $\boldsymbol{CRLB_\theta}$ for $\mathcal{S}^*$ as

$$\boldsymbol{CRLB}_\theta^* \xrightarrow{a.s.} \frac{3}{\beta^2(6M(M-F-1)+(F+1)(2F+1))}\boldsymbol{S}. \tag{3.31}$$

The interpretation of Eq. 3.29 is that if for any reason fewer antennas than available antennas should be used, the optimal choice is to start selecting antennas from the furthest antenna w.r.t. the reference point (whose location is fixed at the top of the antenna array) and move toward it. We recall this set of antennas as the *furthest set*. With this approach, $\boldsymbol{CRLB_\theta}$ will be dramatically reduced relative to the case when we choose antennas from the beginning of the array. For comparison, we write $\boldsymbol{CRLB_\theta}$ when F first antennas (*first set*) are used

$$\boldsymbol{CRLB}_\theta \xrightarrow{a.s.} \frac{3}{\beta^2(F-1)(2F-1)}\boldsymbol{S}. \tag{3.32}$$

It can be seen from Eq. 3.31 and Eq. 3.32 that while $\boldsymbol{CRLB_\theta}$ for the first set is only a function of F, it is a function of both F and M for the furthest set and, increasing total number of available antennas is always beneficial when the furthest antenna selection is applied. In other words, the first set antenna selection approach does not fully appreciate the presence of a large antenna array. Furthermore, $\boldsymbol{CRLB_\theta}$ for the first set is a *decreasing* function of F, however, $\boldsymbol{CRLB}_\theta^*$ of the furthest set will be an *increasing* function of F. The reason for this phenomenon lies within the $M^{-\frac{1}{2}}$ normalization factor in Eq. 3.5 (which becomes $F^{-\frac{1}{2}}$ in the antenna selection scenario) that finally results in the normalization of $tr(\boldsymbol{\Sigma})$. When we start adding antennas from the end of the array, we start from an antenna with the largest contribution to the trace, 1, and minimum normalization cost, 1. Then, a smaller value is added, but as the summation is normalized by the cardinality of the set, it will decrease because for any $1 \leq i \leq F$,

$$1 > \frac{1 + (1 - i/F^2)^2}{2}. \tag{3.33}$$

Therefore, the denominator of $\boldsymbol{CRLB}_\theta$ decreases, and in turn, $\boldsymbol{CRLB}_\theta$ increases. This process is reversed for the first set of antennas. In this case, we start from an antenna with the lowest contribution to the trace and add higher values as we use more antennas. So, the normalized summation is increasing because for any $1 \leq i \leq F$,

$$\frac{1}{F^2} < \frac{1 + (1 + i)^2}{2F^2}. \tag{3.34}$$

Moreover, the physical explanation of this antenna selection strategy can further clarify the behavior of its $\boldsymbol{CRLB}_\theta$. The further an antenna is from the reference point, the more its received signal differs from the signal received in the reference point. This is because it travels through a longer path and has more time to differ from the reference point's signal. On the other hand, due to the $F^{-\frac{1}{2}}$ normalization factor, the total collected power of the system is normalized with the number of utilized antennas. From $\boldsymbol{CRLB}_\theta$ point of view, the system prefers to collect all of the power from the antennas, which provides the maximum possible difference from the reference point. Therefore, when antennas are selected from the end of the array, the system collects its normalized received power from antennas that provide the maximum possible difference with the signal received by the reference point. Furthermore, adding more antennas with this strategy means using more antennas that are relatively closer to the reference point than the last antenna. So, some of the power is collected from the antennas with relatively less difference (due to their shorter path) compared to the last antenna. This explains why the system's performance, in terms of $\boldsymbol{CRLB}_\theta$, degrades when more antennas are selected if the received power is normalized.

If we omit the normalization factor, $\boldsymbol{CRLB}^*_\theta$ will be a decreasing function of F, just with a different slope of $\boldsymbol{CRLB}_\theta$. In other words, this antenna selection strategy reduces the slope of the $CRLB$ decrease but also reduces its initial value significantly. The decrement in the initial point is large enough that for any $F < M$, from Eq. 3.31 and Eq. 3.32, it is evident that $\boldsymbol{CRLB}^*_\theta < \boldsymbol{CRLB}_\theta$, proving that selecting antennas from the furthest set is always beneficial.

So, depending on the method that we select operating antennas, both $CRLB$'s formula and behavior w.r.t. the number of utilized and all available antennas is changed. In this regard, using a set of antennas that are furthest from the reference point minimizes $CRLB$.

If F furthest antennas in the array are selected for localization, LE's formula will change to

$$\begin{aligned} LE_S = & \frac{1}{\sqrt{3}\zeta\sqrt{tr(\boldsymbol{S})}} \\ & \times \frac{K\sqrt{\beta^2(6M(M-F-1)+(F+1)(2F+1))}}{(\frac{W}{L_{BS}}K^F + FP_{BS} + KW\sum_{i=1}^{K}\|s_i\|^2 + KP_{UT} + P_{fix})}. \end{aligned} \tag{3.35}$$

Now that the formula of LE is obtained according to the optimal antenna selection strategy, the following theorem gives the optimal number of antennas when this selection strategy is used.

Theorem 2. *When operating antennas are selected from the furthest set, optimal number of them is*

$$F^* = K + 1. \tag{3.36}$$

Proof. Eq. 3.25 and Eq. 3.31 show that both E_t and $CRLB$ are increasing functions of F. So, maximum value of LE in Eq. 3.35 happens for the minimum possible value of F that is $K + 1$. □

Remark 3. *It should be noted that the furthest antenna selection strategy is optimal as long as the steering vector can be modeled as Eq.3.5. In this equation, it is assumed that the array size is much* *smaller than the distance of UTs from it, so the difference in power of arrival is negligible. When the array becomes too large w.r.t the distance of the UTs from it, the difference in power may be so large that it affects antennas' contribution in different distances from the reference point. Also, for large size arrays, the incident wave cannot be modeled as a plane. So, the proposed antenna selection is optimal as long as the distance from the reference point to the last antenna at the BS is much smaller than the distance of UTs from the BS, and Eq. 3.5 models the steering vector.*

In order to show if (and how) the optimal antenna selection procedure may change if the power normalization in Eq.3.5 is not applied, we study the $\boldsymbol{CRLB_\theta}$ without power normalization. If the $\frac{1}{\sqrt{M}}$ is removed from Eq.3.5, following Eq.3.14, the formulation of $\boldsymbol{CRLB_\theta}$ will change into

$$\boldsymbol{CRLB_\theta} \xrightarrow{a.s.} \frac{3}{\beta^2 M(M-1)(2M-1)}\boldsymbol{S}, \tag{3.37}$$

Considering the fact that the antenna selection optimization problem is how to select the antennas that $tr(\boldsymbol{\Sigma})$ is maximized, removing the $\frac{1}{\sqrt{F}}$ from Eq.3.28 will not change the optimization process and the antenna selection will not change. Moreover, to show if the power normalization will affect the optimal number of antennas, we should analyze the behavior of $\boldsymbol{CRLB_\theta}$ without power normalization. By noting that antenna selection process will not change, without a normalization of power we have

$$\boldsymbol{CRLB^*_{\theta P}} \xrightarrow{a.s.} \frac{3}{\beta^2 F(6M(M-F-1)+(F+1)(2F+1))}\boldsymbol{S}. \tag{3.38}$$

By taking derivative from the $\boldsymbol{CRLB^*_{\theta P}}$ w.r.t. F we have

$$\frac{\partial}{\partial F}\boldsymbol{CRLB^*_{\theta P}} = \frac{3\boldsymbol{S}}{\beta^2}.\frac{-6F^2+(12M-6)F+6M-1}{(F(6M(M-F-1)+(F+1)(2F+1)))^2}. \tag{3.39}$$

As only the nominator of the second fraction will determine the sign of the derivative, we check the zeros of the nominator for F. The zeros of the $-6F^2 + (12M-6)F + 6M - 1$ will be

$$x_{1,2} = \frac{6(2M-1) \pm \sqrt{12(12M^2+1)}}{12} = M - \frac{1}{2} \pm \frac{\sqrt{12(M^2+1)}}{\sqrt{12}}. \quad (3.40)$$

As $\frac{\sqrt{12(M^2+1)}}{\sqrt{12}} > M$, it is seen that smaller zero of $-6F^2 + (12M - 6)F + 6M - 1$ will be negative value and the larger zero of it will be bigger than M. By noting that $-6F^2 + (12M-6)F + 6M - 1$ will have the negative sign of the F^2 multiplier between its zeros, we can deduct that for $0 < F < M$ the derivative of $\boldsymbol{CRLB_\theta}$ will always be positive, meaning that $\boldsymbol{CRLB_\theta}$ will be an increasing function of F. Hence, not normalizing power will not change the optimal number of antennas in Theorem2.

When the effects of the multipath signals are ignored, i.e., $\sigma_h^2 \to 0$, it is seen that $\boldsymbol{CRLB_\theta}$ is still proportional with the inverse of $tr(\boldsymbol{\Sigma})$, which means our results for antenna selection are applicable for this setting, too. Therefore, no matter what the channel model is, by using the proposed antenna selection method, $\boldsymbol{CRLB_\theta}$ can be minimized, and LE can be further improved. The following section presents a case study of how the LE can be formulated for an estimation algorithm.

Remark 4. *The proposed antenna selection strategy remains optimal when the central element of the array is chosen as the reference point. While the choice of the reference antenna can influence the numerical value of the resulting CRLB, the selection criterion itself is not dependent on the absolute values but rather on the functional behavior of the CRLB. Consequently, changing the reference point only affects the lower and upper bounds of the summation in* (B.25)*. However, the fundamental property of the selection process remains unchanged: the antennas located furthest from the reference point always maximize the summation, and therefore, the optimality of the strategy is preserved regardless of the chosen reference.*

3.6 MUSIC Algorithm

The proposed antenna selection in the previous section is a $CRLB$ based antenna selection that creates a higher upper bound for the LE of any estimator. In other words, proposed antenna selection creates a better situation for estimating the AoA. Depending on its procedure, an estimator takes advantage of this better situation at a certain level. To present a heuristic showcase of such a procedure and an example of how the LE can be formulated for any estimator, we study the LE of one of the most known algorithms for AoA estimation, MUSIC, which is used in several applications [51]. After a brief description of its procedure, we calculate the exact amount of calculations required by this algorithm and formulate its LE. Then in section 3.7, we apply the proposed antenna selection to the MUSIC and illustrate the corresponding improvement in LE.

3.6.1 Procedure

Consider that we have a received signal as

$$\boldsymbol{y}_F = \boldsymbol{A}_F \boldsymbol{s} + \boldsymbol{n}_F, \tag{3.41}$$

subscript F shows number of rows, as F antennas are deployed. Sample covariance matrix of this signal can be obtained as [51]

$$\tilde{\boldsymbol{R}}_y = \frac{1}{N}\sum_{i=1}^{N} \boldsymbol{y}_{F_i}\boldsymbol{y}_{F_i}^H. \tag{3.42}$$

In the Eigenvalue Decomposition (EVD) of $\tilde{\boldsymbol{R}}_y$, there will be K eigenvectors corresponding to K UTs and $F-K$ eigenvectors corresponding to the noise. Each noise eigenvector is orthogonal to the columns of $\boldsymbol{A}$. So, by forming $\boldsymbol{E}_n$, composed of noise eigenvectors,

$$\boldsymbol{E}_n = [\boldsymbol{v}_{K+1} \quad \boldsymbol{v}_{K+2} \quad \dots \quad \boldsymbol{v}_F], \tag{3.43}$$

we can form a spatial spectrum function as [51]

$$P(\theta_i) = \frac{1}{\boldsymbol{g}(\theta_i)^H \boldsymbol{E}_n \boldsymbol{E}_n^H \boldsymbol{g}(\theta_i)}, \tag{3.44}$$

in which $\boldsymbol{g}$ is a subset of $\boldsymbol{a}_{Rx,k}$ for the antenna subset that is being used, e.g., if the furthest set of antennas is used it will be

$$\begin{aligned} \boldsymbol{g}(\theta_i) &= \frac{1}{\sqrt{F}}[e^{-j(M-F)\beta\cos(\theta_i)} \quad \ldots \quad e^{-j(M-1)\beta\cos(\theta_i)}]^T, \\ \theta_i &\in [0, \frac{\pi}{Q}, \ldots, \frac{\pi-1}{Q}], \end{aligned} \tag{3.45}$$

where Q is search cardinality. Peaks of $P(\theta)$ happens when $\boldsymbol{g}(\theta)$ corresponds to one of the actual steering vectors. These peaks are estimated as AoAs. Therefore, steps of MUSIC are

i) Observe N snapshots and construct $\tilde{\boldsymbol{R}}_y$ in Eq. 3.42.

ii) Calculate the EVD of $\tilde{\boldsymbol{R}}_y$ and extract $\boldsymbol{E}_n$ in Eq. 3.43.

iii) Construct $P(\theta)$ and extract its maximum points.

3.6.2 Energy Consumption of MUSIC

To accurately determine the required energy consumption of the MUSIC algorithm, we first analyze the number of its required operations. With the help of [52], we evaluate the number of required arithmetic operations to run MUSIC.

In the first step, the algorithm multiplies an $F \times 1$ vector by its conjugate transpose N times, sum them, and then divides all of its elements by N. Every product of the vectors requires F^2 operations, every matrix sum requires F^2 operations, and the final divide needs F^2 operations [52]. So, the first step needs $(2N+1)F^2$ operations.

Generally, EVD of an $F \times F$ matrix by QR decomposition-based algorithm needs at least F^3 operations [52]. So, the second step demands F^3 operations.

In the last step, ignoring the search part, we need to calculate Eq. 3.44, Q times. Product of $\boldsymbol{E}_n\boldsymbol{E}_n^H$ needs $F^2(2(F-K)-1)$ operations and then, multiplying the resulted $F \times F$ matrix by two $F \times 1$ vectors from both sides, needs $(2F-1)(F+1)$ operations. Therefore, third step requires $Q[2F^2(F-K)+F^2+F-1]$ operations.

So, the total number of arithmetic operations of MUSIC is

$$N_A = (2Q+1)F^3 + (2N + Q(1-2K)+1)F^2 + QF - Q. \tag{3.46}$$

Consequently, processing energy consumption of MUSIC will be

$$E_p = \frac{N_A}{L_{BS}} W\zeta. \tag{3.47}$$

Considering same transmitted power for all UTs, p, E_{tr} is

$$E_{tr} = \frac{NW\zeta tr(\boldsymbol{s}\boldsymbol{s}^H)}{\omega} = \frac{NKW\zeta p}{\omega}. \tag{3.48}$$

Hardware energy consumption will be same as Eq. 3.24. Therefore, total energy consumption of localization process using MUSIC algorithm is

$$\begin{aligned} E_t = E_t + E_{tr} + E_h = \underbrace{W\zeta(\frac{2Q+1}{L_{BS}})}_{C_3} F^3 \\ + \underbrace{W\zeta(\frac{2N+1+Q(1-2K)}{L_{BS}})}_{C_2} F^2 + \underbrace{W\zeta(P_{BS} + \frac{Q}{L_{BS}})}_{C_1} F \\ + \underbrace{W\zeta(NKp - \frac{Q}{L_{BS}} + KP_{UT} + P_{fix})}_{C_0} = \sum_{i=0}^{3} C_i F^i. \end{aligned} \tag{3.49}$$

Table 3.1: Simulation parameters

Parameter	**Value**
Bandwidth: W	$50KHz$
Pilot transmission time: ζ	$0.5(ms)$
Noise variance: σ_n^2	$10^{-20}(W/Hz)$
RF amplifier efficiency: ω	0.9
Received pilot power: p	$10^{-19}(W/Hz)$
Operational efficiency: L_{BS}	$30(GFLOP/Joule)$
BS's RF-chain Power consumption: P_{BS}	$1W$
UT's RF-chain Power consumption: P_{UT}	$0.3W$
Fixed power consumption in BS: P_{fix}	$0.5W$
Antenna separation ratio to wavelength: $\frac{d}{\lambda}$	0.5

MSE of the MUSIC algorithm is defined as

$$MSE = \frac{1}{N_{MC}} \sum_{i=1}^{N_{MC}} \sum_{k=1}^{K} (\theta_k - \hat{\theta}_k)^2, \tag{3.50}$$

where N_{MC} is number of Monte-Carlo simulations of MUSIC algorithm.

Finally, we formulate the LE as

$$LE_{MUSIC} = \frac{K}{(E_t)(\sqrt{MSE})}. \tag{3.51}$$

In the next section, the MUSIC algorithm's LE is optimized w.r.t. F, and its behavior when these F antennas are selected from the first and furthest set is illustrated.

3.7 Numerical Results

In this section, we verify our analytical results that are obtained in previous sections. We study the behavior of LE function for different scenarios, using Monte-Carlo simulations when analytical traceability

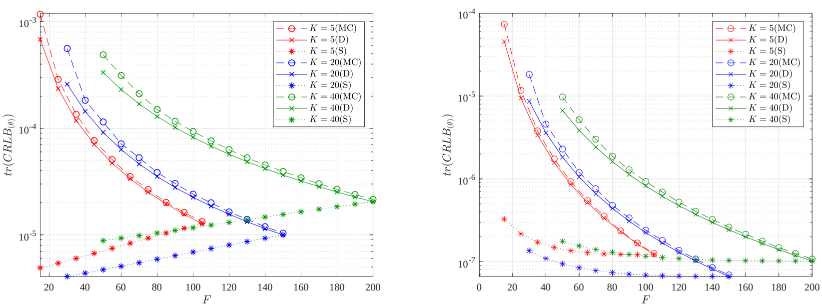

(a) With power normalization. **(b)** Without power normalization.

Figure 3.2: Deterministic and Monte-Carlo simulations of $CRLB_\theta$.

is not possible. In the Monte-Carlo simulations, the random sampling is done over the fast fading channel coefficient between UTs and BS antennas (Eq.3.6). Parameters that we use are listed in Table 3.1, unless otherwise stated.

Fig. 3.2a shows $tr(\boldsymbol{CRLB_\theta})$ in which dashed lines are generated by Monte-Carlo simulations (indicated by MC) while solid lines are computed using deterministic expression in Eq. 3.32 for $K = 5, 20, 40$. For $K = 5$ simulation is done under $\kappa - \mu$ fading model [53]. We used $\kappa = 3$ that indicates the ratio between the total power of the dominant path to the total power of multipath signals, $\mu = 2$ and it is assumed that the dominant component appears in the in-phase [53]. For $K = 20$ we used Nakagami-m fading model with shape parameter $\mu = 2$ and spread parameter $\Omega = 4$. Also, $K = 40$ is simulated in the Rician fading model with a mean equal to 1 and variance of each real and imaginary part $\sigma_h^2 = 0.5$. As $CRLB_\theta$ grows indefinitely when $\theta \to 0$, π, an area of $\frac{\pi}{10}$ from each side is excluded, and UTs' AoAs are placed in equispaced intervals in the remaining area, i.e. $AoA_k = \frac{\pi}{10} + \frac{\pi - \frac{2\pi}{10}}{K}$ for $k = \{1, \ldots, K\}$. Interestingly, deterministic approximation (indicated by D) converges very fast, even when the

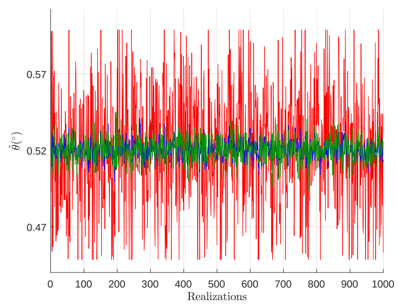

(a) Output of ML estimator in different realizations for various selected antenna sets.

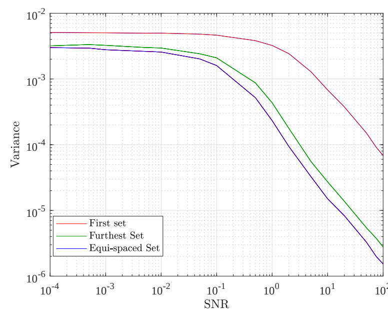

(b) Variance of ML estimator with various selected antenna sets.

Figure 3.3: ML estimation for a single UT with $M = 21$.

number of antennas is not so large. We observe that convergence happens for all of the simulated models, confirming that the deterministic formula is valid for any channel distribution. Also, Eq. 3.32 has the same behavior as Monte-Carlo simulations. It should be noted that as the trace of $\boldsymbol{CRLB_\theta}$ is plotted, the distance between analytical expression and Monte-Carlo simulations will increase for the higher number of UTs since it is the sum of K almost sure convergence. This is why there is a seeming increment between analytical and Monte-Carlo curves in this figure. Furthermore, deterministic $CRLB_\theta$ in Eq.3.31, is plotted (indicated by S) when $M = 100, 155, 205$ for corresponding $K = 5, 20, 40$ curves. We see a significant decrease in $CRLB_\theta$ when the furthest set of antennas is used relative to the case when the first group of them is used, more than two orders of magnitude in some cases. As the number of utilized antennas grows, $CRLB_\theta$ for the furthest set grows and becomes closer to the first set curve until all available antennas are used, when they become the same. The larger the M, the lower the $CRLB_\theta$ will become for the furthest set. Furthermore, Fig. 3.2b presents the $tr(\boldsymbol{CRLB_\theta})$ under the same conditions as in Fig. 3.2a, but this time without applying the power normalization defined in Eq. 3.5. In this case, the expression in Eq. 3.37 is used for computing $CRLB_{\theta}$. The figure indicates that without power normalization, all curves have a steeper descent, due to the higher received SNR. An important observation is related to the furthest antenna selection method: in this case, $tr(\boldsymbol{CRLB}_{\theta})$ begins with considerably lower initial values. However, as additional antennas are selected closer to the reference antenna, the rate of decrease becomes progressively smaller.

In Fig. 3.3, the ML estimator is applied to estimate the AoA of a single UT using different antenna selection strategies. Three strategies are considered: (i) the closest set, which selects antennas nearest to the reference point; (ii) the furthest set, based on the proposed antenna selection method; and (iii) the equi-spaced set, where antennas are chosen at equal spacing along the array. In this example, the array size is $M = 21$, the number of selected antennas is $F = 5$, and the UT's AoA is $\theta = \frac{\pi}{6}$.

As shown in Fig.3.3a, the proposed furthest set achieves significantly lower estimation variance compared to the closest set, thereby demonstrating its superior performance. The equi-spaced set also performs better than the closest set, though it consistently exhibits a higher variance than the furthest set. This behavior is further highlighted in Fig.3.3b, where the estimation variance of the ML estimator is plotted against different SNR values. Across all SNR regimes, the proposed furthest selection maintains the lowest variance, consistently outperforming the other two strategies.

In Fig. 3.4 LE for different numbers of UTs is plotted. In this figure, the left side axis is for LE scale, and solid lines are its corresponding curves. The right side axis is for the $tr(CRLB_{\theta})$, and dashed lines are its corresponding curves. For each scenario, the same colors are used. In this figure, $M = 80$ and for the green curves (Eq. 3.27), in each K, all of the available antennas are used, i.e., no antenna selection. We see that due to high computational complexity, LE drops sharply as K increases. In other two curves (blue for Eq. 3.35 and red

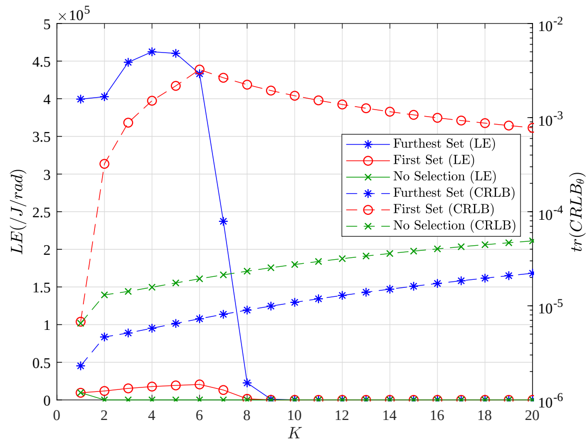

Figure 3.4: Optimal LE for each corresponding K in ML estimation.

for replacing M with F in Eq. 3.27), for each K, LE is maximized w.r.t. F, with constraint $F \geq K$. We see that LE is significantly improved when the optimal number of antennas is used instead of all available antennas. This confirms that using all of the antennas is not always efficient. Moreover, when the optimal number of antennas is selected from the furthest set, LE increases even further, up to 220% in some points, highlighting the advantage of the proposed antenna selection. As K increases, energy consumption increases exponentially, and this causes LE of different scenarios to decrease and become close to each other. However, they are not exactly same until all of the available antennas are used. Furthermore, the $tr(CRLB_\theta)$ indicates the minimum achievable accuracy for each point. One can put a minimum accuracy constraint when optimizing LE depending on one's requirements.

Fig. 3.5 shows corresponding optimal number of antennas for each K that maximize LE in Fig. 3.4. It is seen that due to the exponential growth of energy consumption, F^* decreases very fast for the first set

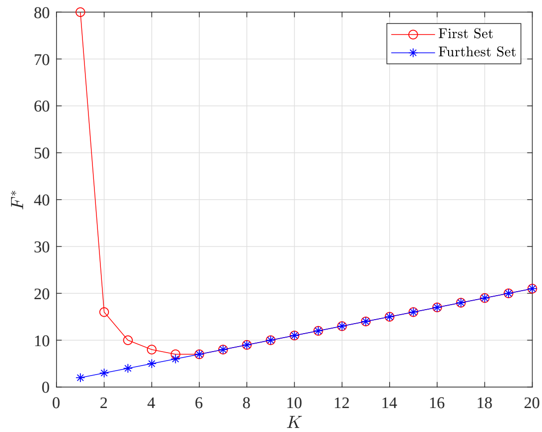

Figure 3.5: Optimal number of antennas for ML.

and reaches saturation point ($F^* = K + 1$) as K increases. Accordingly, this is the point after which LE starts to decrease in Fig. 3.4. Also, as predicted by Eq. 3.36, the optimal number of antennas for the furthest set is always the minimum possible number of antennas, $K + 1$. This illustrates that furthest antenna selection obtains higher LE using fewer antennas, which reduces costs of construction and maintenance of the system.

In Fig.3.6a, our proposed antenna selection is compared with other antenna selection methods for AoA estimation. In [54], it is stated that four smaller subarrays can perform better than one big array in Large Intelligent Surfaces. The same concept with a linear massive MIMO system is tested here. The array is divided into four subarrays, each containing one-fourth of the selected antennas. The distance is the same between these four subarrays. Also, we did the same thing by dividing the array into two subarrays. In [55], four specific solutions are presented for the antenna selection in linear antenna arrays. The pattern of fourth solution is selected ([55], Fig.2 e) and it is named *"Sparsity Enforcing"*. In [56] we showed that a set that contains the

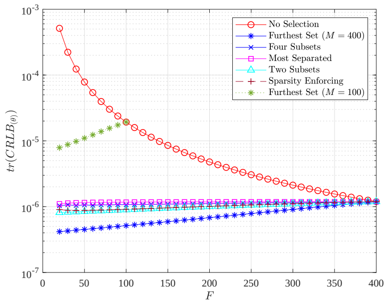

(a) $tr(\boldsymbol{CRLB_\theta})$ for various antenna selection methods.

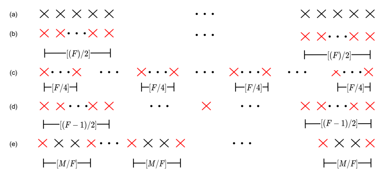

(b) Selection pattern of the compared selection methods. a) Antenna array b) Two subarrays c) Four subarrays d) Sparsity enforcing e) Most separated.

Figure 3.6: Comparison of different antenna selection methods and different M.

most separated antennas could have a relatively high performance in a planar antenna array. Here we applied the same concept to the linear array to see how it performs in the linear arrays (this method is called *"Most Separated"*). The selection pattern of each method is shown in Fig.3.6b. Also, the green curve is plotted to show the benefit of massive antennas at the BS and how our proposed antenna selection results in higher improvement when the number of available antennas is higher. This is also evident from Eq.3.31. The green curve is when $M = 100$ and the blue curve is when $M = 400$. It is seen that the higher M results in higher performance improvement when our proposed antenna selection is used, confirming that the selection method is suitable for massive MIMO systems.

LE of MUSIC algorithm is plotted by Monte-Carlo simulation of Fig. 3.7. The left hand side sub-figures of Fig. 3.7 are for $K = 10$ and $M = 22$, and the right hand side sub-figures are for $K = 20$ and $M = 55$. In this figure, the same AoAs for UTs as Fig. 3.2a are considered,

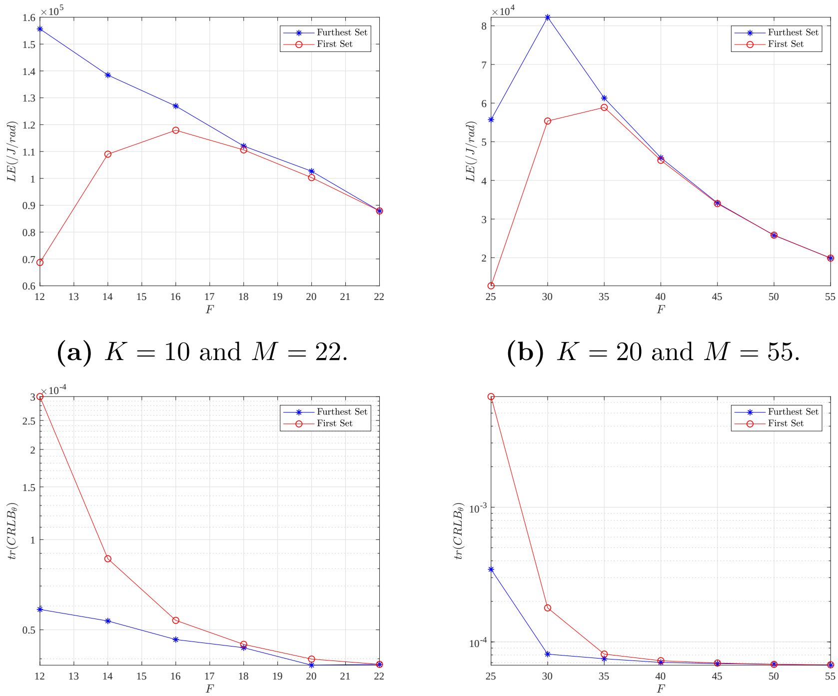

(a) $K = 10$ and $M = 22$.

(b) $K = 20$ and $M = 55$.

(c) $K = 10$ and $M = 22$.

(d) $K = 20$ and $M = 55$.

Figure 3.7: LE and $tr(\boldsymbol{CRLB_\theta})$ of MUSIC algorithm versus F.

only with another exclusion zone that is equal to $\frac{\pi}{7}$, so $AoA_k = \frac{\pi}{7} + \frac{\pi - \frac{2\pi}{7}}{K}$ for $k = \{1, \ldots, K\}$. By selecting antennas from the first set, LE has an optimum point in $F^* = 16$ and $F^* = 35$ in these settings, respectively. On the other hand, for furthest antenna selection, in $K = 10$, LE is always decreasing, and so its optimum point is at minimum number of antennas, but in $K = 20$ LE of the furthest set has an optimum point in $F = 30$. Nevertheless, its optimum point always happens before the first set's optimum point, meaning that the furthest antenna selection needs fewer antennas in this scenario, as well. In addition, the furthest antenna selection always has higher LE than the first antenna selection proving that furthest antenna selection is always beneficial, no matter what the channel model is. Furthermore, it is seen that the obtained $\boldsymbol{CRLB_\theta}$ for the furthest set is always lower than the first set, proving the superiority of the furthest antenna selection, once more.

3.8 Conclusion

This section analyzed $CRLB$ for AoA estimation when the received signal at the BS is accompanied by multipath signals according to the DMC model. With the help of RMT, we proved that regardless of the distribution of multipath signals, $CRLB$ for AoA almost surely converges toward a closed-form expression in the MU massive MIMO setting. This illustrates the contribution of multipath signals in the AoA estimation, providing a theoretical basis for recent studies that estimated location information with the help of multipath signals.

A refined version of the localization efficiency function is presented, which is a ratio of benefits to costs in localization and reflects the trade-off between performance and energy consumption. Contrary to previous studies, we used a comprehensive energy consumption model in this function and showed that there is an optimal number of antennas that maximizes the efficiency in the localization phase. We presented an antenna selection method that minimizes $CRLB$ for AoA when the number of utilized antennas is smaller than the total available antennas. Also, the behavior of both $CRLB$ and LE for this selection scheme is studied. It is shown that the behaviors of both of them change when utilized antennas are selected based on the proposed scheme, which affects the optimal number of antennas that maximizes LE.

Numerical results confirmed the $CRLB$'s convergence, even when the number of antennas is not too large. They showed that the proposed antenna selection strategy dramatically reduces $CRLB$. This phenomenon has been validated by Monte-Carlo simulations, too.

Furthermore, simulation results confirmed significant improvement of LE when our antenna selection approach is utilized. In fact, with the help of the proposed antenna selection method, ML estimation gains a competitive advantage over a certain region in terms of efficiency. In the end, LE of the MUSIC algorithm is studied and simulated, indicating the applicability of our antenna selection strategy even when the contribution of multipath signals is ignored.

CHAPTER 4

Passive Antenna Selection for Azimuth AoA Estimation

Massive MIMO systems provide high angular resolution in the next generation of wireless systems. This opportunity can be used to estimate the location of user terminals (UTs) accurately. In this section, we analyze the Cramer-Rao lower bound (***CRLB***) of planar antenna arrays in Massive MIMO systems for Azimuth Angle of Arrival (AAoA) estimation. With the help of Random Matrix Theory, we prove that for Massive antenna arrays with independent and identically distributed (i.i.d) multipath signals, ***CRLB*** for AAoA estimation converges toward a deterministic value, regardless of channel distribution. In this scenario, ***CRLB*** is a function of channel variance instead of instantaneous realization. Then, antenna selection is studied, and it is shown that using different subsets significantly affects the ***CRLB*** of a planar array.

4.1 Introduction

In the previous chapter, we presented an analysis for $CRLB$ of AoA estimation in DMC channels for a linear antenna array. In this section, we extend the analysis by presenting a deterministic form of $CRLB$ for AoA estimation for a planar antenna array under the DMC model in 3D settings.

In chapter 3 we presented an antenna selection method to maximize the localization efficiency of a linear array. It has been shown that depending on the antenna selection strategy, the behavior of $CRLB$ with respect to (w.r.t) number of antennas changes and the optimal antenna selection method has been presented. In this section, we show that in the case of a planar array, when 3D localization is considered, the optimal antenna selection strategy changes. As the proposed antenna selection is for the Multi-User scenario, it is based on minimizing the expected $CRLB$ over the possible range of UT's AoA. The initial optimal subset of antennas is presented, which serves as the starting point of a greedy algorithm. This algorithm finds the best greedy set of antennas when only a limited number of antennas have to be utilized. The contribution of this section is summarized as following:

- CRLB for AAoA estimation of a MU massive MIMO system with planar antenna array is obtained in a deterministic form when UTs experience a DMC channel.
- A greedy antenna selection with optimal starting point is presented that aims to minimize the expected CRLB of AAOA in planar antenna array.

4.2 System Model

We consider the uplink of a single-cell Multi-User Massive MIMO system with a BS at the center, equipped with $M = M_1 M_2$ antennas. M_1 antennas are installed along the x axis and M_2 antennas along the y axis. On each axis, adjacent antennas are separated by distance

d (Fig 3.1). There are K uniformly distributed single-antenna UTs in the cell. The BS uses pilot signals transmitted by UTs to localize them. The received signal at the BS is

$$\boldsymbol{y} = (\boldsymbol{A}_{Rx} \odot \boldsymbol{H})\boldsymbol{s} + \boldsymbol{n}, \tag{4.1}$$

where $\boldsymbol{s}$ is the vector of transmitted pilots and $\boldsymbol{n} \sim \mathcal{CN}(0, \sigma_n^2 \boldsymbol{I}_M)$ is additive white Gaussian noise. Also,

$$\boldsymbol{A}_{Rx} = [\boldsymbol{a}_R(\theta_1, \varphi_1) \;\; \dots \;\; \boldsymbol{a}_R(\theta_K, \varphi_K)], \tag{4.2}$$

contains K columns of $M \times 1$ steering vectors of BS antenna array response, where θ_k and φ_k are kth UT's azimuth and elevation AoA for $k \in \{1, \dots, K\}$. The mth element of kth steering vector is [57]

$$\begin{aligned} \boldsymbol{a}_R(\theta_k, \varphi_k)_m &= \frac{e^{-j\beta \sin(\varphi_k)((m_1-1)\cos(\theta_k)+(m_2-1)\sin(\theta_k))}}{\sqrt{M}}, \\ m &= (m_2 - 1)M_1 + m_1, \\ m_1 &= 1, \dots, M_1, \quad m_2 = 1, \dots, M_2, \end{aligned} \tag{4.3}$$

where $\beta = \frac{2\pi d}{\lambda}$ and λ is the wavelength of pilots. $\boldsymbol{H} = [\boldsymbol{h}_1 \;\; \dots \;\; \boldsymbol{h}_K]$ is an $M \times K$ matrix whose (m, k)th element, $h_{m,k}$, is the channel coefficient between kth UT and mth BS antenna. The mean of $\boldsymbol{h}_k$ is equal to the channel coefficient of kth UT's dominant path, $\bar{h}_k$. The random part of each elements, $\hat{h}_{m,k}$, accounts for the random effects of aggregated multipath signals at each antenna with limited fourth and eighth moments. The variance of the random part is assumed to be constant and equal to σ_h^2 for every antenna and user [58]

$$h_{m,k} = h^r_{m,k} + jh^i_{m,k}, \tag{4.4}$$

$$\mathbb{E}\{h^r_{m,k}\} = \mathcal{R}e\{\bar{h}_k\}, \;\; \mathbb{E}\{h^i_{m,k}\} = \mathcal{I}m\{\bar{h}_k\},$$

$$var(h^r_{m,k}) = var(h^i_{m,k}) = \sigma_h^2. \tag{4.5}$$

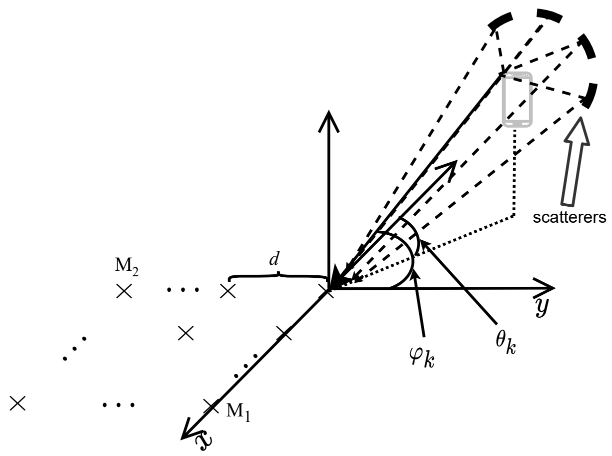

Figure 4.1: Configuration of the antenna array.

4.3 CRLB Analysis

The vector containing desired parameters for estimation is

$$\boldsymbol{\eta} = [\overbrace{\theta_1 \ \ \theta_2 \ \ \dots \ \ \theta_K}^{\boldsymbol{\eta}_\theta} \,|\, \overbrace{\varphi_1 \ \ \dots \ \ \varphi_K}^{\boldsymbol{\eta}_\varphi}]^T. \tag{4.6}$$

Defining $\hat{\boldsymbol{\eta}}$ as the unbiased estimator of $\boldsymbol{\eta}$, its mean square error is lower bounded as [11]

$$\mathbb{E}_{\boldsymbol{y}|\boldsymbol{\eta}}\{(\boldsymbol{\eta} - \hat{\boldsymbol{\eta}})(\boldsymbol{\eta} - \hat{\boldsymbol{\eta}})^T\} \geq \boldsymbol{CRLB} = \boldsymbol{J}^{-1}, \tag{4.7}$$

where $\boldsymbol{J}$ is Fisher Information Matrix (FIM) and can be written in block matrix form as [11]

$$\boldsymbol{J} = \begin{bmatrix} \boldsymbol{J}_{\theta,\theta} & \boldsymbol{J}_{\theta,\varphi} \\ \boldsymbol{J}_{\varphi,\theta} & \boldsymbol{J}_{\varphi,\varphi} \end{bmatrix}, \tag{4.8}$$

and

$$\boldsymbol{J}_{a,b} = \mathcal{R}e[(\frac{\partial \boldsymbol{w}}{\partial \boldsymbol{\eta}_a})^H(\frac{\partial \boldsymbol{w}}{\partial \boldsymbol{\eta}_b})], \tag{4.9}$$

in which $\boldsymbol{w} \triangleq (\boldsymbol{A}_{Rx} \odot \boldsymbol{H})\boldsymbol{s}$ and $a, b \in \{\theta, \varphi\}$. Therefore, using block matrix inversion properties, $CRLB$ of $\boldsymbol{\eta}_\theta$ is

$$\boldsymbol{CRLB}_\theta = \frac{\sigma_n^2}{2}(\boldsymbol{J}_{\theta,\theta} - \boldsymbol{J}_{\theta,\varphi}\boldsymbol{J}_{\varphi,\varphi}^{-1}\boldsymbol{J}_{\varphi,\theta})^{-1}. \tag{4.10}$$

The derivatives of $\boldsymbol{w}$ w.r.t $\boldsymbol{\eta}_\theta$ and $\boldsymbol{\eta}_\varphi$ can be written as

$$\frac{\partial \boldsymbol{w}}{\partial \boldsymbol{\eta}_\theta} = M(\boldsymbol{\Sigma}_2(\boldsymbol{A} + j\boldsymbol{B})\boldsymbol{C}_\theta - \boldsymbol{\Sigma}_1(\boldsymbol{A} + j\boldsymbol{B})\boldsymbol{S}_\theta)\boldsymbol{S}_\varphi, \tag{4.11}$$

$$\frac{\partial \boldsymbol{w}}{\partial \boldsymbol{\eta}_\varphi} = M(\boldsymbol{\Sigma}_1(\boldsymbol{A} + j\boldsymbol{B})\boldsymbol{C}_\theta + \boldsymbol{\Sigma}_2(\boldsymbol{A} + j\boldsymbol{B})\boldsymbol{S}_\theta)\boldsymbol{C}_\varphi, \tag{4.12}$$

where

$$\begin{aligned}
&\boldsymbol{\Sigma}_1 = \beta(\boldsymbol{I}_{M_2} \otimes diag(0, \frac{1}{M}, \ldots, \frac{M_1 - 1}{M})), \\
&\boldsymbol{\Sigma}_2 = \beta(diag(0, \frac{1}{M}, \ldots, \frac{M_2 - 1}{M}) \otimes \boldsymbol{I}_{M_1}), \\
&\boldsymbol{A} = \bar{\boldsymbol{A}} + \sigma_h \hat{\boldsymbol{A}}, \\
&\boldsymbol{B} = \bar{\boldsymbol{B}} + \sigma_h \hat{\boldsymbol{B}}, \\
&\bar{\boldsymbol{A}}_{m,k} = \mathcal{R}e\{\bar{h}_k \boldsymbol{a}_R(\theta_k)_m \boldsymbol{s}_k\}, \bar{\boldsymbol{B}}_{m,k} = \mathcal{I}m\{\bar{h}_k \boldsymbol{a}_R(\theta_k)_m \boldsymbol{s}_k\}, \\
&\hat{\boldsymbol{A}}_{m,k} = \frac{1}{\sigma_h}\mathcal{R}e\{-j\hat{h}_{m,k} s_k(\boldsymbol{a}_R(\theta_k)_m)\}, \\
&\hat{\boldsymbol{B}}_{m,k} = \frac{1}{\sigma_h}\mathcal{I}m\{-j\hat{h}_{m,k} s_k(\boldsymbol{a}_R(\theta_k)_m)\}, \\
&\boldsymbol{S}_a = diag(\sin(a_1), \ldots, \sin(a_K)), \;\; a \in \{\theta, \varphi\} \\
&\boldsymbol{C}_a = diag(\cos(a_1), \ldots, \cos(a_K)). \;\; a \in \{\theta, \varphi\}
\end{aligned} \tag{4.13}$$

By defining $\rho_k \triangleq \frac{|s_k|^2}{\sigma_n^2}$ and $v(m_1, m_2) = (m_1 - 1)(m_2 - 1)$, the following theorem presents a deterministic expression for $\boldsymbol{CRLB}_\theta$ of a planar antenna array.

Theorem 3. *In the Massive MIMO settings, $\boldsymbol{CRLB}_\theta$ almost surely converges toward a deterministic diagonal matrix whose (k,k)th entry is given by*

$$\boldsymbol{CRLB}_\theta(k,k) \xrightarrow{a.s.} \frac{v(M_1,2M_1)\cos^2(\theta_k)+v(M_2,2M_2)sin^2(\theta_k)+3v(M_1,M_2)\cos(\theta_k)\sin(\theta_k)}{\rho_k\beta^2(2\sigma_h^2+|\bar{h}_k|^2)v(M_1,M_2)(\frac{v(2M_1,2M_2)}{3}-\frac{3}{4}v(M_1,M_2))\sin^2(\varphi_k)}. \tag{4.14}$$

Proof. Replacing (4.11) and (4.12) in (5.5), we have

$$\begin{aligned}\boldsymbol{J}_{\theta,\theta} = M^2\boldsymbol{S}_\varphi^T[&\boldsymbol{S}_\theta^T(\boldsymbol{A}^T\boldsymbol{\Sigma}_1^2\boldsymbol{A}+\boldsymbol{B}^T\boldsymbol{\Sigma}_1^2\boldsymbol{B})\boldsymbol{S}_\theta\\ &+\boldsymbol{C}_\theta^T(\boldsymbol{A}^T\boldsymbol{\Sigma}_2^2\boldsymbol{A}+\boldsymbol{B}^T\boldsymbol{\Sigma}_2^2\boldsymbol{B})\boldsymbol{C}_\theta\\ &-\boldsymbol{S}_\theta^T(\boldsymbol{A}^T\boldsymbol{\Sigma}_1\boldsymbol{\Sigma}_2\boldsymbol{A}+\boldsymbol{B}^T\boldsymbol{\Sigma}_1\boldsymbol{\Sigma}_2\boldsymbol{B})\boldsymbol{C}_\theta\\ &-\boldsymbol{C}_\theta^T(\boldsymbol{A}^T\boldsymbol{\Sigma}_2\boldsymbol{\Sigma}_1\boldsymbol{A}+\boldsymbol{B}^T\boldsymbol{\Sigma}_2\boldsymbol{\Sigma}_1\boldsymbol{B})\boldsymbol{S}_\theta]\boldsymbol{S}_\varphi,\end{aligned} \tag{4.15}$$

$$\begin{aligned}\boldsymbol{J}_{\varphi,\varphi} = M^2\boldsymbol{C}_\varphi[&\boldsymbol{C}_\theta^T(\boldsymbol{A}^T\boldsymbol{\Sigma}_1^2\boldsymbol{A}+\boldsymbol{B}^T\boldsymbol{\Sigma}_1^2\boldsymbol{B})\boldsymbol{C}_\theta\\ &+\boldsymbol{S}_\theta^T(\boldsymbol{A}^T\boldsymbol{\Sigma}_2^2\boldsymbol{A}+\boldsymbol{B}^T\boldsymbol{\Sigma}_2^2\boldsymbol{B})\boldsymbol{S}_\theta\\ &+\boldsymbol{C}_\theta^T(\boldsymbol{A}^T\boldsymbol{\Sigma}_1\boldsymbol{\Sigma}_2\boldsymbol{A}+\boldsymbol{B}^T\boldsymbol{\Sigma}_1\boldsymbol{\Sigma}_2\boldsymbol{B})\boldsymbol{S}_\theta\\ &+\boldsymbol{S}_\theta^T(\boldsymbol{A}^T\boldsymbol{\Sigma}_2\boldsymbol{\Sigma}_1\boldsymbol{A}+\boldsymbol{B}^T\boldsymbol{\Sigma}_2\boldsymbol{\Sigma}_1\boldsymbol{B})\boldsymbol{C}_\theta]\boldsymbol{C}_\varphi,\end{aligned} \tag{4.16}$$

$$\begin{aligned}\boldsymbol{J}_{\theta,\varphi} = \boldsymbol{J}_{\varphi,\theta}^T = M^2\boldsymbol{S}_\varphi^T[&-\boldsymbol{S}_\theta^T(\boldsymbol{A}^T\boldsymbol{\Sigma}_1^2\boldsymbol{A}+\boldsymbol{B}^T\boldsymbol{\Sigma}_1^2\boldsymbol{B})\boldsymbol{C}_\theta\\ &+\boldsymbol{C}_\theta^T(\boldsymbol{A}^T\boldsymbol{\Sigma}_2^2\boldsymbol{A}+\boldsymbol{B}^T\boldsymbol{\Sigma}_2^2\boldsymbol{B})\boldsymbol{S}_\theta\\ &-\boldsymbol{S}_\theta^T(\boldsymbol{A}^T\boldsymbol{\Sigma}_1\boldsymbol{\Sigma}_2\boldsymbol{A}+\boldsymbol{B}^T\boldsymbol{\Sigma}_1\boldsymbol{\Sigma}_2\boldsymbol{B})\boldsymbol{S}_\theta\\ &+\boldsymbol{C}_\theta^T(\boldsymbol{A}^T\boldsymbol{\Sigma}_2\boldsymbol{\Sigma}_1\boldsymbol{A}+\boldsymbol{B}^T\boldsymbol{\Sigma}_2\boldsymbol{\Sigma}_1\boldsymbol{B})\boldsymbol{C}_\theta]\boldsymbol{C}_\varphi.\end{aligned} \tag{4.17}$$

From [58] (lemmas 1-3) we know that for $M \to \infty$

$$\boldsymbol{A}^T\boldsymbol{\Sigma}_p\boldsymbol{\Sigma}_q\boldsymbol{A}+\boldsymbol{B}^T\boldsymbol{\Sigma}_p\boldsymbol{\Sigma}_q\boldsymbol{B} \xrightarrow{a.s.} \frac{1}{M}tr(\boldsymbol{\Sigma}_p\boldsymbol{\Sigma}_q)(2\sigma_h^2+\bar{\boldsymbol{H}}) \tag{4.18}$$

for $p, q \in \{1, 2\}$ and $\bar{\boldsymbol{H}} = diag(|\bar{h}_1|^2, \ldots, |\bar{h}_K|^2)$. Also,

$$\begin{aligned} tr(\boldsymbol{\Sigma}_1^2) &= \beta^2(M_1-1)(2M_1-1)/M/6, \\ tr(\boldsymbol{\Sigma}_2^2) &= \beta^2(M_2-1)(2M_2-1)/M/6, \\ tr(\boldsymbol{\Sigma}_1\boldsymbol{\Sigma}_2) &= tr(\boldsymbol{\Sigma}_2\boldsymbol{\Sigma}_1) = \beta^2(M_1-1)(M_2-1)/M/4. \end{aligned} \tag{4.19}$$

Replacing (4.18) and (4.19) in (4.15)-(4.17), we have

$$\begin{aligned} \boldsymbol{J}_{\theta,\theta} \xrightarrow{a.s.} & \beta^2 \boldsymbol{S}_\varphi^T \Big(\frac{v(M_1, 2M_1)}{6}\boldsymbol{S}_\theta^2 + \frac{v(M_2, 2M_2)}{6}\boldsymbol{C}_\theta^2 \\ & - \frac{v(M_1, M_2)}{2}\boldsymbol{C}_\theta\boldsymbol{S}_\theta\Big)\boldsymbol{S}_\varphi(2\sigma_h^2 + \bar{\boldsymbol{H}}), \end{aligned}$$

$$\begin{aligned} \boldsymbol{J}_{\varphi,\varphi} \xrightarrow{a.s.} & \beta^2 \boldsymbol{C}_\varphi^T \Big(\frac{v(M_1, 2M_1)}{6}\boldsymbol{C}_\theta^2 + \frac{v(M_2, 2M_2)}{6}\boldsymbol{S}_\theta^2 \\ & + \frac{v(M_1, M_2)}{2}\boldsymbol{C}_\theta\boldsymbol{S}_\theta\Big)\boldsymbol{C}_\varphi(2\sigma_h^2 + \bar{\boldsymbol{H}}), \end{aligned}$$

$$\begin{aligned} \boldsymbol{J}_{\theta,\varphi} \xrightarrow{a.s.} & \beta^2 \boldsymbol{S}_\varphi^T \Big(\frac{v(M_2, 2M_2) - v(M_1, 2M_1)}{6}\boldsymbol{C}_\theta\boldsymbol{S}_\theta \\ & + \frac{v(M_1, M_2)}{4}(\boldsymbol{C}_\theta^2 - \boldsymbol{S}_\theta^2)\Big)\boldsymbol{C}_\varphi(2\sigma_h^2 + \bar{\boldsymbol{H}}). \end{aligned} \tag{4.20}$$

By replacing (5.7) in (5.6), using the fact that $\boldsymbol{J}_{\theta,\theta}$, $\boldsymbol{J}_{\varphi,\varphi}$, $\boldsymbol{J}_{\theta,\varphi}$ and $\boldsymbol{J}_{\varphi,\theta}$ are diagonal matrices, after some algebraic simplifications, all the elements of $\boldsymbol{CRLB}_\theta$ are obtained as (4.14). □

It is seen that the $CRLB_\theta$ does not depend on individual channel realizations ($h_{m,k}$), but rather on the statistical properties of the channel. In fact, what matters is the variance of these coefficients when large number of antennas are utilized. Also, (4.14) shows that in Massive MIMO systems, AAoA information is (*almost surely*) never lost due to the contribution of the multipath signals. These results, along with those presented in [58] for linear arrays, provide a complementary theoretical basis for AAoA estimation (or refinement) using several path-loss signals with the same order of power, like methods reported in [20, 36].

Now that we have a deterministic value for $\boldsymbol{CRLB}_\theta$, we can use it to study how different antennas contribute in θ estimation and prioritize the antennas with high contribution when only a portion of the total available antennas are utilized.

4.4 Antenna Selection

This section studies the antenna selection for planar antenna array configurations. The expectation of $\boldsymbol{CRLB}_\theta$ is minimized w.r.t set of utilized antennas, using a greedy algorithm whose optimal starting point will be presented.

In the following, we assume that $F \leq M$ number of antennas has to be used. F can be either the number of available RF-chains or the optimal point of the trade-off between $CRLB$ and energy consumption. We assume that array dimensions are much smaller than UTs' distances from it, so the difference of received power for different antennas is negligible.

From (5.6) and Theorem 3 it is seen that $\boldsymbol{CRLB}_\theta$ for a planar array is a function of the traces of squared $\boldsymbol{\Sigma}_1$, $\boldsymbol{\Sigma}_2$, and their product. When F antennas are utilized, $\boldsymbol{\Sigma}_1$ and $\boldsymbol{\Sigma}_2$ will be changed to $\tilde{\boldsymbol{\Sigma}}_1$ and $\tilde{\boldsymbol{\Sigma}}_2$, both with the size of $F \times F$. The diagonal elements of these matrices will be corresponding values of selected antennas from $\boldsymbol{\Sigma}_1$ and $\boldsymbol{\Sigma}_2$. As the antenna selection has to be done before the estimation of θ (and if F is the number of RF-chains, even before reception of the transmitted pilots by the UTs), there is no apriori knowledge about the θ, except its distribution. With this in mind, we minimize $\mathbb{E}_\theta\{tr(\boldsymbol{CRLB}_\theta)\}$. So, noting that when F antennas are utilized, the

$M^{-\frac{1}{2}}$ normalization factor in (5.2) will be changed to $F^{-\frac{1}{2}}$ and uniform distribution of UTs, we obtain

$$\mathbb{E}_\theta\{tr(\boldsymbol{CRLB}_\theta)\} = \frac{F\sum_{k=1}^{K}(\rho_k(2\sigma_h^2+|\bar{h}_k|^2))^{-1}}{8\beta^2\sin^2(\varphi_k)} \times \underbrace{\left(\frac{tr(\tilde{\boldsymbol{\Sigma}}_1^2+\tilde{\boldsymbol{\Sigma}}_2^2)}{tr(\tilde{\boldsymbol{\Sigma}}_1^2)tr(\tilde{\boldsymbol{\Sigma}}_2^2)-(tr(\tilde{\boldsymbol{\Sigma}}_1\tilde{\boldsymbol{\Sigma}}_2))^2}\right)}_{U(\mathcal{S})}, \tag{4.21}$$

where $\mathcal{S}$ is the set of selected antennas according to which the elements of $\tilde{\boldsymbol{\Sigma}}_1$ and $\tilde{\boldsymbol{\Sigma}}_2$ are determined. The only part affected by the selected set of antennas is $U(\mathcal{S})$ (the part inside parentheses), so we just need to minimize it. Minimization of $U(\mathcal{S})$ is a combinatorial optimization problem that we use a greedy algorithm to solve it. $F = 3$ is the minimum possible number of antennas for a planar antenna array (so they form a plane). These first three antennas have to be selected together. After selecting the first three antennas (starting point of the antenna selection), we can proceed with a greedy algorithm that, step by step, selects an antenna that reduces $U(\mathcal{S})$ the most.

Lemma 4. *The best choice for the first three antennas for AAoA estimation is*
$\mathcal{S}_3 = \{(1,1),(M_1,1),(1,M_2)\}$.

Proof. The first choice has to be $(1,1)$th antenna that is the reference point w.r.t which the θ is measured. Moreover, the other two antennas must have different indices in both dimensions, otherwise they compose a linear array. For notation convenience, we define $M_1' = M_1 - 1$ and $M_2' = M_2 - 1$. Let $\bar{\mathcal{S}_3} = \{(1,1),(M_1-a,1+b),(1+c,M_2-d)\}$, for any set of non-negative integers $\{a,b,c,d\}$ where

$$\begin{aligned}&\{a,c\} \le M_1', \ \ \{b,d\} \le M_2',\\ &a+b+c+d \ge 1,\\ &(a+c,b+d) \ne (M_1',M_2'),\end{aligned} \tag{4.22}$$

be a set of three distinctive antennas other than $\mathcal{S}_3$. Evaluating the corresponding $U(\mathcal{S})$ for both $\bar{\mathcal{S}}_3$ and $\mathcal{S}_3$ by using indices of each group in (4.21), we have

$$\begin{aligned} U(\bar{\mathcal{S}}_3) &= \frac{(M_1' - a)^2 + b^2 + c^2 + (M_2' - d)^2}{((M_1' - a)(M_2' - d) - bc)^2}, \\ U(\mathcal{S}_3) &= \frac{M_1'^2 + M_2'^2}{(M_1' M_2')^2}. \end{aligned} \tag{4.23}$$

Accordingly,

$$\begin{aligned} & U(\bar{\mathcal{S}}_3)((M_1'M_2')^2)((M_1' - a)(M_2' - d) - bc)^2 \\ & = (M_1'M_2')^2(M_1' - a)^2 + (M_1'M_2')^2 b^2 \\ & + (M_1'M_2')^2 c^2 + (M_1'M_2')^2 (M_2' - d)^2 \\ & \overset{(e)}{>} (M_1'(M_2' - d))^2 (M_1' - a)^2 + (M_1'^2 + M_2'^2) b^2 c^2 \\ & + ((M_1' - a)M_2')^2 (M_2' - d)^2 \\ & \geq ((M_2' - d)(M_1' - a) - bc)^2 (M_1'^2 + M_2'^2) \\ & = U(\mathcal{S}_3)((M_1'M_2')^2)((M_1' - a)(M_2' - d) - bc)^2, \end{aligned} \tag{4.24}$$

where (e) follows from the fact that $b \leq M_2'$ and $c \leq M_1'$ and if both are equal either to zero or their maximum, due to (4.22), either a or d has to be greater than zero. So,

$$U(\bar{\mathcal{S}}_3) > U(\mathcal{S}_3). \tag{4.25}$$

Based on (4.25), selecting any other set than $\mathcal{S}_3$ results in higher $U(\mathcal{S})$. Therefore, $\mathcal{S}_3$ is the best set of the first three antennas that minimize $U(\mathcal{S})$. □

Now that the optimal start point for selection has been found, the remaining $F - 3$ antennas will be selected using a greedy algorithm. In each step, the antenna that decreases $U(\mathcal{S})$ more than others is added to the $\mathcal{S}$ until all of the required antennas are selected. The

get F
$\mathcal{S} := \mathcal{S}_3$
For $f := 4$ **to** F **do**
For $x := 1$ **to** M_1 **do**
For $y := 1$ **to** M_2 **do**
If $(x, y) \notin \mathcal{S}$ **do**
$\mathcal{S}(f) := (x, y)$
$\boldsymbol{V}(x, y) := U(\mathcal{S})$
EndIf
EndFor
EndFor
$\mathcal{S}(f) := \arg\min_{(x,y)} \boldsymbol{V}$
EndFor
return $\mathcal{S}$

Table 4.1: Greedy algorithm for optimal antenna selection

algorithm is summarized in Table 4.1. It should be noted that as this selection is a static one, the mentioned algorithm is only needed to run once for the antenna configuration of the system. So, although it is low, the algorithm's computational complexity is not of concern because it is not used in real-time.

In Section4.5, it will be shown that although for a $2D$ linear array, the optimal set is composed of furthest antennas from the reference point [58], $\mathcal{S}^*$ of a planar array mostly consists of most separated antennas (whose x and y indices has maximum difference), accompanied by a few numbers of furthest antennas. We compare $\mathcal{S}^*$ with both of these sets separately, in addition to another algorithm that selects the closest antennas to the reference point. The latter's importance is that the behavior of its $CRLB$ w.r.t number of antennas can present some information about designing better antenna arrays when it is not possible to build a larger one.

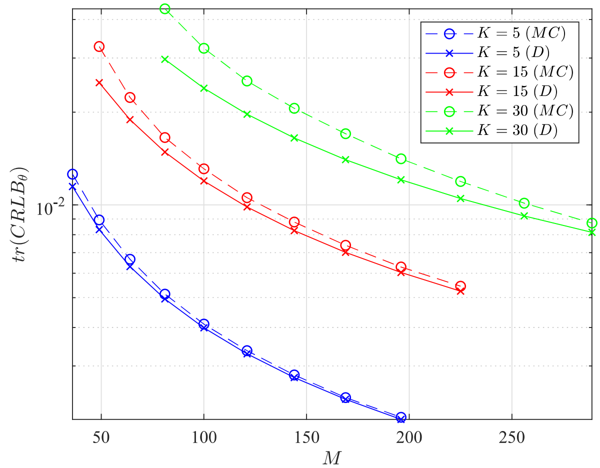

Figure 4.2: Deterministic and MC simulations of $tr(\boldsymbol{CRLB_\theta})$.

4.5 Numerical Results

In this section we verify the analytical results obtained in previous sections using Monte-Carlo (MC) simulations and illustrate the benefits of antenna selection. In the Monte-Carlo simulations, the random sampling is performed on the fast fading channel coefficient between UTs and BS antennas (Eq.4.4). In the following, $\rho_k = 3$, $\frac{d}{\lambda} = 0.5$, $\theta_k = \{0, \frac{2\pi}{K}, \ldots, \frac{2\pi(K-1)}{K}\}$, $\bar{h}_k = 1$ and $\varphi_k = \pi/3$ for $i \in \{1, \ldots, K\}$. Also, channel coefficients are Gaussian distributed random variables with $\sigma_h^2 = 0.5$.

Fig. 4.2 shows the values of $tr(\boldsymbol{CRLB_\theta})$ in which dashed lines are generated by MC simulations of (5.6), while solid ones are computed using the deterministic expression in (4.14), when $M_1 = M_2$ for $K = 5, 15, 30$. It should be noted that as the trace of $\boldsymbol{CRLB_\theta}$ is plotted, the gap between deterministic and MC curves is actually the sum of K errors of each almost sure convergence in (4.14). This explains

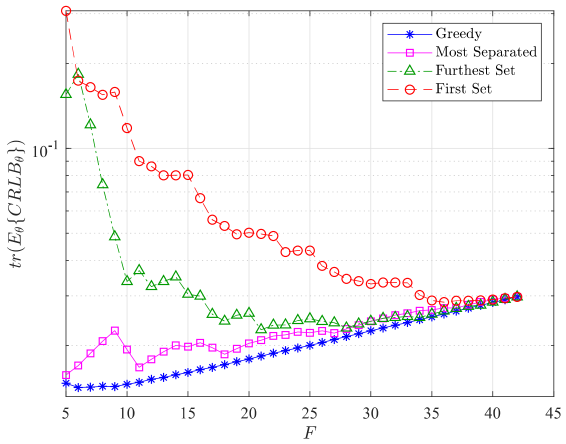

Figure 4.3: $\mathbb{E}_\theta\{tr(\boldsymbol{CRLB_\theta})\}$ for various antenna selection strategies.

the seeming increment of the gap between MC and deterministic corresponding curves as K grows. It is seen that (4.14) completely mimics the behavior of actual $\boldsymbol{CRLB_\theta}$ with high accuracy. In the rest of the figures, we only use deterministic formula.

Fig. 4.3 represents $\mathbb{E}_\theta\{tr(\boldsymbol{CRLB_\theta})\}$ for four different antenna selection algorithms, when $M_1 = 7$, $M_2 = 6$ and $K = 5$. The reason that $\mathbb{E}_\theta\{tr(\boldsymbol{CRLB_\theta})\}$ has increasing behavior for some algorithms stems from the fact that the received power is normalized w.r.t the number of utilized antennas (5.2). So, for certain F, some algorithms have lower $\mathbb{E}_\theta\{tr(\boldsymbol{CRLB_\theta})\}$ compared to the case when all of the M antennas are used (where all curves merge). The scenario where the power is not normalized is also presented in Fig. 4.5. It is seen that using the greedy algorithm, $\mathbb{E}_\theta\{tr(\boldsymbol{CRLB_\theta})\}$ is significantly reduced. Also, using antenna selection, there will be a global optimal point in which $\mathbb{E}_\theta\{tr(\boldsymbol{CRLB_\theta})\}$ is minimized. In other words, there is an optimal point for the trade-off between number of utilized antennas and

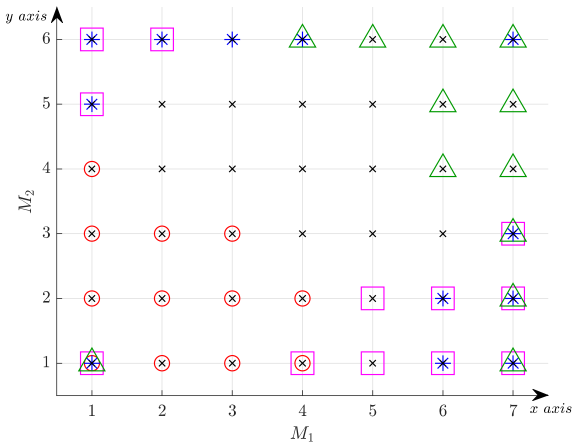

Figure 4.4: Selected antennas of each selection method for $F = 12$.

$\mathbb{E}_\theta\{tr(\boldsymbol{CRLB}_\theta)\}$ that happens before using all of the available antennas. In this regard, the greedy algorithm obtains its minimum for $F = 6$, which is the lowest among all algorithms. Moreover, other algorithms experience several rapid deterioration and refinements, that is due to disordered addition of antennas with low and high contributions in $\mathbb{E}_\theta\{tr(\boldsymbol{CRLB}_\theta)\}$, respectively. In order to clarify these behaviors, Fig. 4.4 shows the antenna configurations associated with different algorithms, when $F = 12$, for the same setting as that of Fig. 4.3. Selected antennas of each method are specified using the same color and marker as Fig. 4.3. The first set algorithm tries to complete a square in each step. The 12th selected antenna of this method is $(4, 2)$, which has a mild effect in reducing $CRLB$ in Fig. 4.3, while the previous two antennas, $(4, 1)$ and $(1, 4)$, decreased the $CRLB$ relatively more. Therefore, sudden decreases happen when the added antenna belongs to the most separated set. This shows that in a planar array, antennas inside the array shape do not contribute as high as those on the sides in terms of the $CRLB$. The same phenomenon

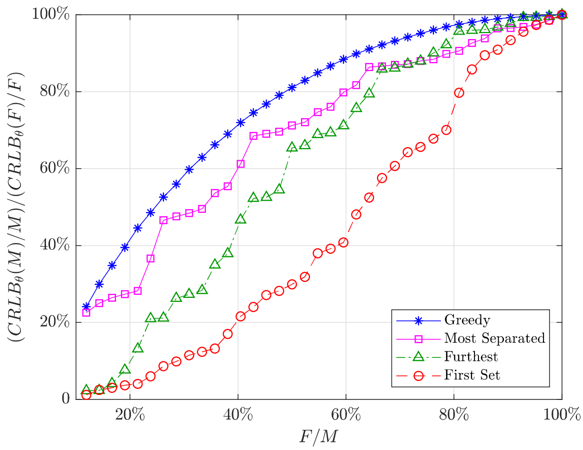

Figure 4.5: Ratio of obtained $CRLB_\theta$ versus ratio of utilized antennas.

(with different intensities) happens with the furthest and most separated sets at different points. Finally, the greedy algorithm selects some of the most separated antennas alongside some of the furthest ones (mostly from the former) to achieve the best possible outcome. All in all, Fig. 4.3 and Fig. 4.4 show that antennas on the boundary sides of the array have higher contributions than those in the middle, i.e., the further away from the main diagonal an antenna is, the more the contribution it has. Interestingly, we see that the optimal selection strategy creates a collection of four divided sub-arrays for AAoA estimation. This effect that four smaller but separated sub-arrays can have better performance in localization rather than one big array has also been reported in [54] for systems that utilize large intelligent surfaces. Our results show that similar effects happen for the Massive MIMO systems, and the best performance is obtained when the sub-arrays vary in size.

Fig. 4.5 illustrates the percentage of achieved $CRLB_\theta$ versus the percentage of utilized antennas when the $M^{-\frac{1}{2}}$ normalization factor in

(5.2) is removed. $\boldsymbol{CRLB}_\theta(f)$ is the $CRLB$ when f antennas are used. This figure indicates the efficiency of hardware usage when antenna selection is utilized, corresponding to the selection method. It is seen that by using the greedy antenna selection method, more than 80% of the best possible performance is achieved, only by using half of the antennas on the array (i.e., the $\boldsymbol{CRLB}_\theta$ by using half of the total available antennas is only $\frac{1}{0.8} = 1.25$ times the $\boldsymbol{CRLB}_\theta$ when all of antennas are used). This can significantly increase both the hardware and energy efficiency of the system. Therefore, with or without the normalization factor, antenna selection has its advantages, especially with the optimal selection method.

Fig. 4.6 presents the $\mathbb{E}_\theta\{tr(\boldsymbol{CRLB}_\theta)\}$ for $K = 5$, when number of selected antennas is constant, $F = 16$, and the array size increases with $M_1 = M_2 + 2$. This figure shows how different methods appreciate the size of the antenna array. Clearly, the first antenna set will remain constant as it does not care about the total array size. The greedy algorithm and most separated have a uni-mode behavior as the size increases. For the furthest set, as long as the array is small enough, it will contain more antennas on the array's boundary sides relative to those near the main diagonal. As the array size grows, the ratio of antennas from the boundary to near diagonal ones will decrease. Eventually, selected antennas will form a square (or a rectangle) shape, in which the ratio will remain the same. When this ratio starts to decrease, the $\boldsymbol{CRLB}_\theta$ rises, and after the formation of the square (or the rectangle), $\boldsymbol{CRLB}_\theta$ remains the same. So, only the greedy and most separated methods always take full advantage of the total array size.

4.6 Conclusion

In this chapter, we have investigated the behavior of $CRLB$ for AAoA estimation for planar antenna arrays in Multi-User Massive MIMO system by using Random Matrix Theory. We showed that in the asymptotic case, regardless of the distribution of channel coefficients,

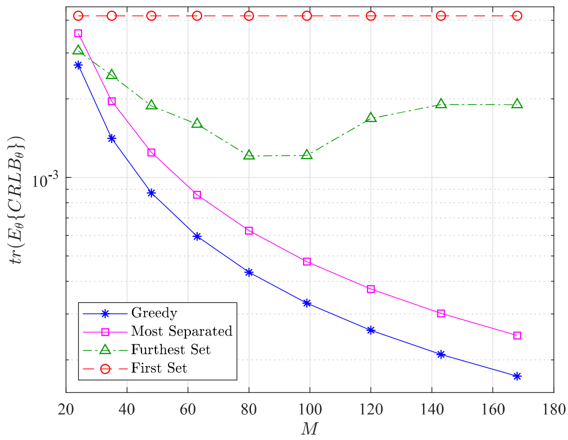

Figure 4.6: $\mathbb{E}_\theta\{tr(\boldsymbol{CRLB}_\theta)\}$ versus M for $F = 16$.

$CRLB$ almost surely converges toward a deterministic expression that depends on system parameters, namely the channel's variance, instead of its instantaneous realizations. This means that when dominant path is in poor condition, AAoA information is not lost and theoretically confirms the results of recent works that use multipath signals to refine their estimation. Moreover, antenna selection for minimizing the $CRLB$ is studied, and the best method to minimize the expected $CRLB$ when a fraction of available antennas have to be used is presented as a greedy algorithm. As a benchmark, other antenna selection methods are also compared with the output of the greedy algorithm. We showed that a greedy antenna selection significantly increases system performance in terms of AAoA estimation.

CHAPTER 5

Real-Time CRLB based Antenna Selection

Estimation of User Terminals' (UTs') AoA plays a significant role in the next generation of wireless systems. Due to high demands, energy efficiency concerns, and scarcity of available resources, it is pivotal how these resources are used. Installed antennas and their corresponding hardware at the Base Station (BS) are of these resources. In this section, we address the problem of antenna selection to minimize Cramer-Rao Lower Bound (CRLB) of a planar antenna array when fewer antennas than total available antennas have to be used for a UT. First, the optimal antenna selection strategy to minimize the expected CRLB is proposed. Then, using this strategy as a preliminary step, we present a two-stage greedy antenna selection method whose goal is to minimize the instantaneous CRLB. The optimal start point of the greedy algorithm is presented alongside some methods to reduce the algorithm's computational complexity.

5.1 Introduction

Localization of UTs is an indispensable part of wireless systems. On the one hand, many applications, like auto-driving cars and health services, directly require continuous tracking of UT's locations. On the other hand, using location information, higher data rates with higher efficiencies can be transferred to the UTs [9]. The AoA information plays a key role in these applications.

A general criterion to evaluate the capability of a system to localize UTs is CRLB. Numerous works have studied the CRLB in different system models [11, 56]. Many parameters of a system affect the CRLB. In particular, the arrangement of antennas on the receiver side substantially influences the ability of AoA estimation. A linear [58], concentric [59], or planar [57] antenna array each has certain pros and cons. Planar antenna array provides wide aperture and uses assigned space for antenna array more efficiently (making them a suitable choice for Massive MIMO systems) [60]. Also, studies for planar antenna arrays can be easily generalized to the newly emerging concept of Reconfigurable Intelligent Surfaces (RIS) [61, 62].

Antenna selection is a solution for various challenges in multi-antenna systems. Energy efficiency concerns may limit the number of active antennas [19], hardware shortage or complexity [63], or multicasting services where different antennas provide different services to different UTs [64]. It is shown that by using antenna selection, the system's energy efficiency can be improved up to 220% [58]. Also, in [65] it is shown that by using 20% of total available antennas, more than 60% of total localization accuracy can be obtained, resulting in improved hardware usage efficiency. Another motivation for antenna selection is that using all of the available antennas may surpass the required accuracy of the system [66]. In RIS and massive MIMO systems, antenna selection is used to balance performance and hardware complexity [67, 68]. When fewer antennas than the total available antennas have to be used in a wireless network, active antennas can be selected to improve certain aspects of the system, e.g., the ability to estimate AoA with higher accuracy.

In this regard, [69] proposes a neural network selection method to minimize the log-determinant of CRLB in a radar system with a linear array. The log determinant of the CRLB is used as the cost function, and the neural network is trained by feeding the actual AoA of training samples. In [70] deep learning is used to minimize CRLB for cognitive radars with linear, circular, and randomly distributed antenna arrays. In [65] authors present a greedy algorithm for sensor selection in distributed radars where the objective function to minimize is the probability of error in a Maximum a Posteriori (MAP) localization method. It is shown that a greedy algorithm can yield outstanding performance with low complexity and low run time. Another use of greedy algorithms to solve the combinatorial optimization problem of antenna selection is studied in [66] where the goal is to minimize minimum square error in a distributed system, using a knapsack problem formulation. In [71] authors introduced a real-time antenna selection strategy that uses a cyclic algorithm to minimize posterior CRLB (PCRLB) in a 2D scenario for a compact MIMO radar. The PCRLB is the optimization criterion as the prefiltering of the radar will not affect PCRLB. In [72] authors used a Dinkelbach type algorithm to minimize CRLB of AoA when desired parameters for estimation were AoA and azimuth of a UT. An unsupervised online learning method is used to minimize total CRLB for azimuth and elevation of a UT in [73], with three orders of magnitude lower complexity compared to [72] to make it possible to run in real-time.

In works that aim to minimize CRLB, like [72,73], the actual AoAs are used in the optimization process, and this brings the question of how one can feed their proposed algorithm with AoAs when they are unknown. The main point in minimizing CRLB for AoA in the 3D scenario is that as it is a combined function of both antenna set and AoAs, without knowledge of AoAs, it will not be possible to minimize CRLB. If AoAs are known, there will be no need to minimize them. The primary contribution of this work is to address this issue to minimize the CRLB.

Greedy algorithms have been widely used for solving antenna selection problems [65, 66, 68]. A key feature of the greedy algorithm is its simplicity, making it possible to run it quickly. However, a major difference between employing a greedy algorithm in a compact planar antenna array with the distributed case, like the ones considered in [65, 66], is that in the case of a compact array, the first three antennas have to be chosen together. At each step of the greedy algorithm, one antenna is selected. To do this, the $CRLB$ is checked for every possible antenna, and the one that results in the minimum $CRLB$ will be selected at the corresponding step. However, as the $CRLB$ is calculated for a planar array, the antenna set that is put in $CRLB$'s formula must compose a plane, otherwise, it will result in infinity. So, the minimum requirement to start the greedy algorithm is a set of antennas that create a plane. As the minimum number of points that create a plane is three, the start point of the greedy algorithm needs to be a set of three antennas that are not in a line. After that, the greedy algorithm can continue by selecting one antenna at each step without facing the infinite $CRLB$ problem.

In chapter 4, we studied the problem of antenna selection for a planar array whose reference point is at its corner under DMC model. A greedy-based antenna selection strategy whose cost function is the expected $CRLB$ was proposed with an optimal start point. With the help of the expectation (over all possible values of AAoA), it is possible to remove the effects of the instantaneous AAoA and minimize it. In the first part of this work, in continuation of our previous work [56], the $CRLB$ for a planar array whose reference point is at its center in the 3D setting is calculated where the effects of unknown elevation are also considered in the calculation. Then, (instead of using a greedy method), an optimal antenna selection strategy to minimize the expected CRLB of a planar antenna array is proposed. This antenna selection strategy only requires the possible range of AAoA and its distribution to take the expectation from the CRLB. The advantage of this selection procedure is that the antenna selection priority can be determined prior to system implementation.

In the next part, to address the problem of lack of knowledge about AAoA, we present a two-stage antenna selection procedure that aims to minimize the instantaneous CRLB of AAoA. In the first step, a crude estimation of AAoA is made using selected antennas to minimize expected CRLB. Then based on this estimation, a greedy algorithm with an optimal start point is employed to minimize the instantaneous CRLB. To reduce the computational complexity of the greedy algorithm, especially for its initial start set, we present the optimal start set for every value of AAoA. Furthermore, by using the characteristics of the CRLB, we prove that in each step of the greedy algorithm, by searching only half of the available antennas, the contribution of all antennas can be evaluated. This proposition will further reduce the computational complexity of utilizing the greedy algorithm.

The contributions of this chapter are summarized as the following:

- The optimal antenna selection strategy to minimize the expected CRLB of AAoA estimation in planar antenna arrays in a 3D scenario is presented.
- By using the antenna selection for minimizing the expected CRLB, a two-stage antenna selection method is developed that aims to minimize instantaneous CRLB of AAoA.
- The presented algorithm is designed to have low complexity to be suited for real-time applications. To do this, the optimal start point of the greedy algorithm is analytically presented alongside a lemma to reduce the search pool.

5.2 System Model

We consider the uplink of a single-cell MIMO system with a BS at the center, equipped with $(M+1)^2$ antennas. $M+1$ antennas are installed along x and y axes. For mathematical tractability and clarity, it is assumed that M is an even number. On each axis, adjacent antennas are separated by distance d (Fig.5.1). There is a UT in the cell, and

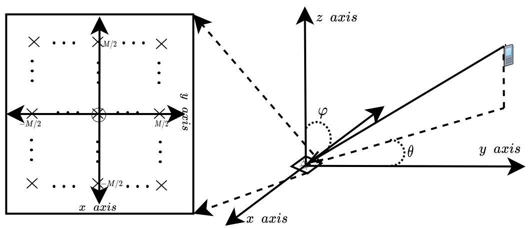

Figure 5.1: Antenna configuration at the BS w.r.t the UT.

the BS uses pilot signals transmitted by the UT to localize the UT[1]. For clarity, we assume that there is only one dominant path. The received signal at the BS is

$$\boldsymbol{y} = \boldsymbol{a}_R h_d s + \boldsymbol{n}, \tag{5.1}$$

where h_d is the channel coefficient for the dominant path of the UT, s is the transmitted pilot by the UT with $\mathbb{E}\{s\} = 0$ and $\mathbb{E}\{|s|^2\} = p_r$, and $\boldsymbol{n} \sim \mathcal{CN}(0, \sigma_n^2 \boldsymbol{I}_M)$ is additive white Gaussian noise. Also, $\boldsymbol{a}_R$ is the steering vector of BS antenna array response, where θ and φ are the UT's azimuth and elevation AoAs. The mth element of $\boldsymbol{a}_R$ is [57]

$$\begin{aligned}
&\boldsymbol{a}_R(\theta, \varphi)_m = e^{-j\beta \sin(\varphi)((m_1-1)\cos(\theta)+(m_2-1)\sin(\theta))}, \\
&m = (m_2 - 1)(M + 1) + m_1, \\
&m_1 = 1, \ldots, M + 1, \quad m_2 = 1, \ldots, M + 1,
\end{aligned} \tag{5.2}$$

where $\beta = \frac{2\pi d}{\lambda}$ and λ is the wavelength of pilots.

5.3 CRLB

In this part, we obtain the formulation of $CRLB_\theta$ that is the CRLB for the estimation of the θ, when $F \leq (M+1)^2$ antennas are activated

[1]Indeed, there can be more than one UT, but they have to use different frequency or time slot and the following concepts can be applied to each of them.

(and the rest of them are not used). As the CRLB of θ in a planar antenna array is well studied in the literature (namely in [56, 72]), we just briefly explain how the same results can match our system model with minor changes in the $CRLB$ calculations[2].

The vector of the desired variable is $\eta = [\theta \;\; \varphi]$. Defining $\hat{\boldsymbol{\eta}}$ as the unbiased estimator of $\boldsymbol{\eta}$, its mean square error is lower bounded as

$$\mathbb{E}_{\boldsymbol{y}|\boldsymbol{\eta}}\{(\boldsymbol{\eta}-\hat{\boldsymbol{\eta}})(\boldsymbol{\eta}-\hat{\boldsymbol{\eta}})^T\} \geq \boldsymbol{CRLB} = \boldsymbol{J}^{-1}, \tag{5.3}$$

where $\boldsymbol{J}$ is Fisher information matrix and can be written in block matrix form as [11]

$$\boldsymbol{J} = \begin{bmatrix} J_{\theta,\theta} & J_{\theta,\varphi} \\ J_{\varphi,\theta} & J_{\varphi,\varphi} \end{bmatrix}, \tag{5.4}$$

and

$$J_{a,b} = \mathcal{R}e[(\frac{\partial \boldsymbol{w}}{\partial \boldsymbol{\eta}_a})^H(\frac{\partial \boldsymbol{w}}{\partial \boldsymbol{\eta}_b})], \tag{5.5}$$

in which $\boldsymbol{w} \triangleq \boldsymbol{a}_R h_d s$ and $a, b \in \{\theta, \varphi\}$. Therefore, using block matrix inversion properties, $CRLB_\theta$ is

$$CRLB_\theta = \frac{\sigma_n^2}{2}(J_{\theta,\theta} - J_{\theta,\varphi}J_{\varphi,\varphi}^{-1}J_{\varphi,\theta})^{-1}. \tag{5.6}$$

From [56], equations (18-19), we know that

$$\begin{aligned} J_{\theta,\theta} &= \beta^2|h_d|^2\sin^2(\varphi)(tr(\tilde{\boldsymbol{\Sigma}}_1^2)\sin^2(\theta) + tr(\tilde{\boldsymbol{\Sigma}}_2^2)\cos^2(\theta) \\ &\quad - 2tr(\tilde{\boldsymbol{\Sigma}}_1\tilde{\boldsymbol{\Sigma}}_2)\cos(\theta)\sin(\theta)), \\ J_{\varphi,\varphi} &= \beta^2|h_d|^2\cos^2(\varphi)(tr(\tilde{\boldsymbol{\Sigma}}_1^2)\cos^2(\theta) + tr(\tilde{\boldsymbol{\Sigma}}_2^2)\sin^2(\theta) \\ &\quad + 2tr(\tilde{\boldsymbol{\Sigma}}_1\tilde{\boldsymbol{\Sigma}}_2)\cos(\theta)\sin(\theta)), \\ J_{\theta,\varphi} &= \beta^2|h_d|^2\sin(\varphi)\cos(\varphi)(tr(\tilde{\boldsymbol{\Sigma}}_2^2 - \tilde{\boldsymbol{\Sigma}}_1^2)\sin(\theta)\cos(\theta) \\ &\quad + tr(\tilde{\boldsymbol{\Sigma}}_1\tilde{\boldsymbol{\Sigma}}_2)(\cos^2(\theta) - \sin^2(\theta)). \end{aligned} \tag{5.7}$$

[2] For detailed calculation, please refer to [56], section III.

where $\tilde{\boldsymbol{\Sigma}}_1$ and $\tilde{\boldsymbol{\Sigma}}_2$ are $F \times F$ selected matrices from $(M+1)^2 \times (M+1)^2$ $\boldsymbol{\Sigma}_1$ and $\boldsymbol{\Sigma}_2$ matrices and

$$\begin{aligned}\boldsymbol{\Sigma}_1 &= \boldsymbol{I}_M \otimes diag(-M/2, \ldots, M/2),\\ \boldsymbol{\Sigma}_2 &= diag(-M/2, \ldots, M/2) \otimes \boldsymbol{I}_M.\end{aligned} \tag{5.8}$$

The main points of obtaining (5.7) from [56] are two. First, due to absence of multi-path signals (caused by a different system model), the almost sure convergence in [56] is replaced with equality in (5.7). Second, because there is only one UT, most of matrices are converted to scalars (including the $CRLB_\theta$). By defining $\rho \triangleq \frac{p_r}{\sigma_n^2}$ and replacing (5.7) in (5.6) and after some algebraic operations, we obtain the $CRLB_\theta$ as

$$CRLB_\theta = \frac{tr(\tilde{\boldsymbol{\Sigma}}_1^2)\cos^2(\theta) + tr(\tilde{\boldsymbol{\Sigma}}_2^2)sin^2(\theta) + 2tr(\tilde{\boldsymbol{\Sigma}}_1\tilde{\boldsymbol{\Sigma}}_2)\cos(\theta)\sin(\theta)}{2\rho\beta^2|h_d|^2(tr(\tilde{\boldsymbol{\Sigma}}_1^2)tr(\tilde{\boldsymbol{\Sigma}}_2^2) - tr(\tilde{\boldsymbol{\Sigma}}_1\tilde{\boldsymbol{\Sigma}}_2)^2)\sin^2(\varphi)}. \tag{5.9}$$

By definition, $CRLB_\theta$ indicates the lowest possible error variance for any estimator for the considered system model. In this regard, $CRLB_\theta$ can be seen as an intrinsic characteristic of the system, as it is a function of system settings. Any unbiased estimator is bound to have a higher or equal variance as $CRLB_\theta$. This makes it a valuable parameter for various optimizations, namely antenna selection. If $CRLB_\theta$ is optimized, the performance of any estimator utilized in the system will be improved. Based on this, we choose $CRLB_\theta$ as the cost function of the antenna selection optimization problem, so its outcome can be used for any estimation method.

5.4 Antenna Selection

In this section, the antenna selection in the localization phase is studied, and two antenna selection methods are proposed. In the first selection method, we use the expected value of $CRLB_\theta$ as the cost function to minimize. Then, using this method, we develop another antenna selection strategy whose cost function is instantaneous $CRLB_\theta$. We focus on the selection process and assume that the number of required antennas, F, is given.

Antenna selection is one of the proposed solutions in the literature to address hardware shortage [74], or energy efficiency [19]. The general goal of antenna selection is to select a subset of antennas that results in the highest possible performance for the number of selected antennas. In [56] we have proposed a greedy antenna selection strategy that aims to minimize expected $CRLB_\theta$ for a planar antenna array, where the expectation is over all possible realizations of AAoA.

In [72] authors presented an antenna selection to minimize $CRLB_\theta$ for a planar antenna array whose reference point is at the center of the array. The antenna set is selected based on the actual AoAs using the Dinkelbach algorithm for minimization. The problem with this approach is that AAoAs have to be known before minimization. This means that the antenna selection cannot be used for the AAoA estimation phase. Moreover, the complexity of the Dinkelbach algorithm may increase the time consumption of the antenna selection procedure. To overcome these problems, we propose a real-time antenna selection approach.

Our method is composed of two phases. The first phase is when the transmission of pilot signals by UT has not yet begun. In this phase, the only available information at the BS is the possible range and distribution of the AAoA. For example, if the space division multiplexing is not used and the BS has to cover all of the cell, this range would be $[0, 2\pi)$. In this step, we turn on F_p antennas to make a crude estimation of the received AAoA to have a general idea about where the UT is. The value of F_p can be defined by other criteria, like the total energy consumption of the BS. These F_p antennas are selected to minimize the expected $CRLB_\theta$ over the possible range of the AAoA. In this step, we will use a certain percentage of the total transmitted pilot snapshots to acquire a preliminary estimation of the AAoA (we call this estimation θ_p).

Minimizing (5.9) is a Combinatorial optimization problem. After acquiring the θ_p, we can use it to minimize the $CRLB_\theta$. By virtue of the θ_p, we can select a subset of the antennas that specifically minimize the $CRLB_\theta$ instead of its expectation. We use a greedy algorithm and present its optimal starting point. In the greedy approach, one antenna that reduces the $CRLB_\theta$ more than others is selected in each step. The greedy algorithm is chosen for the optimization due to two main reasons. First, it can be run in real-time and very fast, thanks to its simplicity. The running time is significant because this part of the selection process is done while BS receives the pilot signals. Extra delay in the selection process will result in missing transmitted snapshots by the UT. Second, the greedy algorithm has a high level of performance. Later in the numerical result section, we show that the greedy algorithm (with the optimal starting point) obtains almost the same performance as the global search with much lower computational complexity.

Therefore, the steps of the antenna selection algorithm can be summarized as the following:

1. *Preliminary stage*: $F_p \geq 3$ antennas are selected in a way to minimize $\mathbb{E}_\theta\{CRLB_\theta\}$. BS turns on these antennas and awaits the reception of the pilot signals from the UT. Then, it uses these antennas alongside a percentage of the total snapshots to make a Preliminary estimation of θ (that is called θ_p).

2. *Main stage*: Based on the θ_p, a set of antennas are selected to minimize $CRLB_\theta$ using a greedy algorithm. This set will use the remaining snapshots of the pilot signals to estimate θ.

Remark 5. *In addition to helping the antenna selection procedure, θ_p can be used to reduce the computational complexity of the estimation* *of θ in the Main stage. For example, in methods like ML or MUSIC, where a certain range has to be searched for the estimation, only the vicinity of θ_p (with a certain margin) can be the prime candidate to be searched. This reduces the search area and reduces estimation time.*

In the following subsections, the antenna selection of each step is explained.

5.4.1 Preliminary Stage

In this stage, the only available information is the total possible range of θ. As $CRLB_\theta$ is a function of both antennas set and θ, we have to remove its dependency to θ (based on the available information) to be able to use $CRLB_\theta$ as a cost function for minimization. In order to do so, by noting that $\theta \sim U[0, 2\pi)$, the expectation of $CRLB_\theta$ over θ will be

$$\begin{aligned} \mathbb{E}_\theta\{CRLB_\theta\} = & \frac{1}{2\rho\beta^2|h_d|^2\sin^2(\varphi)} \\ & \times \underbrace{\left(\frac{tr(\tilde{\mathbf{\Sigma}}_{p_1}^2) + tr(\tilde{\mathbf{\Sigma}}_{p_2}^2)}{(tr(\tilde{\mathbf{\Sigma}}_{p_1}^2)tr(\tilde{\mathbf{\Sigma}}_{p_2}^2) - tr(\tilde{\mathbf{\Sigma}}_{p_1}\tilde{\mathbf{\Sigma}}_{p_2})^2)} \right)}_{U(\mathcal{S})}, \end{aligned} \tag{5.10}$$

where $\tilde{\mathbf{\Sigma}}_{p_1}$ and $\tilde{\mathbf{\Sigma}}_{p_2}$ contain the corresponding values of F_p selected antennas from $\mathbf{\Sigma}_1$ and $\mathbf{\Sigma}_2$, respectively and $\mathcal{S}$ is the set of selected antennas. The only part related to the antenna set in (5.10) is $U(\mathcal{S})$, so we have to minimize it. First, we explain the process in detail, and then we present and prove it in a theorem.

The optimal antenna selection strategy to minimize $U(\mathcal{S})$ is composed of various steps that depend on the value of the F_p. If $F_p \leq 5$, in addition to the reference point, the four antennas at the corners of the array (i.e. $S_{p_1} = \{(\frac{M}{2}, \frac{M}{2}), (-\frac{M}{2}, \frac{M}{2}), (\frac{M}{2}, -\frac{M}{2}), (-\frac{M}{2}, -\frac{M}{2})\}$) are optimal choices and all of them have the same priority to be selected. This means that if, for example, $F_p = 4$, either combination of three antennas from S_{p_1} (in addition to the reference point) will result in the same value of $U(\mathcal{S})$. So, for $F_p = 4$ any of the following sets are optimal choices with the same values for $U(\mathcal{S})$:

$$\{(0,0),(\frac{M}{2},\frac{M}{2}),(-\frac{M}{2},\frac{M}{2}),(\frac{M}{2},-\frac{M}{2})\},$$
$$\{(0,0),(-\frac{M}{2},-\frac{M}{2}),(-\frac{M}{2},\frac{M}{2}),(\frac{M}{2},-\frac{M}{2})\},$$
$$\{(0,0),(\frac{M}{2},\frac{M}{2}),(-\frac{M}{2},-\frac{M}{2}),(\frac{M}{2},-\frac{M}{2})\},$$
$$\{(0,0),(\frac{M}{2},\frac{M}{2}),(-\frac{M}{2},\frac{M}{2}),(-\frac{M}{2},-\frac{M}{2})\}.$$

For $5 < F_p \leq 13$, the next optimal choices are neighboring antennas of the four antennas at S_{p_1} in the outer most rectangle of the array, i.e. $S_{p_2} = \{(\frac{M}{2}-1,\frac{M}{2}),(1-\frac{M}{2},\frac{M}{2}),(\frac{M}{2},\frac{M}{2}-1),(-\frac{M}{2},\frac{M}{2}-1),(\frac{M}{2},1-\frac{M}{2}),(-\frac{M}{2},1-\frac{M}{2}),(\frac{M}{2}-1,-\frac{M}{2}),(1-\frac{M}{2},-\frac{M}{2})\}$. Again, all of the antennas at S_{p_2} have the same priority to be selected, and if $5 < F_p < 13$, any combination from S_{p_2} (in addition to all of the antennas in S_{p_1} and the reference point) will result in the same value for $U(\mathcal{S})$. For $13 < F_p \leq 21$, the neighbors of the ones selected for $5 < F_p \leq 13$ in the outermost rectangle of the array are optimal choices and so on. Therefore, the process is to start with the four antennas at S_{p_1} at the corners, select their neighbor antennas, and move toward other corners. An example of this process for $M = 6$ is represented graphically in Fig. 5.2. In this figure, four red antennas have the highest priority to be selected. After selecting them, we move in both available directions (shown by solid arrows) to select antennas with blue markers. All antennas with blue markers have the same priority. Then the same procedure is continued by moving in the same directions (showed by dashed arrows) to obtain the next set of antennas, marked by green markers. When all antennas from the outermost rectangle are selected, the same process is repeated from the second outermost rectangle. The following theorem summarizes the optimal selection procedure.

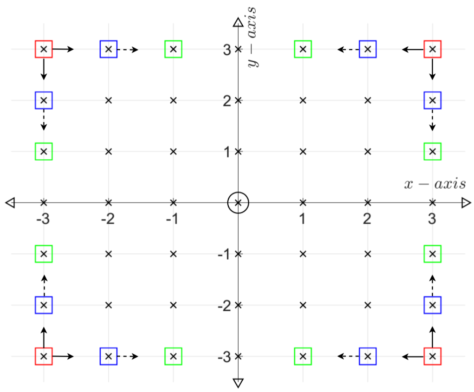

Figure 5.2: Selection Process for θ_p estimation stage.

Theorem 4. *The optimal antenna selection strategy to minimize $\mathbb{E}_\theta\{CRLB_\theta\}$ for $\theta \sim U[0, 2\pi)$ is to start from the four antennas at the corner of the array and then, from each corner, move toward other two corners, selecting antennas from the outermost rectangle. Antennas that have the same distance from their closest corner antenna, have the same priority for selection. When all antennas at the outermost rectangle are selected, the same procedure is repeated in the second outermost rectangle and so on.*

Proof. Please see Appendix C. □

Theorem4 presents the optimal selection strategy when the goal is to minimize $\mathbb{E}_\theta\{CRLB_\theta\}$. This is an extension of our previous work in [56] where we used a greedy algorithm to minimize $\mathbb{E}_\theta\{CRLB_\theta\}$. This strategy itself can be used as an independent selection method. The most important advantage of this method is that the desired set can be determined offline, and there is no need for online calculations, which leads to fast and easy implementation. For the rest of the section, this method of antenna selection is referred to as *expected* method.

Another important aspect of Theorem4 is the shape of the selected antennas. When $F \leq 4(M-1)$, the optimal choice creates four subarrays of antennas. This is in accordance with the same results presented in [54] for large intelligent surfaces, which shows that four smaller subarrays perform better than one big antenna array for AAoA estimation. We saw the same results in [56] when the greedy algorithm is utilized to select antennas, where the goal is to minimize the $\mathbb{E}_\theta\{CRLB_\theta\}$. Furthermore, we will see in Section5.5 that for the real-time antenna selection, where the goal is to minimize $CRLB_\theta$, the greedy algorithm will again create smaller subarrays that are separated from one another.

5.4.2 Main Antenna selection

In this part, we select the total number of desired antennas based on the θ_p, acquired in the previous step. We use a greedy algorithm in this stage to minimize the $CRLB_\theta$. Because $CRLB_\theta$ in (5.9) is for a planar antenna array, the greedy algorithm requires a starting point composed of three antennas selected simultaneously. This means that the first three antennas (the minimum number to form a plane) must be selected together and cannot be selected in a greedy approach. The search for selecting these three antennas together to initiate the greedy algorithm is usually very costly in terms of computational complexity. This is because one has to go through all possible combinations of choosing three antennas over $(M+1)^2$. However, with the help of the following theorem, this complexity will be reduced to only two possible choices for any M. In the following Theorem, we provide the optimal starting set for the greedy algorithm and prove that this set is the best possible choice. The coordinates of the optimal choices are extracted from the pattern observed in the simulations.

Theorem 5. *The optimal first three antennas that minimize $CRLB_\theta$ for different values of θ in the first quarter of the trigonometric circle are as the following:*

If $0 \leq \theta \leq \frac{\pi}{4} - \theta_0$,

$$\mathcal{S}_3 = \{(0,0), (-\frac{M}{2}, \frac{M}{2}), (x_2, \frac{M}{2})\}, \tag{5.11}$$

where

$$x_2 = \begin{cases} \lfloor \frac{M(1-2\alpha)}{2} \rfloor & \textit{if } g_x(\lfloor \frac{M(1-2\alpha)}{2} \rfloor) \leq g_x(\lceil \frac{M(1-2\alpha)}{2} \rceil) \\ \lceil \frac{M(1-2\alpha)}{2} \rceil & \textit{if } g_x(\lfloor \frac{M(1-2\alpha)}{2} \rfloor) > g_x(\lceil \frac{M(1-2\alpha)}{2} \rceil), \end{cases}$$

If $\frac{\pi}{4} - \theta_0 < \theta < \frac{\pi}{4} + \theta_1$,

$$\mathcal{S}_3 = \{(0,0), (-\frac{M}{2}, \frac{M}{2} - 1), (1 - \frac{M}{2}, \frac{M}{2})\}, \tag{5.12}$$

If $\frac{\pi}{4} + \theta_1 \leq \theta \leq \frac{\pi}{2}$,

$$\mathcal{S}_3 = \{(0,0), (-\frac{M}{2}, \frac{M}{2}), (-\frac{M}{2}, y_2)\}, \tag{5.13}$$

where

$$y_2 = \begin{cases} \lfloor \frac{M(2-\alpha)}{2\alpha} \rfloor & \textit{if } g_y(\lfloor \frac{M(2-\alpha)}{2\alpha} \rfloor) \leq g_y(\lceil \frac{M(2-\alpha)}{2\alpha} \rceil) \\ \lceil \frac{M(2-\alpha)}{2\alpha} \rceil & \textit{if } g_y(\lfloor \frac{M(2-\alpha)}{2\alpha} \rfloor) > g_y(\lceil \frac{M(2-\alpha)}{2\alpha} \rceil), \end{cases}$$

$\alpha = \tan(\theta)$,

$$g_x(x) = \frac{(1-\alpha)^2 + (\frac{2}{M}x + \alpha)^2}{(\frac{M}{2} + x)^2}, \tag{5.14}$$

$$g_y(x) = \frac{(1-\alpha)^2 + (\frac{2\alpha}{M}x - 1)^2}{(\frac{M}{2} - x)^2}, \tag{5.15}$$

$\theta_0 = \tan^{-1}(x_2)$ *and* $\theta_1 = \tan^{-1}(\frac{M^2(3M^2-6M+2)x_1}{(M-2)(3M-2)(M^2-2M+2)})$ *where* x_2 *and* x_1 *are the bigger and the smaller root of the following equation (solved* *for x), respectively*

$$
\begin{aligned}
&M^2(3M^2-6M+2)x^2-2M(3M^3-10M^2+12M-4)x\\
&+(M-2)(3M-2)(M^2-2M+2)=0.
\end{aligned}
\tag{5.16}
$$

Proof. Please see Appendix D. $\square$

Using same procedure the following sets are the optimal start set for other ranges of θ:

If $\frac{\pi}{2} < \theta \leq \frac{3\pi}{4} - \theta_0$,

$$\mathcal{S}_3 = \{(0,0), (\frac{M}{2}, \frac{M}{2}), (\frac{M}{2}, y_2)\}, \tag{5.17}$$

where

$$y_2 = \begin{cases} \lfloor\frac{-M(2+\alpha)}{2\alpha}\rfloor & \textit{if } g_{2,y}(\lfloor\frac{-M(2+\alpha)}{2\alpha}\rfloor) \leq g_{2,y}(\lceil\frac{-M(2+\alpha)}{2\alpha}\rceil) \\ \lceil\frac{-M(2+\alpha)}{2\alpha}\rceil & \textit{if } g_{2,y}(\lfloor\frac{-M(2+\alpha)}{2\alpha}\rfloor) > g_{2,y}(\lceil\frac{-M(2+\alpha)}{2\alpha}\rceil), \end{cases}$$

If $\frac{3\pi}{4} - \theta_0 < \theta < \frac{3\pi}{4} + \theta_1$,

$$\mathcal{S}_3 = \{(0,0), (\frac{M}{2}, \frac{M}{2} - 1), (\frac{M}{2} - 1, \frac{M}{2})\}, \tag{5.18}$$

If $\frac{3\pi}{4} + \theta_1 \leq \theta < \pi$,

$$\mathcal{S}_3 = \{(0,0), (\frac{M}{2}, \frac{M}{2}), (x_2, \frac{M}{2})\}, \tag{5.19}$$

where

$$x_2 = \begin{cases} \lfloor\frac{-M(1+2\alpha)}{2}\rfloor & \textit{if } g_{2,x}(\lfloor\frac{-M(1+2\alpha)}{2}\rfloor) \leq g_{2,x}(\lceil\frac{-M(1+2\alpha)}{2}\rceil) \\ \lceil\frac{-M(1+2\alpha)}{2}\rceil & \textit{if } g_{2,x}(\lfloor\frac{-M(1+2\alpha)}{2}\rfloor) > g_{2,x}(\lceil\frac{-M(1+2\alpha)}{2}\rceil), \end{cases}$$

$$g_{2,x}(x) = \frac{(1+\alpha)^2 + (\frac{2}{M}x + \alpha)^2}{(\frac{M}{2} - x)^2}, \tag{5.20}$$

$$g_{2,y}(x) = \frac{(1+\alpha)^2 + (\frac{2\alpha}{M}x + 1)^2}{(\frac{M}{2} - x)^2}. \tag{5.21}$$

For $\pi < \theta \leq \frac{5\pi}{4} - \theta_0$, $\frac{5\pi}{4} - \theta_0 < \theta < \frac{5\pi}{4} + \theta_1$, $\frac{5\pi}{4} + \theta_1 \leq \theta < \frac{3\pi}{2}$, $\frac{3\pi}{2} < \theta \leq \frac{7\pi}{4} - \theta_0$, $\frac{7\pi}{4} - \theta_0 < \theta < \frac{7\pi}{4} + \theta_1$ and $\frac{7\pi}{4} + \theta_1 \leq \theta < 2\pi$ the optimal choices are exactly same as the ones for $0 < \theta \leq \frac{\pi}{4} - \theta_0$, $\frac{\pi}{4} - \theta_0 < \theta < \frac{\pi}{4} + \theta_1$, $\frac{\pi}{4} + \theta_1 \leq \theta < \frac{\pi}{2}$, $\frac{\pi}{2} < \theta \leq \frac{3\pi}{4} - \theta_0$, $\frac{3\pi}{4} - \theta_0 < \theta < \frac{3\pi}{4} + \theta_1$ and $\frac{3\pi}{4} + \theta_1 \leq \theta < \pi$, respectively.

By virtue of Theorem 5, the choice of the first three antennas for any M is reduced to only two sets. For example, suppose we have an array of 81 antennas. In that case, the total number of possible sets for the start point is $\binom{80}{2} = 3160$ cases. Such a search pool can prevent antenna selection in real-time, but this problem is solved with the help of Theorem 5. Now that we have an optimal starting point for the greedy algorithm, by using the characteristics of the $CRLB_\theta$ formulation, it is possible to reduce the search area of the greedy algorithm to half.

Corollary 5.1. *Every antenna selected in the Main Stage, either for the start set or by the greedy algorithm, has the same contribution in the* $CRLB_\theta$ *as its reciprocal counterpart w.r.t the reference point and can be replaced with it.*

Proof. Consider that in the nth step of the greedy algorithm if $(-x_1, -y_1)$ is added instead of (x_1, y_1). By noting the formulation of $U(s)$, at the numerator all the elements of both $\tilde{\mathbf{\Sigma}}_1$ and $\tilde{\mathbf{\Sigma}}_2$ are squared before addition. So, all x and y elements are squared and changing the sign of those elements will not affect the nominator. In the denominator, again the $tr(\tilde{\mathbf{\Sigma}}_1^2)tr(\tilde{\mathbf{\Sigma}}_2^2)$ will not be affected due to the fact that their elements are squared. For $tr(\tilde{\mathbf{\Sigma}}_1\tilde{\mathbf{\Sigma}}_1)$, each x is multiplied by its corresponding y, so if the sign of both of them are changed simultaneously, the final result will not change. $\square$

By virtue of the Corollary 5.1, the search area of the greedy algorithm will be restricted only to half of the antenna array. This is because when the contribution of the antennas in the first half is calculated, the contribution of all of the antennas in the other half will be the same as the first one. This significantly reduces the computational complexity of the greedy algorithm, which is essential for real-time utilization. The complete procedure of the real-time antenna selection algorithm is presented in Table. 5.1.

Contrary to previous implementations of greedy algorithms for antenna selection, the real-time antenna selection algorithm presented in Table.1 uses the instantaneous $CRLB_\theta$ of a planar antenna array as its cost function. This feature is possible due to two main entries that are fed into the algorithm. First is the preliminary estimation (θ_p) acquired in the algorithm's preliminary stage. Second, the optimal start point for every θ_p composed of three antennas. Calling the total number of antennas N, and noting that only the Main stage is going to be run in real-time, the algorithm at the fth stage has to search an antenna pool composed of $N-(F-3)$ antennas. So, the total number of iterations to select F antennas is

$$\sum_{f=1}^{F-3}(N-f)=(F-3)N-\frac{(F-3)(F-2)}{2}=(F-3)(N-\frac{F}{2}+1). \tag{5.22}$$

The highest order of complexity in (5.22) is $\mathcal{O}(NF)$. The presented algorithms in [72] and [73] have complexity order of $\mathcal{O}(N^3)$ and $\mathcal{O}(N^6)$, respectively. By noting $F<N$, we have $\mathcal{O}(NF)<\mathcal{O}(N^3)<\mathcal{O}(N^6)$, meaning that our algorithm has much lower computational complexity compared to these works. Also, methods in [72, 73] have an optimization inside their algorithm, where we only have a simple calculation of the $CRLB$ function that further reduces the computational complexity.

In certain applications where the AAoA of a UT is being tracked like [20, 75], the preliminary stage of the antenna selection can be ignored. Suppose the frequency of tracking estimation is fast enough that the AAoA of the UT is not hugely changed. In that case, based on the previous estimation of the UT's AAoA, the system has a fair idea of the current AAoA. So, the preliminary estimation stage can be removed, and θ_p can be replaced with the estimation of the previous AAoA. This will help such applications implement real-time antenna selection with even lower computational complexity.

Remark 6. *From* (5.9)*,* (5.10)*,* (D.1) *and the presented results in [56], it is evident that changing the channel model to the DMC model does not affect the antenna selection procedure. The real-time antenna selection can also be used in the DMC channels. Also, in the presence of inter-symbol interference (ISI) with independent channel coefficients and AAoAs will not change the antenna selection part in* (5.9)*,* (5.10) *and* (D.1)*. So, the presented antenna selection methods can be implemented for any distribution of channel coefficients and/or in the presence of independent ISI.*

5.5 Numerical Results

In this section, we test the presented theorems by various simulations. As a benchmark, the performance of real-time antenna selection is compared with the expected antenna selection method. In the expected method, only the preliminary stage (presented in section5.4.1), of the proposed antenna selection is used (also related to our work previous work [56]). Also, we compare both selection methods with a strategy in which the preliminary stage is done, but the start point of the greedy algorithm is randomly selected, and θ_p is only used in the greedy algorithm's cost function (i.e. Theorem5 is not used)[3]. Unless otherwise stated, in the following figures, $\frac{d}{\lambda} = 0.5$,

[3] Unlike [65, 67, 71], we do not compare our results with total random selection method (in which all of the antennas are selected randomly) as it performs so poorly that it distorts the scale of plots. One can better appreciate small differences in different selection methods in the current view.

get F_p, F	
Select F_p antennas based on Theorem4. Estimate θ_p.	Preliminary Stage

Using θ_p, select $\mathcal{S}_3$ based on Theorem5.
$\mathcal{S} := \mathcal{S}_3$
For $f := 4$ **to** F **do**
    For $x := 0$ **to** $M/2$ **do**
        For $y := 0$ **to** $M/2$ **do**
            If $(x, y) \notin \mathcal{S}$ **do**
                $\mathcal{S}(f) := (x, y)$
                $\boldsymbol{V}(x, y) := CRLB_\theta(\mathcal{S})$
            EndIf
        EndFor
    EndFor
    $\mathcal{S}(f) := \arg\min_{(x,y)} \boldsymbol{V}$
EndFor
return $\mathcal{S}$
	Main Stage

Table 5.1: Real-time antenna selection algorithm.

$|h_d|^2 = 1$, $\rho = 0dB$ and $\varphi = \frac{\pi}{3}$.

Fig. 5.3 shows the $CRLB_\theta$ for all possible AAoAs when only three antennas are selected, using different methods for $M = 6$. The red curve is $CRLB_\theta$ when three antennas are selected to minimize $\mathbb{E}_\theta\{CRLB_\theta\}$. The blue and green curves result from selecting antennas to minimize instantaneous $CRLB_\theta$, using Theorem 5 and global search, respectively. Moreover, the dotted lines show $\theta_0 = 43.1352°$ and $\theta_1 = 46.8648°$, where the optimal choices change according to (5.12) and (5.16). It is seen that Theorem 5 is perfectly capable of predicting the optimal set for the first three antennas.

Fig. 5.4a indicates the resulted $CRLB_\theta$ versus θ for different antenna selection strategies and scenarios. In this figure, $M = 6$ and $F = 13$. The magenta curve results when antennas are selected to

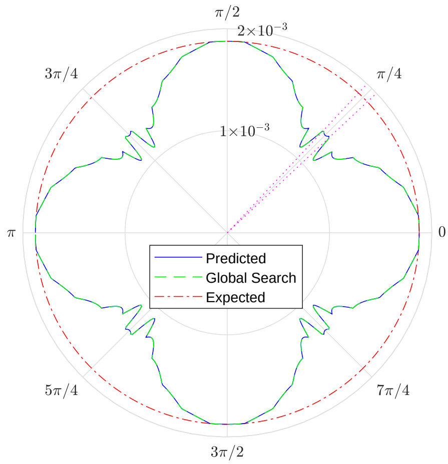

Figure 5.3: $CRLB_\theta$ versus θ for $F = 3$ and different selection methods.

minimize $\mathbb{E}_\theta\{CRLB_\theta\}$. The cyan curve is for the case when all of the available antennas are used ($F = (M+1)^2$). The green curve results from the real-time greedy method, when AAoA is perfectly known, i.e., $\theta_p =$AAoA. It is seen that the real-time antenna selection method secures between 52% and 68% of total performance (depending on the value of θ), only by using a quarter of the total available antennas. Moreover, the expected antenna selection method achieves %45 of total performance. The star markers ($*$) show the $CRLB_\theta$ that is obtained through global search, i.e., the global minimum for $F = 13$. It is seen that the greedy algorithm obtains a very close performance to global search with much less computational complexity, indicating that the greedy algorithm with an optimal start point is a reasonable choice for antenna selection. In the blue curve, constant noise is added to the θ_p to show how the selection strategy performs when $\theta_p \neq$ AAoA. The noise value is 2.5° with a random positive or negative sign, i.e., $\theta_p =$AAoA$\pm 2.5^\circ$. It should be noted that the $CRLB_\theta$ is in the order of 3×10^{-4} ($\approx 0.01^\circ$), and the added error is more than two orders of magnitude higher than $CRLB_\theta$. It is seen that even with this amount of error, the selection process is performing so close to the optimal case. Also, this curve shows that different AAoAs have different tolerances against error in θ_p. It should be noted that an error in θ_p affects both parts of the real-time selection algorithm, the start set and the greedy part. This amount of error tolerance can motivate one to create a look-up table for the real-time antenna selection by selecting a set for every $2.5°$ (or any other value) and using a proper set according to the value of θ_p to extremely simplify the antenna selection procedure. The red curve with a random start set is plotted to see the effects of the optimal start set. In this curve, the optimal start set proposed by Theorem5 is not used. Instead, two random antennas are selected in addition to the reference point. The greedy part is the same as the blue curve, and θ_p is used in the greedy part of the red curve. It is seen that, in general, $CRLB_\theta$ deteriorates when the optimal start point is not used, sometimes even worse than the expected method. This highlights the importance of the optimal start point, presented in Theorem5.

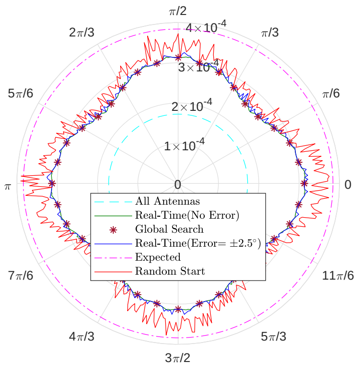

(a) $F = 13$ and $M = 6$.

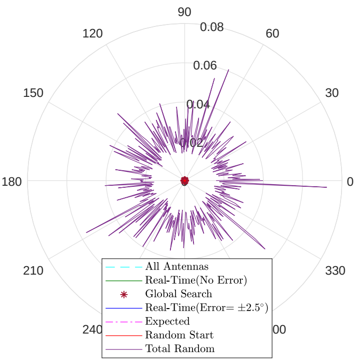

(b) $F = 13$ and $M = 6$.

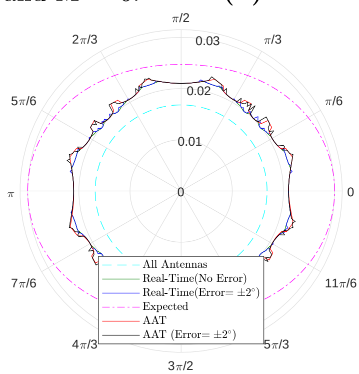

(c) $F = 11$ and $M = 4$.

Figure 5.4: $CRLB_\theta$ versus θ for different selection strategies and scenarios.

In Fig.5.4b the same curves are plotted Fig.5.4a, in addition to the resulted $CRLB_\theta$ when all of the antennas are selected randomly. As seen, the total random selection distorts the scale of the plot so much that it is impossible to appreciate the differences of other methods from one another, indicating the significant advantage of using an antenna selection method that take into account the $CRLB_\theta$ of the system.

In Fig.5.4c, our proposed method is compared with another antenna selection method proposed in [72]. In [72], a Dinklebach type algorithm is used in CVX to minimize the $CRLB$. This selection method is named AAT. AAT is compared in two scenarios in Fig. 5.4c, first actual θ is fed into the algorithm, and second, 2° of error is added when feeding the algorithm. Our proposed real-time method is also simulated in the same scenarios. In all the cases, $F = 11$. It is seen that with the same inputs, when actual θ is used, the real-time algorithm is always better. Also, when there is an error, the real-time algorithm performs better in most points. Our algorithm obtains this performance with much less computational complexity (resulting in lower run time) and the possibility of being implemented in real-world scenarios.

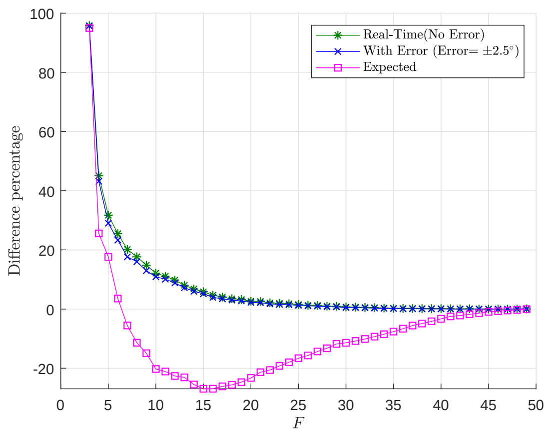

Figure 5.5: Performance improvement percentage of different methods relative to real-time method with random start point.

Fig. 5.5 shows the relative advantage of real-time and expected antenna selection methods to the selection method in which only the start point is selected randomly, i.e., θ_p is only used in the greedy part.

For all curves, each point is calculated as $\frac{\sum_{\theta=0}^{2\pi}([CRLB_{\theta}]_R - [CRLB_{\theta}]_A)}{N\sum_{\theta=0}^{2\pi}[CRLB_{\theta}]_R}$, where $[CRLB_{\theta}]_A$ means the $CRLB_{\theta}$ resulted by using method A, and A can be real-time (either with or without error) or expected method, $[CRLB_{\theta}]_R$ means the $CRLB_{\theta}$ resulted by using real-time method with random start point and N is total number of angles that have been summed. This figure aims to show that for every F, how using proposed methods, namely real-time with optimal start point, increases the performance w.r.t the case in which the real-time method is utilized but with the random start point. It is seen that when F is relatively small, by using the presented optimal start set, the performance increases significantly. As F grows, the difference in performance decreases. This is because as more and more antennas are selected, even if the start set is selected randomly, other antennas that are selected in the greedy section by the random algorithm will make up a considerable portion of the total selected antennas. So the contribution of two optimally selected antennas for the start set will decrease. Therefore, as more antennas are selected, the importance of the optimal start set reduces because antennas with high contributions will be selected one way or another. Another point of Fig. 5.5 is the behavior of the curve for the expected antenna selection method. First, it has a positive relative performance. Then it becomes negative, meaning that for certain F expected method is better than the real-time with a random start point. As F increases, the real-time approach, even with a random start point, is better than the expected method.

In Fig. 5.6, antenna selection is applied to the Maximum-likelihood estimator. In this figure, $\theta = \pi/6$, $\varphi = \pi/3$, $F_p = 4$ and, $M = 6$. Fig. 5.6a indicates the estimation variance for different numbers of selected antennas. As predicted by Fig. 5.5, soon after small values of F, real-time antenna selection performs better than the expected method. Also, as F increases, real-time selection with optimal and random start become closer. In Fig. 5.6b, the percentage of obtained performance versus the percentage of utilized antennas are plotted to

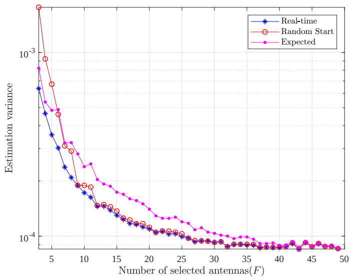

(a) Variance of ML estimator for different number of antennas.

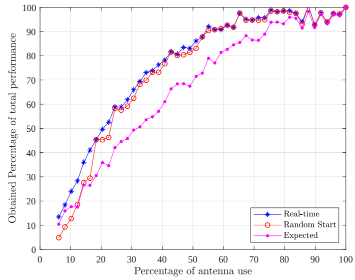

(b) Percentage of obtained performance versus percentage of used antennas.

Figure 5.6: Performance analysis of ML estimator with different antenna selection methods.

show the effectiveness of each antenna selection method. The real-time antenna selection obtains more than 80% of total performance only by using half of the available antennas, showing the effectiveness of antenna selection in improving both hardware and energy efficiency.

Fig. 5.7 is plotted to further examine how the main real-time antenna selection method (the one that takes advantage of the optimal start set) performs compared to the expected method. This figure represents how error tolerant the real-time antenna selection is, compared with the expected antenna selection method. In this figure, the x-axis is the AAoA, and the y-axis is the number of selected antennas. For each point in this 2D plane, the color indicates how much error the real-time algorithm can bear in the preliminary stage and still have lower $CRLB_\theta$ than the antenna selection method that minimizes expected $CRLB_\theta$. A deep blue color means lower error tolerance, and the more the color of a point becomes reddish, the higher the error can be tolerated by the real-time algorithm. It is seen that starting after $\frac{\pi}{3}$ up to around $\frac{\pi}{2}$, between $5 \leq F \leq 20$ for $M = 4$ and between $10 \leq F \leq 40$ for $M = 6$, the real-time algorithm shows its highest resistance. Moreover, increasing the number of antennas makes the

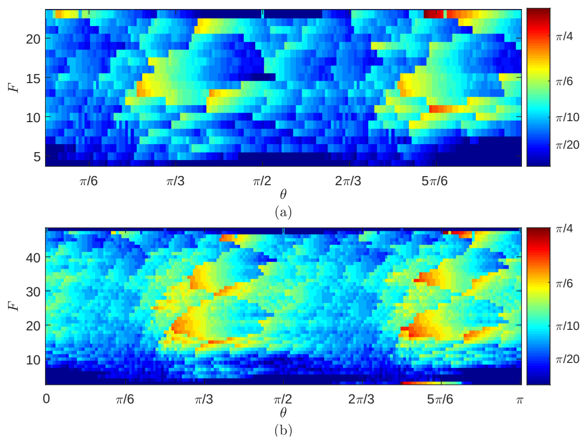

Figure 5.7: Error tolerance of real-time antenna selection strategy for: (a) $M = 4$ and (b) $M = 6$.

real-time algorithm more error tolerant. This means that the real-time selection method performs very well when F is around half of the M, i.e., for relatively moderate values of F. Also, it should be noted that the reason for the low error tolerance in higher values of F is that as most of the antennas are already selected by both selection strategies, the $CRLB_\theta$ is reaching its final value (that is using $(M+1)^2$ antennas) and then even selecting one antenna with lower priority results in a very small but higher value for $CRLB_\theta$, so error tolerance is low. However, despite lower tolerance, the value of resulted $CRLB_\theta$ is very close for both strategies.

In Fig. 5.8, the inverse product of F and $CRLB_\theta$ is plotted for $M = 6$ and $M = 4$ to show how efficiently each selection strategy is using its selected antennas. This can be seen as a basic study and can be modified for any efficiency study, like the energy efficiency of AoA estimation introduced in chapter 3. In this figure, in both real-time and expected selection methods for each F, the average value for all possible θs are plotted, i.e. $\frac{1}{N}\sum_{\theta=0}^{2\pi} CRLB_\theta$ where N is total

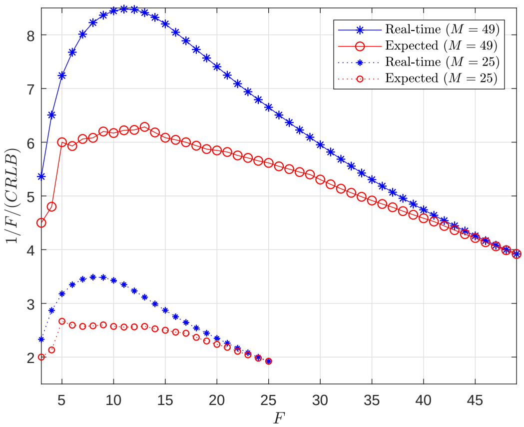

Figure 5.8: The inverse of the product of $CRLB$ and F, versus F.

number of θs that are summed. It is seen that the real-time selection method always obtains higher efficiency in terms of antenna usage. As expected from Fig. 5.7, the region where real-time selection has the highest efficiency difference w.r.t the expected antenna selection corresponds to the same region where real-time selection also has higher error tolerance. Also, noting that the endpoints of the curves indicate the efficiency of antenna usage without antenna selection, significantly higher efficiencies can be obtained by making use of antenna selection.

Finally, in Fig. 5.9 an example of the selected antennas by the presented algorithms for $M = 6$, $F = 20$ and $\theta = \frac{\pi}{3}$ is plotted. In this figure, square markers show the selected antennas by the real-time antenna selection (without error). The blue squares indicate start points for the greedy algorithm, and the greedy algorithm selected magenta ones. Also, green circles demonstrate the selected antennas by the expected algorithm. We observe that the greedy algorithm creates two separate subarrays to estimate AAoA. This result that several smaller subarrays perform better than one big array is also reported for large

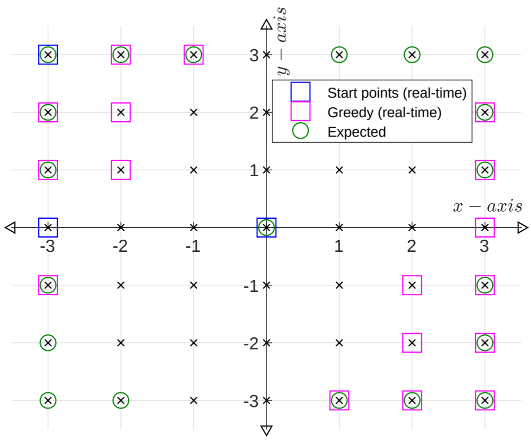

Figure 5.9: Selected antennas by both real-time and expected algorithms for $F = 20$ and $\theta = \frac{\pi}{3}$.

intelligent surfaces in [54] and Massive MIMO systems in [56]. Our results for both expected and real-time antenna selection methods are in accordance with these results.

5.6 Conclusion

This section studied antenna selection for AAoA estimation for a square planar antenna array. We proposed two CRLB based antenna selection methods for AAoA estimation. In the first method, motivated by our previous studies, the goal is to minimize the expected value of the $CRLB_\theta$. The optimal strategy for antenna selection in this scenario is presented.

Next, a two-step real-time antenna selection method is developed using the first introduced antenna selection method. This method selects an initial set of antennas to minimize the expected $CRLB_\theta$. Using this set, a fast and crude estimation of AAoA is done. Then the estimated AAoA is used in a greedy algorithm whose objective function is to minimize instantaneous $CRLB_\theta$. The optimal start point of the algorithm is presented to make the algorithm fast enough (so it can be run in real-time). Moreover, a corollary that reduces the search space to half the available antennas is presented to reduce the algorithm's computational complexity.

Numerical results show a considerable gain in performance when either one of the methods is employed. Also, it is shown that a greedy algorithm with an optimal starting point obtains quite close performance to global search. Furthermore, both presented algorithms' error tolerance and efficiency of antenna usage are compared with one another and with the real-time method, whose start point is random. It is seen that for a moderate number of active antennas, the real-time antenna selection (with optimal start point) has its highest error tolerance and efficiency w.r.t the antenna selection method that aims to minimize expected $CRLB_\theta$.

CHAPTER 6

Conclusion

This thesis has focused on improving energy efficiency and performance in the localization phase of massive MIMO systems, addressing key challenges and proposing solutions in the context of AoA estimation.

In Chapter 3, we analyzed the CRLB for AoA estimation in the presence of multipath signals using the DMC model. Utilizing Random Matrix Theory, we demonstrated that the CRLB for AoA converges toward a deterministic expression independent from the multipath signals distribution in MU massive MIMO settings. This finding underscores the significant role of multipath signals in enhancing AoA estimation accuracy, providing a theoretical foundation for recent studies that take advantage of multipath signals to extract location information. Furthermore, we introduced a refined LE metric, which balances performance and energy consumption in localization. Through a comprehensive energy consumption model, we identified an optimal number of antennas that maximizes LE for a linear antenna array and proposed an antenna selection method that minimizes CRLB for AoA.

In Chapter 4, we extended our investigation to planar antenna arrays in MU massive MIMO systems. By applying RMT, we showed that the CRLB for AAoA estimation converges to a deterministic expression dependent on system parameters rather than instantaneous channel realizations. This result indicates that AAoA information remains robust even under poor dominant path conditions, validating the effectiveness of using multipath signals for refined estimation. We also studied the antenna selection problem in planar antenna arrays. To address the problem of lack of knowledge of the AAoA to minimize the CRLB, we used the ECRLB, where the expectation is over all possible realizations of AAoAs. We concluded that a greedy algorithm with ECRLB as its cost function and optimal starting set, significantly enhances AAoA estimation performance compared to other benchmarks.

Chapter 5 focused on antenna selection for AAoA estimation using a square planar antenna array. We proposed a two step CRLB-based antenna selection method that minimizes the instantaneous CRLB. In the first stage, that aims at minimizing the ECRLB for AAoA, we presented an optimal strategy for antenna selection. Building on this, we developed a two-step real-time antenna selection method. This method initially selects antennas to minimize the expected CRLB, followed by a crude AAoA estimation used to further refine the selection through a greedy algorithm, whose cost function is instantaneous CRLB. The optimal starting point for this algorithm is also presented to ensure real-time feasibility. To the best of our knowledge, the proposed solution is the first presented solution to address the problem of instantaneous CRLB minimization.

In summary, this thesis has contributed to the field of massive MIMO systems by improving the accuracy and energy efficiency of the localization phase. Our work on CRLB convergence, refined LE metrics, and antenna selection strategies provides a solid foundation for future research and practical implementations in next-generation wireless networks.

6.1 Future Works

This thesis has provided the ground for further research in several directions. By virtue of a deterministic CRLB for MU Massive MIMO systems, a more realistic CRLB is now available for AoA estimation methods that make use of multipath signals. This can result in better tuning of algorithms and methods that incorporate multipath signals to estimate AoA.

Furthermore, another possible direction is further investigations of resource allocation and antenna selection strategies in the localization phase. For instance, the study of optimal antenna selection strategies in scenarios where designers want to simultaneously minimize the instantaneous CRLBs for both azimuth and elevation AoAs. This topic requires a minimization of combined CRLBs. How should one combine these two CRLBs and what are the pros and cons of different combinations can also be studied to provide comprehensive options for designing any type of wireless networks.

In this work, we have focused on optimizing antenna selection based on the CRLB as a measure of estimation accuracy. While the CRLB provides a fundamental limit on the variance of unbiased estimators, it does not explicitly account for resolution capabilities, which are also critical in many sensing and estimation applications. Incorporating resolution-related metrics (e.g., ambiguity function properties or sidelobe suppression) could further refine the antenna selection process, particularly in scenarios where distinguishing closely spaced sources is essential. Future extensions of this work could explore multi-objective optimization frameworks that jointly consider accuracy (CRLB) and resolution, thereby offering a more comprehensive approach to antenna selection.

APPENDIX A

Proof of Lemma 3

By defining $\gamma = \beta(\cos(\theta_1) - \cos(\theta_2))$, from [76] we know that when $\gamma \neq 0$

$$\lim_{M\to\infty} \underbrace{\frac{1}{M^3}\sum_{m=1}^{M} m^2 \cos(m\gamma)}_{\triangleq V(M,\gamma)} = 0. \tag{A.1}$$

Also, we know that $-2\beta < \gamma < 2\beta$, therefore by defining the set A as

$$A = \{\gamma \in (-2\beta, 2\beta) : \lim_{M\to\infty} V(M,\gamma) = 0\} \tag{A.2}$$

we have

$$P(A) = P(\cos(\theta_1) \neq \cos(\theta_2)) \tag{A.3}$$

By noting that $\theta \sim U[0,\pi]$, we know that the probability of two users having exact same AoA is zero, therefore, $P(A) = 1$. So, as $M \to \infty$, $V(M,\gamma)$ is zero with probability one, that is the definition of the almost sure convergence.

APPENDIX B

Proof of Theorem 1

Generally, $\boldsymbol{X}$ is a complex matrix, composed from two real and imaginary parts, so we can write it as

$$\boldsymbol{X} = M\boldsymbol{\Sigma}^{\frac{1}{2}}(\boldsymbol{A} + j\boldsymbol{B})\boldsymbol{D}, \tag{B.1}$$

where

$$\boldsymbol{\Sigma} = \beta^2 diag(0, \frac{1}{M^2}, \frac{4}{M^2}, \ldots, \frac{(M-1)^2}{M^2}), \tag{B.2}$$

$$\boldsymbol{D} = diag(\sin^2(\theta_1)|s_1|\sqrt{l(r_1)}, \ldots, \sin^2(\theta_K)|s_K|\sqrt{l(r_K)}), \tag{B.3}$$

As $\boldsymbol{\Sigma}$ is a diagonal matrix, its singular values are its diagonal elements. From Eq. B.3, the largest singular value of $\boldsymbol{\Sigma}$ is equal to 1. Therefore, the spectral norm of $\boldsymbol{\Sigma}$ is bounded [52]. If we replace Eq. B.1 in $\boldsymbol{X}^H\boldsymbol{X}$, we have

$$\begin{aligned}\boldsymbol{X}^H\boldsymbol{X} &= M^2\boldsymbol{D}(\boldsymbol{A} + j\boldsymbol{B})^H\boldsymbol{\Sigma}(\boldsymbol{A} + j\boldsymbol{B})\boldsymbol{D} \\ &= M^2\boldsymbol{D}(\boldsymbol{A}^T\boldsymbol{\Sigma}\boldsymbol{A} + \boldsymbol{B}^T\boldsymbol{\Sigma}\boldsymbol{B})\boldsymbol{D} + jM^2\boldsymbol{D}(\boldsymbol{A}^T\boldsymbol{\Sigma}\boldsymbol{B} - \boldsymbol{B}^T\boldsymbol{\Sigma}\boldsymbol{A})\boldsymbol{D}.\end{aligned} \tag{B.4}$$

Therefore

$$\mathcal{R}e(\boldsymbol{X}^H\boldsymbol{X}) = M^2\boldsymbol{D}(\boldsymbol{A}^T\boldsymbol{\Sigma}\boldsymbol{A} + \boldsymbol{B}^T\boldsymbol{\Sigma}\boldsymbol{B})\boldsymbol{D}. \tag{B.5}$$

We can decompose $(\boldsymbol{A}^T\boldsymbol{\Sigma}\boldsymbol{A} + \boldsymbol{B}^T\boldsymbol{\Sigma}\boldsymbol{B})$ as

$$\boldsymbol{A}^T\boldsymbol{\Sigma}\boldsymbol{A}+\boldsymbol{B}^T\boldsymbol{\Sigma}\boldsymbol{B} = (\bar{\boldsymbol{A}}^T\boldsymbol{\Sigma}\bar{\boldsymbol{A}}+\bar{\boldsymbol{B}}^T\boldsymbol{\Sigma}\bar{\boldsymbol{B}})+\sigma_h^2(\hat{\boldsymbol{A}}^T\boldsymbol{\Sigma}\hat{\boldsymbol{A}}+\hat{\boldsymbol{B}}^T\boldsymbol{\Sigma}\hat{\boldsymbol{B}}), \tag{B.6}$$

in which

$$\begin{aligned}
\bar{\boldsymbol{A}}_{m,k} &= \mathcal{R}e\{\bar{h}_k e^{-j(m\beta\cos(\theta_k)+\varphi_k)}\}, \\
\bar{\boldsymbol{B}}_{m,k} &= \mathcal{I}m\{\bar{h}_k e^{-j(m\beta\cos(\theta_k)+\varphi_k)}\}, && \text{(B.7)} \\
\hat{\boldsymbol{A}}_{m,k} &= \frac{1}{\sqrt{\sigma_h^2}}\mathcal{R}e\{\hat{h}_{m,k} e^{-j(m\beta\cos(\theta_k)+\varphi_k)}\}, \\
\hat{\boldsymbol{B}}_{m,k} &= \frac{1}{\sqrt{\sigma_h^2}}\mathcal{I}m\{\hat{h}_{m,k} e^{-j(m\beta\cos(\theta_k)+\varphi_k)}\}, && \text{(B.8)}
\end{aligned}$$

and φ_k is phase of kth transmitted pilot. So, Eq.B.5 can be written as

$$\begin{aligned}
\mathcal{R}e(\boldsymbol{X}^H\boldsymbol{X}) = {} & M^2\boldsymbol{D}(\bar{\boldsymbol{A}}^T\boldsymbol{\Sigma}\bar{\boldsymbol{A}} + \bar{\boldsymbol{B}}^T\boldsymbol{\Sigma}\bar{\boldsymbol{B}})\boldsymbol{D} \\
& + M^2\sigma_h^2\boldsymbol{D}(\hat{\boldsymbol{A}}^T\boldsymbol{\Sigma}\hat{\boldsymbol{A}} + \hat{\boldsymbol{B}}^T\boldsymbol{\Sigma}\hat{\boldsymbol{B}})\boldsymbol{D}. && \text{(B.9)}
\end{aligned}$$

Now, we investigate the behavior of both parts of the right hand side of Eq. B.9 separately. First, we analyze $\bar{\boldsymbol{A}}^T\boldsymbol{\Sigma}\bar{\boldsymbol{A}} + \bar{\boldsymbol{B}}^T\boldsymbol{\Sigma}\bar{\boldsymbol{B}}$. The (k_1, k_2)th element of this matrix will be

$$\begin{aligned}
(\bar{\boldsymbol{A}}^T\boldsymbol{\Sigma}\bar{\boldsymbol{A}} + \bar{\boldsymbol{B}}^T\boldsymbol{\Sigma}\bar{\boldsymbol{B}})_{k_1,k_2} = {} & \mathcal{R}e\{\bar{h}_{k_1}\boldsymbol{a}_{Rx}(\theta_{k_1})^T\}\boldsymbol{\Sigma}\mathcal{R}e\{\bar{h}_{k_2}\boldsymbol{a}_{Rx}(\theta_{k_2})\} \\
& + \mathcal{I}m\{\bar{h}_{k_1}\boldsymbol{a}_{Rx}(\theta_{k_1})^T\}\boldsymbol{\Sigma}\mathcal{I}m\{\bar{h}_{k_2}\boldsymbol{a}_{Rx}(\theta_{k_2})\}.
\end{aligned} \tag{B.10}$$

For any two random variables p and q, we have

$$\mathcal{R}e\{pq^*\} = \mathcal{R}e\{p\}\mathcal{R}e\{q\} + \mathcal{I}m\{p\}\mathcal{I}m\{q\}. \tag{B.11}$$

So

$$(\bar{\boldsymbol{A}}^T \boldsymbol{\Sigma} \bar{\boldsymbol{A}} + \bar{\boldsymbol{B}}^T \boldsymbol{\Sigma} \bar{\boldsymbol{B}})_{k_1,k_2}$$
$$= \mathcal{R}e\{\bar{h}_{k_1}^* \bar{h}_{k_2} e^{j(\varphi_{k_1} - \varphi_{k_2})} \boldsymbol{a}_{Rx}(\theta_{k_1})^H \boldsymbol{\Sigma} \boldsymbol{a}_{Rx}(\theta_{k_2})\}. \tag{B.12}$$

Using Lemma 3, we obtain

$$\bar{\boldsymbol{A}}^T \boldsymbol{\Sigma} \bar{\boldsymbol{A}} + \bar{\boldsymbol{B}}^T \boldsymbol{\Sigma} \bar{\boldsymbol{B}} \xrightarrow{a.s.} \frac{tr(\boldsymbol{\Sigma})}{M} diag(|\bar{h}_1|^2, \ldots, |\bar{h}_K|^2) \tag{B.13}$$

Now, we analyze the second part of the right hand side of Eq. B.6. Choosing an arbitrary element of $\hat{\boldsymbol{A}}$, we have

$$\begin{aligned}\hat{\boldsymbol{A}}_{m,k} &= \frac{1}{\sqrt{M\sigma_h^2}} \mathcal{R}e\{h_{m,k} e^{-j(m\beta\cos(\theta_k) + \varphi_k)}\} \\ &= \frac{1}{\sqrt{M\sigma_h^2}} (h_{m,k}^r \cos(m\beta\cos(\theta_k) + \varphi_k) \\ &\qquad + h_{m,k}^i \sin(m\beta\cos(\theta_k) + \varphi_k)).\end{aligned} \tag{B.14}$$

So the variance of each element will be

$$\begin{aligned}\mathbb{E}\{\hat{\boldsymbol{A}}_{m,k} \hat{\boldsymbol{A}}_{m,k}^*\} &= \frac{1}{M\sigma_h^2} \mathbb{E}\{|h_{m,k}^r|^2\} \cos^2((m-1)\sqrt{\beta}\cos(\theta_k) + \varphi_k) \\ &\quad + \frac{1}{M\sigma_h^2} \mathbb{E}\{|h_{m,k}^i|^2\} \sin^2((m-1)\sqrt{\beta}\cos(\theta_k) + \varphi_k) \\ &= \frac{1}{M}.\end{aligned} \tag{B.15}$$

Similarly, $\mathbb{E}\{\hat{\boldsymbol{B}}_{m,k} \hat{\boldsymbol{B}}_{m,k}^*\} = \frac{1}{M}$. For the fourth order moment we have

$$\begin{aligned}\mathbb{E}\{|\hat{\boldsymbol{A}}_{m,k}|^4\} &= \mathbb{E}\{\hat{\boldsymbol{A}}_{m,k} \hat{\boldsymbol{A}}_{m,k}^* \hat{\boldsymbol{A}}_{m,k} \hat{\boldsymbol{A}}_{m,k}^*\} \\ &= \frac{1}{M^2\sigma_h^4} \mathbb{E}\{(h_{m,k}^r \cos((m-1)\beta\cos(\theta_k) + \varphi_k) \\ &\quad + h_{m,k}^i \sin((m-1)\beta\cos(\theta_k) + \varphi_k))^4\}\end{aligned} \tag{B.16}$$

After some algebraic simplification and using the fact that h^r and h^i are independent from each other, we obtain the following term for the fourth order moment

$$\begin{aligned}\mathbb{E}\{|\hat{\boldsymbol{A}}_{m,k}|^4\} = \frac{1}{M^2\sigma_h^4}&[\mathbb{E}\{|h^r_{m,k}|^4\}\cos^4((m-1)\beta\cos(\theta_k)+\varphi_k)\\ &+\mathbb{E}\{|h^i_{m,k}|^4\}\sin^4((m-1)\beta\cos(\theta_k)+\varphi_k)]\\ &+\frac{6}{M^2}[\cos^2((m-1)\beta\cos(\theta_k)+\varphi_k)\\ &\qquad\times\sin^2((m-1)\beta\cos(\theta_k)+\varphi_k)].\end{aligned} \tag{B.17}$$

Noting the fact that channel distribution is independent from the number of antennas at the BS, from Eq. B.17 it is evident that for a bounded $\mathbb{E}\{|h^r_{m,k}|^4\}$ and $\mathbb{E}\{|h^i_{m,k}|^4\}$, fourth moment of all elements of $\boldsymbol{A}$ are in the order of $\mathcal{O}(\frac{1}{M^2})$. Same condition is held for all the elements of $\boldsymbol{B}$. Using same approach, it can be shown that the order of eighth moment of all the elements of both $\boldsymbol{A}$ and $\boldsymbol{B}$ are in the order of $\mathcal{O}(\frac{1}{M^4})$.

Rewriting $\hat{\boldsymbol{A}}$ as

$$\hat{\boldsymbol{A}} = [\hat{\boldsymbol{a}}_1\hat{\boldsymbol{a}}_2\ldots\hat{\boldsymbol{a}}_K]. \tag{B.18}$$

From Lemma 1 and Lemma 2 we have

$$\begin{aligned}&\hat{\boldsymbol{a}}_1^H\boldsymbol{\Sigma}\hat{\boldsymbol{a}}_1-\frac{1}{M}tr(\boldsymbol{\Sigma})\xrightarrow{a.s.}0,\\ &\hat{\boldsymbol{a}}_2^H\boldsymbol{\Sigma}\hat{\boldsymbol{a}}_2-\frac{1}{M}tr(\boldsymbol{\Sigma})\xrightarrow{a.s.}0,\\ &\hat{\boldsymbol{a}}_1^H\boldsymbol{\Sigma}\hat{\boldsymbol{a}}_2\xrightarrow{a.s.}0,\\ &\hat{\boldsymbol{a}}_2^H\boldsymbol{\Sigma}\hat{\boldsymbol{a}}_1\xrightarrow{a.s.}0.\end{aligned}$$

So, we can write

$$\begin{bmatrix}\hat{\boldsymbol{a}}_1^H\\ \hat{\boldsymbol{a}}_2^H\end{bmatrix}\boldsymbol{\Sigma}\begin{bmatrix}\hat{\boldsymbol{a}}_1 & \hat{\boldsymbol{a}}_2\end{bmatrix}-\frac{1}{M}\begin{bmatrix}tr(\boldsymbol{\Sigma}) & 0\\ 0 & tr(\boldsymbol{\Sigma})\end{bmatrix}\xrightarrow{a.s.}\mathbf{0}_2. \tag{B.19}$$

After repeating this process for K columns of $\boldsymbol{A}$, we will have

$$\hat{\boldsymbol{A}}^H \boldsymbol{\Sigma} \hat{\boldsymbol{A}} - \frac{1}{M} tr(\boldsymbol{\Sigma}) \boldsymbol{I}_K \xrightarrow{a.s.} 0. \tag{B.20}$$

Similarly,

$$\hat{\boldsymbol{B}}^H \boldsymbol{\Sigma} \hat{\boldsymbol{B}} - \frac{1}{M} tr(\boldsymbol{\Sigma}) \boldsymbol{I}_K \xrightarrow{a.s.} 0. \tag{B.21}$$

Based on B.20 and B.21 and the fact that both $\boldsymbol{A}$ and $\boldsymbol{B}$ consist of real elements, we can write

$$\hat{\boldsymbol{A}}^T \boldsymbol{\Sigma} \hat{\boldsymbol{A}} + \hat{\boldsymbol{B}}^T \boldsymbol{\Sigma} \hat{\boldsymbol{B}} - \frac{2}{M} tr(\boldsymbol{\Sigma}) \boldsymbol{I}_K \xrightarrow{a.s.} 0. \tag{B.22}$$

By replacing Eq. B.13 and Eq. B.22 in Eq. B.6, we obtain

$$\boldsymbol{A}^T \boldsymbol{\Sigma} \boldsymbol{A} + \boldsymbol{B}^T \boldsymbol{\Sigma} \boldsymbol{B} \xrightarrow{a.s.} \frac{tr(\boldsymbol{\Sigma})}{M} (2\sigma_h^2 + diag(|\bar{h}_1|^2, \ldots, |\bar{h}_K|^2)). \tag{B.23}$$

Consequently

$$(\boldsymbol{A}^T \boldsymbol{\Sigma} \boldsymbol{A} + \boldsymbol{B}^T \boldsymbol{\Sigma} \boldsymbol{B})^{-1} \xrightarrow{a.s.} \frac{M}{2tr(\boldsymbol{\Sigma})} (2\sigma_h^2 + diag(|\bar{h}_1|^2, \ldots, |\bar{h}_K|^2))^{-1}. \tag{B.24}$$

Defining $\boldsymbol{S} \triangleq \sigma_n^2 \boldsymbol{D}^{-2}$ and noticing that

$$tr(\boldsymbol{\Sigma}) = \frac{\beta^2}{M^2} \sum_{m=0}^{M-1} m^2 = \frac{\beta^2 M(M-1)(2M-1)}{6M^2}, \tag{B.25}$$

we obtain

$$\boldsymbol{CRLB}_\theta = \frac{\sigma_n^2}{2} (\mathbb{E}_{\boldsymbol{h}|\boldsymbol{\eta}_\theta} \{\mathcal{R}e(\boldsymbol{X}^H \boldsymbol{X})\})^{-1} \xrightarrow{a.s.} \frac{3}{\beta^2 (M-1)(2M-1)} \boldsymbol{S}. \tag{B.26}$$

APPENDIX C

Proof of Theorem 4

The process of proof is to show that for every step, the presented set in Theorem4 obtains the lowest possible value for $U(\mathcal{S})$. We show this for the first two steps, i.e. for $F_p \leq 5$ and $5 < F_p \leq 13$. The rest of the proof is exactly the same as these steps and can be simply repeated until any arbitrary F_p.

For $F_p = 5$, selecting S_{p_1} will result in $U(\mathcal{S}_{p_1}) = \frac{2}{M^2}$. Now we show that any other set than S_{p_1}, results in higher value for $U(\mathcal{S})$. Assume any $\bar{S}_{p_1} = \{(0,0),(x_1,y_1),(x_2,y_2),(x_3,y_3),(x_4,y_4)\}$ to be a set of antennas which at least has one different antenna from S_{p_1}, we have

$$U(\bar{\mathcal{S}}_{p_1}) = \frac{\sum_{i=1}^{5}(x_i^2+y_i^2)}{(\sum_{i=1}^{5} x_i^2)(\sum_{i=1}^{5} y_i^2) - (\sum_{i=1}^{5} x_i y_i)^2}. \tag{C.1}$$

Because at least one antenna in $\bar{\mathcal{S}}_{p_1}$ has at least one different coordinate from the antennas in the $\mathcal{S}_{p_1}$, so at least either $\sum_{i=1}^{5} x_i^2 < M^2$ or

$\sum_{i=1}^{5} y_i^2 < M^2$, so

$$(M^2 - \sum_{i=1}^{5} y_i^2) \sum_{i=1}^{5} x_i^2 + (M^2 - \sum_{i=1}^{5} x_i^2) \sum_{i=1}^{5} y_i^2$$
$$= M^2 \sum_{i=1}^{5} (x_i^2 + y_i^2) - 2(\sum_{i=1}^{5} x_i^2)(\sum_{i=1}^{5} y_i^2) > 0 \geq -2(\sum_{i=1}^{5} x_i y_i)^2. \quad \text{(C.2)}$$

Therefore

$$M^2 \sum_{i=1}^{5} x_i^2 + y_i^2 > 2((\sum_{i=1}^{5} x_i^2)(\sum_{i=1}^{5} y_i^2) - (\sum_{i=1}^{5} x_i y_i)^2). \quad \text{(C.3)}$$

By noting that $(\sum_{i=1}^{5} x_i^2)(\sum_{i=1}^{5} y_i^2) - (\sum_{i=1}^{5} x_i y_i)^2 > 0$ due to Cauchy-Schwarz inequality, we obtain

$$\frac{\sum_{i=1}^{5}(x_i^2 + y_i^2)}{(\sum_{i=1}^{5} x_i^2)(\sum_{i=1}^{5} y_i^2) - (\sum_{i=1}^{5} x_i y_i)^2} > \frac{2}{M^2}. \quad \text{(C.4)}$$

When, $3 < F_p < 5$, all of greater signs ($>$) in (C.2)-(C.4) will be replaced with the greater or equal sign ($\geq$), with equality happening for any two subsets of $\mathcal{S}_{p_1}$.

For $F_p = 13$, the antennas set of $\mathcal{S}_{p_2}$ will result in $U(\mathcal{S}_{p_1} \bigcup \mathcal{S}_{p_2}) = \frac{2}{2M^2+4(\frac{M}{2}-1)^2}$. For this set, $\sum_{i=1}^{5} x_i^2 = \sum_{i=1}^{5} y_i^2 = 2M^2+4(\frac{M}{2}-1)^2$. We call $\bar{\mathcal{S}}_{p_2}$ a set in which at least one of the coordinates of one antenna is different from the $\mathcal{S}_{p_1} \bigcup \mathcal{S}_{p_2}$. In this case, depending on the fact that which coordinate is different, three scenarios will happen. First scenario is that either $\sum_{i=1}^{5} x_i^2$ or $\sum_{i=1}^{5} y_i^2$ is reduced and the other one remains constant. Second scenario is when both of them are reduced and the third scenario is when one is increased and the other one is reduced. It should be noted that no other choice for first 13 antenna other than antennas in $\mathcal{S}_{p_2}$ can simultaneously increase both $\sum_{i=1}^{5} x_i^2$ and $\sum_{i=1}^{5} y_i^2$. This is because expect the reference point, all of antennas in $\mathcal{S}_{p_2}$ are the ones whose x_is and y_is are simultaneously maximized.

In the aforementioned scenarios, the values of $\sum_{i=1}^{5} x_i^2$ and $\sum_{i=1}^{5} y_i^2$ for $\mathcal{S}_{p_2}$ will change to

$$\sum_{i\in\bar{\mathcal{S}}_{p_2}} x_i^2 = 2M^2 + 4(\frac{M}{2} - 1)^2 - a,$$
$$\sum_{i\in\bar{\mathcal{S}}_{p_2}} y_i^2 = 2M^2 + 4(\frac{M}{2} - 1)^2 - b, \tag{C.5}$$

We have

$$\begin{aligned}
&(2M^2 + 4(\frac{M}{2} - 1)^2)(\sum_{i\in\bar{\mathcal{S}}_{p_2}} x_i^2 + y_i^2) - 2(\sum_{i\in\bar{\mathcal{S}}_{p_2}} x_i^2)(\sum_{i\in\bar{\mathcal{S}}_{p_2}} y_i^2) \\
&= (2M^2 + 4(\frac{M}{2} - 1)^2)(\sum_{i\in\mathcal{S}_{p_2}} x_i^2 + y_i^2 - a - b) \\
&- 2(\sum_{i\in\mathcal{S}_{p_2}} x_i^2 - a)(\sum_{i\in\mathcal{S}_{p_2}} y_i^2 - b) \\
&= (2M^2 + 4(\frac{M}{2} - 1)^2)(\sum_{i\in\mathcal{S}_{p_2}} x_i^2 + y_i^2) - 2(\sum_{i\in\mathcal{S}_{p_2}} x_i^2)(\sum_{i\in\mathcal{S}_{p_2}} y_i^2) \\
&+ (2M^2 + 4(\frac{M}{2} - 1)^2)(a+b) - 2ab \\
&= \underbrace{\left(2M^2 + 4(\frac{M}{2} - 1)^2 - \sum_{i\in\mathcal{S}_{p_2}} y_i^2\right)}_{=0} \sum_{i\in\mathcal{S}_{p_2}} x_i^2 \\
&+ \underbrace{\left(2M^2 + 4(\frac{M}{2} - 1)^2 - \sum_{i\in\mathcal{S}_{p_2}} x_i^2\right)}_{=0} \sum_{i\in\mathcal{S}_{p_2}} y_i^2 \\
&+ (2M^2 + 4(\frac{M}{2} - 1)^2)(a+b) - 2ab.
\end{aligned} \tag{C.6}$$

Now, (C.6) is a linear equation w.r.t a and b. Its derivative w.r.t a is

$$2M^2 + 4(\frac{M}{2} - 1)^2 - 2b, \tag{C.7}$$

and (C.7) is always positive because the maximum value of b is $4(\frac{M^2}{4})$. So, the slope of (C.6) is always positive. The most negative value of a happens when all of four antennas with $x = \frac{M}{2} - 1$ in $\mathcal{S}_{p_1}$ are replaced with $\frac{M}{2}$ in $\bar{\mathcal{S}}_{p_1}$. This replacement will result in $a = 4((\frac{M}{2} - 1)^2 - (\frac{M}{2})^2)$ and $b = 4((\frac{M}{2})^2 - (\frac{M}{2} - 2)^2)$. Therefore, $a + b > 0$ in the most negative value of a. So, a starts from a positive value with a positive slope, meaning that (C.6) is positive for every possible value of a. Same thing can be shown w.r.t b. Therefore,

$$\begin{aligned}
&(2M^2 + 4(\frac{M}{2} - 1)^2)(\sum_{i \in \bar{\mathcal{S}}_{p_2}} x_i^2 + y_i^2) - 2(\sum_{i \in \bar{\mathcal{S}}_{p_2}} x_i^2)(\sum_{i \in \bar{\mathcal{S}}_{p_2}} y_i^2) \\
&= (2M^2 + 4(\frac{M}{2} - 1)^2 - b)a + (2M^2 + 4(\frac{M}{2} - 1)^2 - a)b \\
&> 0 \geq -2\left(\sum_{i \in \bar{\mathcal{S}}_{p_2}} x_i y_i\right)^2.
\end{aligned} \tag{C.8}$$

So, for any $\bar{\mathcal{S}}_{p_2}$ we have

$$\frac{\sum_{i=1}^{13} x_i^2 + y_i^2}{(\sum_{i=1}^{13} x_i^2)(\sum_{i=1}^{5} y_i^2) - (\sum_{i=1}^{13} x_i y_i)^2} > \frac{2}{(2M^2 + 4(\frac{M}{2} - 1))^2}. \tag{C.9}$$

If $5 < F_p < 13$, all of the greater signs ($>$) in (C.8) and (C.9) will be replaced by greater or equal sign ($\geq$), with equality happening for any two subsets of $\mathcal{S}_{p_1} \bigcup \mathcal{S}_{p_2}$.

For $14 \leq F < 21$ and other steps the proof is exactly same as $5 < F_p \leq 13$. When all of antennas in the outer most rectangle are selected, then the proof of the next step that is the selection of the four antennas at the corner of the second most outer rectangle, is same as $F_p \leq 5$. Then the process of rest antennas in the same rectangle is same as $5 < F_p \leq 13$, and so on. This process can be repeated for any desired F_p.

APPENDIX D

Proof of Theorem 5

As the main reference for the system, the antenna that is considered as the reference point has to be in the selected set. Then, the $CRLB_\theta$ for any set of three selected antennas $\{(0,0),(x_1,y_1),$ $(x_2,y_2)\}$, will have the following form

$$CRLB_{\theta,3} = A \times \underbrace{\left(\frac{(x_1+\alpha y_1)^2+(x_2+\alpha y_2)^2}{(x_1y_2-x_2y_1)^2}\right)}_{Q_\theta(x_1,y_1,x_2,y_2)}, \tag{D.1}$$

where $A = \frac{\cos^2(\theta)}{2\rho\beta^2|h_d|^2\sin^2(\varphi)}$ and it is independent from selected antennas. So, $Q_\theta(x_1,y_1,x_2,y_2)$ should be minimized with respect to (w.r.t) x_1, y_1, x_2 and y_2

$$\min_{x_1,y_1,x_2,y_2} Q_\theta(x_1,y_1,x_2,y_2), \tag{D.2a}$$

$$s.t.\;\; x_1,y_1,x_2,y_2 \in \{-\frac{M}{2},\ldots,0,\ldots,\frac{M}{2}\}, \tag{D.2b}$$

$$(x_1,y_1) \neq (ax_2,ay_2) \quad for \quad a \in \mathbb{R}, \tag{D.2c}$$

$$(x_1,y_1) \neq (0,0), \quad (x_2,y_2) \neq (0,0), \tag{D.2d}$$

where (D.2c) and (D.2d) ensure that an antenna is not selected twice, and three selected antennas do not compose a line.

For $0 < \theta \leq \frac{\pi}{4} - \theta_0$, first we relax the integer constraint only on x_2 and prove that any other choice than $(x_1^*, y_1^*, x_2^*, y_2^*) = (-\frac{M}{2}, \frac{M}{2}, \frac{M(1-2\alpha)}{2}, \frac{M}{2})$ results in higher $Q_\theta(x_1, y_1, x_2, y_2)$. Then the problem boils down to the choice between two upper and lower integers in the vicinity of x_2, that can be efficiently solved by directly checking which one results in lower value for $Q_\theta(x_1, y_1, x_2, y_2)$.

By replacing $(x_1^*, y_1^*, x_2^*, y_2^*) = (-\frac{M}{2}, \frac{M}{2}, \frac{M(1-2\alpha)}{2}, \frac{M}{2})$ in Q_θ, we have

$$Q_\theta(x_1^*, y_1^*, x_2^*, y_2^*) = \frac{2}{M^2}. \tag{D.3}$$

Now we show that for any combination of (x_1, y_1, x_2, y_2),

$$\frac{(x_1 + \alpha y_1)^2 + (x_2 + \alpha y_2)^2}{(x_1 y_2 - x_2 y_1)^2} \geq \frac{2}{M^2}. \tag{D.4}$$

By multiplying both sides of (D.4) by $M^2(x_1 y_2 - x_2 y_1)^2$, we have

$$\begin{aligned}
&M^2((x_1 + \alpha y_1)^2 + (x_2 + \alpha y_2)^2) \\
&= M^2(x_1^2 + \alpha^2 y_1^2 + 2\alpha x_1 y_1 + x_2^2 + \alpha^2 y_2^2 + 2\alpha x_2 y_2) \\
&= 2\frac{M^2}{4}x_1^2 + M^2\alpha^2 y_1^2 + 2M^2\alpha x_1 y_1 + 2\frac{M^2}{4}x_2^2 + M^2\alpha^2 y_2^2 + 2M^2\alpha x_2 y_2 \\
&+ 2\frac{M^2}{4}(x_1^2 + x_2^2) \\
&= M^2\alpha^2 y_1^2 + M^2\alpha^2 y_2^2 + 2M^2\alpha x_1 y_1 + 2M^2\alpha x_2 y_2 + 2x_2^2 y_1^2 + 2x_1^2 y_2^2 \\
&+ 2\frac{M^2}{4}(x_1 - x_2)^2 \\
&- 4x_1 x_2 y_1 y_2 + 2((\frac{M^2}{4} - y_2^2)x_1^2 + (\frac{M^2}{4} - y_1^2)x_2^2) + 4x_1 x_2(\frac{M^2}{4} + y_1 y_2).
\end{aligned} \tag{D.5}$$

Now we show the fact that the following phrase is always non-negative

$$\begin{aligned} A(M,\alpha) &= M^2\alpha^2 y_1^2 + M^2\alpha^2 y_2^2 + 2\alpha M^2 x_1 y_1 + 2\alpha M^2 x_2 y_2 \\ &\quad + 2((\frac{M^2}{4} - y_2^2)x_1^2 + (\frac{M^2}{4} - y_1^2)x_2^2) + 2\frac{M^2}{4}(x_1 - x_2)^2 \\ &\quad + 4x_1 x_2(\frac{M^2}{4} + y_1 y_2). \end{aligned} \tag{D.6}$$

By rewriting $A(M,\alpha)$ we have

$$\begin{aligned} A(M,\alpha) &= M^2(y_1^2 + y_2^2)\alpha^2 + 2M^2(x_1 y_1 + x_2 y_2)\alpha \\ &\quad + (M^2(x_1^2 + x_2^2) - 2(x_1 y_2 - x_2 y_1)^2). \end{aligned} \tag{D.7}$$

After some algebraic operations, the discriminant of $A(M,\alpha)$ will be obtained as

$$\Delta_A = 4M^2(x_1 y_2 - x_2 y_1)^2(2(y_1^2 + y_2^2) - M^2) \leq 0, \tag{D.8}$$

where the last inequality results from the fact that $|y_1| \leq \frac{M}{2}$ and $|y_2| \leq \frac{M}{2}$. Because $\Delta_A \leq 0$ (and $M^2(y_1^2 + y_2^2) > 0$), for any value of α any combination of x_1, x_2, y_1 and y_2, $A(M,\alpha)$ will be non-negative. Therefore, we continue (D.5) as

$$\begin{aligned} &M^2((x_1 + \alpha y_1)^2 + (x_2 + \alpha y_2)^2) \\ &= A(M,\alpha) + 2x_2^2 y_1^2 + 2x_1^2 y_2^2 - 4x_1 x_2 y_1 y_2 \\ &\geq 2x_2^2 y_1^2 + 2x_1^2 y_2^2 - 4x_1 x_2 y_1 y_2 = 2(x_1 y_2 - x_2 y_1)^2. \end{aligned} \tag{D.9}$$

So, $(x_1^*, y_1^*, x_2^*, y_2^*) = (-\frac{M}{2}, \frac{M}{2}, \frac{M(1-2\alpha)}{2}, \frac{M}{2})$ is the optimal choice to minimize $Q_\theta(x_1, y_1, x_2, y_2)$. However, $\frac{M(1-2\alpha)}{2}$ may not be an integer value. In order to decide whether higher or lower integer is the better choice, we simply check both of them in the function of

$Q_\theta(x_1, y_1, x_2, y_2)$. The $Q_\theta(-\frac{M}{2}, \frac{M}{2}, x, \frac{M}{2})$ will be

$$Q_\theta(-\frac{M}{2}, \frac{M}{2}, x, \frac{M}{2}) = \frac{(1-\alpha)^2 + (\frac{2}{M}x + \alpha)^2}{(\frac{M}{2} + x)^2}.$$

As $\theta \to \frac{\pi}{4}$, $\frac{M(1-2\alpha)}{2} \to -\frac{M}{2}$, but because one antenna cannot be selected twice, the system will have to choose $1 - \frac{M}{2}$ for x_2. The selection of $(-\frac{M}{2}, \frac{M}{2}, 1-\frac{M}{2}, \frac{M}{2})$ happens when $\theta \geq \tan^{-1}(\frac{M-1}{M})$. Although this choice is optimal for a certain range of θ, after a point it will not be the best choice and $(x_1, y_1, x_2, y_2) = (-\frac{M}{2}, \frac{M}{2} - 1, 1 - \frac{M}{2}, \frac{M}{2})$ results in lower $Q_\theta(x_1, y_1, x_2, y_2)$. To obtain the range of θ that the latter set is the optimal choice, we have to solve the following inequality for α

$$Q_\theta(-\frac{M}{2}, \frac{M}{2} - 1, 1 - \frac{M}{2}, \frac{M}{2}) < Q_\theta(-\frac{M}{2}, \frac{M}{2}, 1 - \frac{M}{2}, \frac{M}{2}). \quad \text{(D.10)}$$

By replacing the actual values of both sides, we have

$$\frac{(\alpha-1)^2(\frac{M^2}{2} - M + 1) + 2\alpha}{(M-1)^2} < (\alpha - 1)^2 + \frac{(M(\alpha-1)+2)^2}{M^2}. \quad \text{(D.11)}$$

After some algebraic operations, (D.11) simplifies to

$$\begin{aligned} B(M,\alpha) = {} & M^2(3M^2 - 6M + 2)\alpha^2 - 2M(3M^3 - 10M^2 + 12M - 4)\alpha \\ & + (M-2)(3M-2)(M^2 - 2M + 2) > 0. \end{aligned} \quad \text{(D.12)}$$

Calling α_{b_1} the smaller root and α_{b_2} the bigger root of $B(M,\alpha)$, for $M \geq 1 + \frac{1}{\sqrt{3}}$ [1] (which is the case because $M \geq 2$), the inequality of (D.12) is held when either $\alpha \leq \alpha_{b_1}$ or $\alpha_{b_2} \leq \alpha$. To find out which root indicates the value of θ_0, after which $(x_1, y_1, x_2, y_2) = (-\frac{M}{2}, \frac{M}{2} - 1, 1 - \frac{M}{2}, \frac{M}{2})$ is the optimal choice, we investigate the sign of $B(M,\alpha)$ in a critical point in which $x_2 = \frac{M(1-2\alpha)}{2}$ is an integer and therefore $(x_1, y_1, x_2, y_2) = (-\frac{M}{2}, \frac{M}{2}, \frac{M(1-2\alpha)}{2}, \frac{M}{2})$ is still the optimal

[1] The roots of $(3M^2 - 6M + 2)$ are $1 \pm \frac{1}{\sqrt{3}}$ and for $M \geq 1 + \frac{1}{\sqrt{3}}$, the multiplier of α^2 will be always positive.

choice. This point is $\alpha = \frac{M-1}{M}$. By replacing $\alpha = \frac{M-1}{M}$ in $B(M, \alpha)$ and simplifying it, we obtain

$$B(M, \frac{M-1}{M}) = -M^2 - 2M + 2. \tag{D.13}$$

The roots of $B(M, \frac{M-1}{M})$ are $-\sqrt{3} - 1$ and $\sqrt{3} - 1$. So, for $M \geq 2$, (D.13) will always be negative (sign of M^2). This means that $\alpha = \frac{M-1}{M}$ is between the roots of $B(M, \alpha)$ (this is because for $M \geq 2$ the sign of $B(M, \alpha)$ is negative only between its root). We know that for $\alpha \leq \frac{M-1}{M}$, the optimal choice is $(x_1, y_1, x_2, y_2) = (-\frac{M}{2}, \frac{M}{2}, \frac{M(1-2\alpha)}{2}, \frac{M}{2})$ and therefore, the minimum α that changes the optimal choice, must be bigger than $\frac{M-1}{M}$. So, the minimum α after which the optimal choice becomes $(x_1, y_1, x_2, y_2) = (-\frac{M}{2}, \frac{M}{2} - 1, 1 - \frac{M}{2}, \frac{M}{2})$ is the bigger root of $B(M, \alpha)$ (solved for α). By noting that $\alpha = \tan(\theta)$, we obtain $\theta_0 = \tan^{-1}(\alpha_{b_2})$.

For $\theta_1 \leq \theta < \frac{\pi}{2}$, we relax the integer constraint only on y_2 to show that $(x_1, y_1, x_2, y_2) = (-\frac{M}{2}, \frac{M}{2}, -\frac{M}{2}, \frac{M(2-\alpha)}{2\alpha})$ is the optimal choice. By replacing $(x_1^*, y_1^*, x_2^*, y_2^*) = (-\frac{M}{2}, \frac{M}{2}, -\frac{M}{2}, \frac{M(2-\alpha)}{2\alpha})$ in (D.1) we have

$$f(x_1^*, y_1^*, x_2^*, y_2^*) = \frac{2\alpha}{M^2}. \tag{D.14}$$

The process to show that any other choice than $(x_1, y_1, x_2, y_2) = (-\frac{M}{2}, \frac{M}{2}, -\frac{M}{2}, \frac{M(2-\alpha)}{2\alpha})$ results in higher Q_θ is same as the process of (D.5). The only difference is that instead of showing $A(M, \alpha) \geq 0$, we should show that the following equation is non-negative:

$$\begin{aligned} C(M, \alpha) = {} & (M^2(y_1^2 + y_2^2) - 2(x_1 y_2 - x_2 y_1)^2)\alpha^2 \\ & + 2M^2(x_1 y_1 + x_2 y_2)\alpha + M^2(x_1^2 + x_2^2). \end{aligned} \tag{D.15}$$

The discriminant of $C(M, \alpha)$ will be obtained as

$$\Delta_C = 4M^2(x_1 y_2 - x_2 y_1)^2(2(x_1^2 + x_2^2) - M^2) \leq 0. \tag{D.16}$$

Same as (D.8), Δ_C in (D.16) is always non-positive, that confirms $C(M,\alpha) \geq 0$.

When θ is around $\frac{\pi}{4}$, $\frac{M(2-\alpha)}{2\alpha}$ is close to $\frac{M}{2}$ but as one antenna cannot be selected twice, system has to select $\frac{M}{2}-1$ for y_2. This obligation causes the choice of $(1-\frac{M}{2}, \frac{M}{2}, -\frac{M}{2}, \frac{M}{2}-1)$ to be the optimal choice for a certain range (same as the case of $\theta_0 < \theta < \frac{\pi}{4}$). To obtain this range, we have to solve the following inequality

$$Q_\theta(-\frac{M}{2}, \frac{M}{2}-1, 1-\frac{M}{2}, \frac{M}{2}) < Q_\theta(-\frac{M}{2}, \frac{M}{2}, -\frac{M}{2}, \frac{M}{2}-1). \quad \text{(D.17)}$$

By replacing the actual values of both sides and simplifying the inequality we obtain

$$\begin{aligned} D(M,\alpha) &= (M-2)(3M-2)(M^2-2M+2)\alpha^2 \\ &\quad - 2M(3M^3-10M^2+12M-4)\alpha \\ &\quad + M^2(3M^2-6M+2) > 0. \end{aligned} \quad \text{(D.18)}$$

Calling α_{d_1} the small root and α_{d_2} the big root of $D(M,\alpha)$, for $M > 2$ the inequality of (D.18) is held when either $\alpha \leq \alpha_{d_1}$ or $\alpha_{d_2} \leq \alpha$. To find out which root indicates the value of θ_1, before which $(x_1, y_1, x_2, y_2) = (-\frac{M}{2}, \frac{M}{2}-1, 1-\frac{M}{2}, \frac{M}{2})$ is the optimal choice, we investigate the sign of $D(M,\alpha)$ in a critical point in which $y_2 = \frac{M(2-\alpha)}{2\alpha}$ is an integer and therefore $(x_1, y_1, x_2, y_2) = (-\frac{M}{2}, \frac{M}{2}, -\frac{M}{2}, \frac{M(2-\alpha)}{2\alpha})$ is still the optimal choice. This point is $\alpha = \frac{M}{M-1}$. By replacing $\alpha = \frac{M}{M-1}$ in $D(M,\alpha)$ and simplifying it, we obtain

$$D(M, \frac{M}{M-1}) = (-M^2-2M+2)(\frac{M}{M-1})^2. \quad \text{(D.19)}$$

As $(\frac{M}{M-1})^2$ is always positive and the roots of $(-M^2-2M+2)$ are $-1 \pm \sqrt{3}$, for $M > 1$, $D(M, \frac{M}{M-1}) < 0$. This means that $\alpha = \frac{M}{M-1}$ is between the roots of (D.18). We know that for $\alpha \geq \frac{M}{M-1}$, the optimal choice is $(x_1, y_1, x_2, y_2) = (-\frac{M}{2}, \frac{M}{2}, -\frac{M}{2}, \frac{M(2-\alpha)}{2\alpha})$ and therefore, the maximum α before which the optimal choice is $(x_1, y_1, x_2, y_2) = (-\frac{M}{2}, \frac{M}{2} - 1, 1 - \frac{M}{2}, \frac{M}{2})$ has to be the smaller root of (D.18). By noting that $\alpha = \tan(\theta)$, we obtain $\theta_1 = \tan^{-1}(\alpha_{d_1})$.

By comparing the (D.12) and (D.18) we see that both have same coefficient for α, and the α^2 coefficient in (D.12) is the constant term of (D.18) and vice versa. We know that the roots of $ax^2 + bx + c$ are $x_{1,2} = \frac{-b\pm\sqrt{b^2-4ac}}{2a}$ and the roots of cx^2+bx+a are $x_{3,4} = \frac{-b\pm\sqrt{b^2-4ac}}{2c} = \frac{a}{c}x_{1,2}$. Therefore

$$\alpha_{d_1} = \frac{\alpha_{b_1} M^2(3M^2 - 6M + 2)}{(M-2)(3M-2)(M^2 - 2M + 2)}, \tag{D.20}$$

$$\theta_1 = \tan^{-1}(\alpha_{d_1}) = \tan^{-1}\left(\frac{M^2(3M^2 - 6M + 2)\alpha_{b_1}}{(M-2)(3M-2)(M^2 - 2M + 2)}\right). \tag{D.21}$$

APPENDIX E

List of Publications

Journal Paper

[1] **Arash. M**, Stupia. I and Vandendorpe. L. Real-Time CRLB based Antenna Selection in Planar Antenna Arrays. *IEEE Transactions on Wireless Communications*, vol. 22, no. 6, pp. 4043-4056, June 2023.

[2] **Arash. M**, Mirghasemi. H, Stupia. I and Vandendorpe. L. Energy Efficiency of Angle of Arrival estimation in Massive MIMO Systems. *IEEE Transactions on Communications*, vol. 70, no. 6, pp. 4175-4188, June 2022.

Conference Papers

[3] **Arash. M**, Mirghasemi. H, Stupia. I and Vandendorpe. L. Analysis of CRLB for AoA estimation in Massive MIMO systems. *2021 IEEE Annual International Symposium on Personal, Indoor and Mobile Radio Communications (PIMRC), pp. 1395-1400. IEEE, 2021.*

Bibliography

[1] T. L. Marzetta, “Noncooperative cellular wireless with unlimited numbers of base station antennas,” *IEEE Transactions on Wireless Communications*, vol. 9, no. 11, pp. 3590–3600, 2010.

[2] E. G. Larsson, O. Edfors, F. Tufvesson, and T. L. Marzetta, “Massive mimo for next generation wireless systems,” *IEEE communications magazine*, vol. 52, no. 2, pp. 186–195, 2014.

[3] L. Lu, G. Y. Li, A. L. Swindlehurst, A. Ashikhmin, and R. Zhang, “An overview of massive mimo: Benefits and challenges,” *IEEE Journal of Selected Topics in Signal Processing*, vol. 8, no. 5, pp. 742–758, 2014.

[4] G. Auer, V. Giannini, C. Desset, I. Godor, P. Skillermark, M. Olsson, M. A. Imran, D. Sabella, M. J. Gonzalez, O. Blume, and A. Fehske, “How much energy is needed to run a wireless network?” *IEEE Wireless Communications*, vol. 18, no. 5, pp. 40–49, 2011.

[5] M. Giordani and M. Zorzi, "Toward 6g networks: Use cases and technologies," *IEEE Communications Magazine*, vol. 58, no. 3, pp. 55–61, 2020.

[6] R. Liu, M. Li, and Q. Liu, "Joint transmit/receive antenna selection and beamforming design for isac systems," in *GLOBECOM 2023-2023 IEEE Global Communications Conference*. IEEE, 2023, pp. 3118–3123.

[7] H. Li, L. Song, and M. Debbah, "Energy efficiency of large-scale multiple antenna systems with transmit antenna selection," *IEEE Transactions on Communications*, vol. 62, no. 2, pp. 638–647, 2014.

[8] Z. Liu, W. Du, and D. Sun, "Energy and spectral efficiency tradeoff for massive mimo systems with transmit antenna selection," *IEEE Transactions on Vehicular Technology*, vol. 66, no. 5, pp. 4453–4457, 2016.

[9] H. Wymeersch, G. Seco Granados, G. Destino, D. Dardari, and F. Tufvesson, "5g mmwave positioning for vehicular networks," *IEEE Wireless Communications*, vol. 24, no. 6, pp. 80–86, 2017.

[10] Z. Abu-Shaban, X. Zhou, T. Abhayapala, G. Seco-Granados, and H. Wymeersch, "Error bounds for uplink and downlink 3d localization in 5g millimeter wave systems," *IEEE Transactions on Wireless Communications*, vol. 17, no. 8, pp. 4939–4954, 2018.

[11] A. Shahmansoori, G. E. Garcia, G. Destino, G. Seco-Granados, and H. Wymeersch, "Position and orientation estimation through millimeter-wave mimo in 5g systems," *IEEE Transactions on Wireless Communications*, vol. 17, no. 3, pp. 1822–1835, 2017.

[12] K. Mahler, W. Keusgen, F. Tufvesson, T. Zemen, and G. Caire, "Tracking of wideband multipath components in a vehicular communication scenario," *IEEE Transactions on Vehicular Technology*, vol. 66, no. 1, pp. 15–25, 2016.

[13] E. Björnson, L. Sanguinetti, J. Hoydis, and M. Debbah, "Optimal design of energy-efficient multi-user mimo systems: Is massive mimo the answer?" *IEEE Transactions on Wireless Communications*, vol. 14, no. 6, pp. 3059–3075, 2015.

[14] L. Zhao, G. Geraci, T. Yang, D. W. K. Ng, and J. Yuan, "A tone-based aoa estimation and multiuser precoding for millimeter wave massive mimo," *IEEE Transactions on Communications*, vol. 65, no. 12, pp. 5209–5225, 2017.

[15] R. Schmidt, "Multiple emitter location and signal parameter estimation," *IEEE transactions on antennas and propagation*, vol. 34, no. 3, pp. 276–280, 1986.

[16] R. Roy, A. Paulraj, and T. Kailath, "Estimation of signal parameters via rotational invariance techniques-esprit," in *MILCOM 1986-IEEE Military Communications Conference: Communications-Computers: Teamed for the 90's*, vol. 3. IEEE, 1986, pp. 41–6.

[17] E. Christopher, H. S. Dhillon, and R. M. Buehrer, "A statistical characterization of localization performance in wireless networks," *IEEE Transactions on Wireless Communications*, vol. 17, no. 9, pp. 5841–5856, 2018.

[18] S. M. Kay, *Fundamentals of statistical signal processing.* Prentice Hall PTR, 1993.

[19] M. Arash, E. Yazdian, M. S. Fazel, G. Brante, and M. A. Imran, “Employing antenna selection to improve energy efficiency in massive mimo systems,” *Transactions on Emerging Telecommunications Technologies*, vol. 28, no. 12, p. e3212, 2017.

[20] X. Li, E. Leitinger, M. Oskarsson, K. Åström, and F. Tufvesson, “Massive mimo-based localization and mapping exploiting phase information of multipath components,” *IEEE transactions on wireless communications*, vol. 18, no. 9, pp. 4254–4267, 2019.

[21] A. Guerra, F. Guidi, and D. Dardari, “Position and orientation error bound for wideband massive antenna arrays,” in *2015 IEEE International Conference on Communication Workshop (ICCW)*. IEEE, 2015, pp. 853–858.

[22] X. Wei, W. Peng, D. Chen, D. W. K. Ng, and T. Jiang, “Joint channel parameter estimation in multi-cell massive mimo system,” *IEEE Transactions on Communications*, vol. 67, no. 5, pp. 3251–3264, 2019.

[23] N. Garcia, H. Wymeersch, E. G. Larsson, A. M. Haimovich, and M. Coulon, “Direct localization for massive mimo,” *IEEE Transactions on Signal Processing*, vol. 65, no. 10, pp. 2475–2487, 2017.

[24] X. Sun, X. Gao, G. Y. Li, and W. Han, “Single-site localization based on a new type of fingerprint for massive mimo-ofdm systems,” *IEEE Transactions on Vehicular Technology*, vol. 67, no. 7, pp. 6134–6145, 2018.

[25] H. Elsawy, W. Dai, M.-S. Alouini, and M. Z. Win, “Base station ordering for emergency call localization in ultra-dense cellular networks,” *IEEE Access*, vol. 6, pp. 301–315, 2017.

[26] A. Wang, L. Liu, and J. Zhang, "Low complexity direction of arrival (doa) estimation for 2d massive mimo systems," in *2012 IEEE Globecom Workshops*. IEEE, 2012, pp. 703–707.

[27] D. Fan, F. Gao, Y. Liu, Y. Deng, G. Wang, Z. Zhong, and A. Nallanathan, "Angle domain channel estimation in hybrid millimeter wave massive mimo systems," *IEEE Transactions on Wireless Communications*, vol. 17, no. 12, pp. 8165–8179, 2018.

[28] J. Salmi, A. Richter, and V. Koivunen, "Detection and tracking of mimo propagation path parameters using state-space approach," *IEEE Transactions on Signal Processing*, vol. 57, no. 4, pp. 1538–1550, 2008.

[29] D. Asztély and B. Ottersten, "The effects of local scattering on direction of arrival estimation with music and esprit," in *IEEE International Conference on Acoustics, Speech and Signal Processing, ICASSP*, vol. 6. IEEE, 1998, pp. 3333–3336.

[30] L. Liu, C. Oestges, J. Poutanen, K. Haneda, P. Vainikainen, F. Quitin, F. Tufvesson, and P. De Doncker, "The cost 2100 mimo channel model," *IEEE Wireless Communications*, vol. 19, no. 6, pp. 92–99, 2012.

[31] J. Poutanen, J. Salmi, K. Haneda, V.-M. Kolmonen, and P. Vainikainen, "Angular and shadowing characteristics of dense multipath components in indoor radio channels," *IEEE Transactions on Antennas and Propagation*, vol. 59, no. 1, pp. 245–253, 2010.

[32] J. Poutanen, J. Salmi, K. Haneda, V.-M. Kolmonen, F. Tufvesson, and P. Vainikainen, "Propagation characteristics of dense

multipath components," *IEEE Antennas and Wireless Propagation Letters*, vol. 9, pp. 791–794, 2010.

[33] C. A. B. Camargo, G. Fraidenraich, and L. L. Mendes, "Probability of detection of the angle of arrival for massive mimo arrays," *IEEE Access*, vol. 6, pp. 65 109–65 117, 2018.

[34] R. Miller and C. Chang, "A modified cramér-rao bound and its applications (corresp.)," *IEEE Transactions on Information theory*, vol. 24, no. 3, pp. 398–400, 1978.

[35] A. N. D'Andrea, U. Mengali, and R. Reggiannini, "The modified cramer-rao bound and its application to synchronization problems," *IEEE Transactions on Communications*, vol. 42, no. 234, pp. 1391–1399, 1994.

[36] S. De Bast and S. Pollin, "Mamimo csi-based positioning using cnns: Peeking inside the black box," in *2020 IEEE International Conference on Communications Workshops (ICC Workshops)*, 2020, pp. 1–6.

[37] S. Wielandt and L. D. Strycker, "Indoor multipath assisted angle of arrival localization," *Sensors*, vol. 17, no. 11, 2017.

[38] E. Björnson, J. Hoydis, M. Kountouris, and M. Debbah, "Massive mimo systems with non-ideal hardware: Energy efficiency, estimation, and capacity limits," *IEEE Transactions on Information Theory*, vol. 60, no. 11, pp. 7112–7139, 2014.

[39] X. Gao, O. Edfors, F. Tufvesson, and E. G. Larsson, "Massive mimo in real propagation environments: Do all antennas contribute equally?" *IEEE Transactions on Communications*, vol. 63, no. 11, pp. 3917–3928, 2015.

[40] F. Reichenbach, J. Blumenthal, and D. Timmermann, "Comparing the efficiency of localization algorithms with the power-error-product (pep)," in *2008 The 28th International Conference on Distributed Computing Systems Workshops*. IEEE, 2008, pp. 150–155.

[41] D. Lieckfeldt, J. You, J. Salzmann, R. Behnke, and D. Timmermann, "Characterizing the energy efficiency of localization algorithms in wireless sensor networks," in *Proceedings of the 2009 International Conference on Wireless Communications and Mobile Computing: Connecting the World Wirelessly*. ACM, 2009, pp. 839–843.

[42] V. Chakravarthy, P. Chowdary, G. Panda, J. Anguera, A. Andújar, and B. Majhi, "On the linear antenna array synthesis techniques for sum and difference patterns using flower pollination algorithm," *Arabian Journal for Science and Engineering*, vol. 43, no. 8, pp. 3965–3977, 2018.

[43] S. De Bast, A. P. Guevara, and S. Pollin, "Csi-based positioning in massive mimo systems using convolutional neural networks," in *2020 IEEE 91st Vehicular Technology Conference (VTC2020-Spring)*. IEEE, 2020, pp. 1–5.

[44] R. Couillet and M. Debbah, *Random matrix methods for wireless communications*. Cambridge University Press, 2011.

[45] C. Steiner and A. Wittneben, "Efficient training phase for ultrawideband-based location fingerprinting systems," *IEEE Transactions on Signal Processing*, vol. 59, no. 12, pp. 6021–6032, 2011.

[46] W. W.-L. Li, Y. Shen, Y. J. Zhang, and M. Z. Win, "Robust power allocation for energy-efficient location-aware networks," *IEEE/ACM Transactions on Networking*, vol. 21, no. 6, pp. 1918–1930, 2013.

[47] H. Sallouha, A. Chiumento, S. Rajendran, and S. Pollin, "Localization in ultra narrow band iot networks: Design guidelines and tradeoffs," *IEEE Internet of Things Journal*, vol. 6, no. 6, pp. 9375–9385, 2019.

[48] Y. Shen and M. Z. Win, "Fundamental limits of wideband localization part i: A general framework," *IEEE Transactions on Information Theory*, vol. 56, no. 10, pp. 4956–4980, 2010.

[49] A. C. Gurbuz and B. A. Cetiner, "Crlb based mode selection and enhanced doa estimation for multifunctional reconfigurable arrays," *Physical Communication*, vol. 38, p. 100894, 2020.

[50] Y. Chen, D. Chen, and T. Jiang, "Non-uniform quantization codebook-based hybrid precoding to reduce feedback overhead in millimeter wave mimo systems," *IEEE Transactions on Communications*, vol. 67, no. 4, pp. 2779–2791, 2018.

[51] X. Zhang, L. Xu, L. Xu, and D. Xu, "Direction of departure (dod) and direction of arrival (doa) estimation in mimo radar with reduced-dimension music," *IEEE communications letters*, vol. 14, no. 12, pp. 1161–1163, 2010.

[52] S. Boyd and L. Vandenberghe, *Convex optimization.* Cambridge university press, 2004.

[53] U. S. Dias and M. D. Yacoub, “The κ-μ phase-envelope joint distribution,” *IEEE Transactions on Communications*, vol. 58, no. 1, pp. 40–45, 2010.

[54] S. Hu, F. Rusek, and O. Edfors, “Beyond massive mimo: The potential of positioning with large intelligent surfaces,” *IEEE Transactions on Signal Processing*, vol. 66, no. 7, pp. 1761–1774, 2018.

[55] V. Roy, S. P. Chepuri, and G. Leus, “Sparsity-enforcing sensor selection for doa estimation,” in *2013 5th IEEE International Workshop on Computational Advances in Multi-Sensor Adaptive Processing (CAMSAP)*. IEEE, 2013, pp. 340–343.

[56] M. Arash, H. Mirghasemi, I. Stupia, and L. Vandendorpe, “Analysis of crlb for aoa estimation in massive mimo systems,” in *2021 IEEE 32nd Annual International Symposium on Personal, Indoor and Mobile Radio Communications (PIMRC)*. IEEE, 2021, pp. 1395–1400.

[57] A. Hu, T. Lv, H. Gao, Z. Zhang, and S. Yang, “An esprit-based approach for 2d localization of incoherently distributed sources in massive mimo systems,” *IEEE Journal of Selected Topics in Signal Processing*, vol. 8, no. 5, pp. 996–1011, 2014.

[58] M. Arash, H. Mirghasemi, I. Stupia, and L. Vandendorpe, “Localization efficiency in massive mimo systems,” *arXiv preprint arXiv:2003.07978*, 2020.

[59] Q. Li, T. Su, and K. Wu, “Accurate doa estimation for large-scale uniform circular array using a single snapshot,” *IEEE Communications Letters*, vol. 23, no. 2, pp. 302–305, 2019.

[60] N. H. M. Adnan, I. M. Rafiqul, and A. Z. Alam, "Effects of inter element spacing on large antenna array characteristics," in *2017 IEEE 4th International Conference on Smart Instrumentation, Measurement and Application (ICSIMA).* IEEE, 2017, pp. 1–5.

[61] E. Bjornson, L. Sanguinetti, H. Wymeersch, J. Hoydis, and T. L. Marzetta, "Massive mimo is a reality what is next?: Five promising research directions for antenna arrays," *Digital Signal Processing*, vol. 94, pp. 3–20, 2019.

[62] C. Huang, G. C. Alexandropoulos, A. Zappone, M. Debbah, and C. Yuen, "Energy efficient multi user miso communication using low resolution large intelligent surfaces," in *2018 IEEE Globecom Workshops (GC Wkshps).* IEEE, 2018, pp. 1–6.

[63] A. M. Elbir and K. V. Mishra, "Joint antenna selection and hybrid beamformer design using unquantized and quantized deep learning networks," *IEEE Transactions on Wireless Communications*, vol. 19, no. 3, pp. 1677–1688, 2019.

[64] A. S. Khan, I. Chatzigeorgiou, S. Lambotharan, and G. Zheng, "Network-coded noma with antenna selection for the support of two heterogeneous groups of users," *IEEE Transactions on Wireless Communications*, vol. 18, no. 2, pp. 1332–1345, 2019.

[65] A. Bhattacharya, C. Zhan, A. Maji, H. Gupta, S. R. Das, and P. M. Djurićc, "Selection of sensors for efficient transmitter localization," *IEEE/ACM Transactions on Networking*, 2021.

[66] H. Godrich, A. P. Petropulu, and H. V. Poor, "Sensor selection in distributed multiple radar architectures for localization: A

knapsack problem formulation," *IEEE Transactions on Signal Processing*, vol. 60, no. 1, pp. 247–260, 2011.

[67] J. He, K. Yu, Y. Shi, Y. Zhou, W. Chen, and K. B. Letaief, "Reconfigurable intelligent surface assisted massive mimo with antenna selection," *IEEE Transactions on Wireless Communications*, 2021.

[68] M. O. Mendonça, P. S. Diniz, T. N. Ferreira, and L. Lovisolo, "Antenna selection in massive mimo based on greedy algorithms," *IEEE Transactions on Wireless Communications*, vol. 19, no. 3, pp. 1868–1881, 2020.

[69] S. Mulleti, C. Saha, H. S. Dhillon, and Y. C. Eldar, "A fast-learning sparse antenna array," in *2020 IEEE Radar Conference (RadarConf20)*. IEEE, 2020, pp. 1–6.

[70] A. M. Elbir, K. V. Mishra, and Y. C. Eldar, "Cognitive radar antenna selection via deep learning," *IET Radar, Sonar & Navigation*, vol. 13, no. 6, pp. 871–880, 2019.

[71] H. Zhang, J. Shi, Q. Zhang, B. Zong, and J. Xie, "Antenna selection for target tracking in collocated mimo radar," *IEEE Transactions on Aerospace and Electronic Systems*, vol. 57, no. 1, pp. 423–436, 2020.

[72] X. Wang, E. Aboutanios, and M. G. Amin, "Adaptive array thinning for enhanced doa estimation," *IEEE Signal Processing Letters*, vol. 22, no. 7, pp. 799–803, 2014.

[73] E. Aboutanios, H. Nosrati, and X. Wang, "Online antenna selection for enhanced doa estimation," in *ICASSP 2021-2021 IEEE*

International Conference on Acoustics, Speech and Signal Processing (ICASSP). IEEE, 2021, pp. 8468–8472.

[74] J. M. Romero-Jerez and A. J. Goldsmith, "Performance of multichannel reception with transmit antenna selection in arbitrarily distributed nagakami fading channels," *IEEE Transactions on Wireless Communications*, vol. 8, no. 4, pp. 2006–2013, 2009.

[75] M. Zhu, J. Vieira, Y. Kuang, K. Åström, A. F. Molisch, and F. Tufvesson, "Tracking and positioning using phase information from estimated multi-path components," in *2015 IEEE International Conference on Communication Workshop (ICCW).* IEEE, 2015, pp. 712–717.

[76] P. Stoica, R. L. Moses, B. Friedlander, and T. Soderstrom, "Maximum likelihood estimation of the parameters of multiple sinusoids from noisy measurements," *IEEE Transactions on Acoustics, Speech, and Signal Processing*, vol. 37, no. 3, pp. 378–392, 1989.

[77] A. Guerra, F. Guidi, and D. Dardari, "Single-anchor localization and orientation performance limits using massive arrays: Mimo vs. beamforming," *IEEE Transactions on Wireless Communications*, vol. 17, no. 8, pp. 5241–5255, 2018.

[78] R. Di Taranto, S. Muppirisetty, R. Raulefs, D. Slock, T. Svensson, and H. Wymeersch, "Location-aware communications for 5g networks: How location information can improve scalability, latency, and robustness of 5g," *IEEE Signal Processing Magazine*, vol. 31, no. 6, pp. 102–112, 2014.

[79] D. Astely and B. Ottersten, "The effects of local scattering on direction of arrival estimation with music," *IEEE transactions on Signal Processing*, vol. 47, no. 12, pp. 3220–3234, 1999.

[80] A. I. Akin, I. Stupia, and L. Vandendorpe, "On the effect of blockage objects in dense mimo swipt networks," *IEEE Transactions on Communications*, vol. 67, no. 2, pp. 1059–1069, 2018.

[81] S. Jang and C. Lee, "New view of learning-aided channel estimation for movable antenna systems," *IEEE Transactions on Wireless Communications*, 2025.

[82] D. Wang, M. Fattouche, and F. M. Ghannouchi, "Bounds of mmwave-based ranging and positioning in multipath channels," in *2017 IEEE Globecom Workshops (GC Wkshps)*. IEEE, 2017, pp. 1–6.

[83] K. B. Petersen, M. S. Pedersen *et al.*, "The matrix cookbook," *Technical University of Denmark*, vol. 7, no. 15, p. 510, 2008.

[84] T. W. Anderson, *An introduction to multivariate statistical analysis*, 1962.

[85] M.-T. Chao and W. Strawderman, "Negative moments of positive random variables," *Journal of the American Statistical Association*, vol. 67, no. 338, pp. 429–431, 1972.

[86] A. M. Tulino, S. Verdú *et al.*, "Random matrix theory and wireless communications," *Foundations and Trends® in Communications and Information Theory*, vol. 1, no. 1, pp. 1–182, 2004.

[87] P. Charge, Y. Wang, and J. Saillard, "An extended cyclic music algorithm," *IEEE Transactions on Signal Processing*, vol. 51, no. 7, pp. 1695–1701, 2003.

[88] C. Stoeckle, J. Munir, A. Mezghani, and J. A. Nossek, "Doa estimation performance and computational complexity of subspace- and compressed sensing-based methods," in *WSA 2015; 19th International ITG Workshop on Smart Antennas.* VDE, 2015, pp. 1–6.

[89] S. Buzzi and C. D'Andrea, "Doubly massive mmwave mimo systems: Using very large antenna arrays at both transmitter and receiver," in *2016 IEEE Global Communications Conference (GLOBECOM).* IEEE, 2016, pp. 1–6.

[90] X. Chen, X. Xu, and X. Tao, "Adaptive antenna selection for energy-efficient mimo systems with user demand awareness," *IEEE Transactions on Wireless Communications*, vol. 15, no. 4, pp. 2437–2451, 2016.

[91] H. Li, G. P. Koudouridis, and J. Zhang, "Antenna selection schemes for energy efficiency in distributed antenna systems," in *2012 IEEE International Conference on Communications (ICC).* IEEE, 2012, pp. 5619–5623.